AUTOMATED LATTICE PERTURBATION THEORY

FOR IMPROVED QUARK AND GLUON ACTIONS

by

Matthew A. Nobes

B.Sc. University of Waterloo, 1997

M.Sc. Simon Fraser University, 2000

THESIS SUBMITTED IN PARTIAL FULFILLMENT

OF THE REQUIREMENTS FOR THE DEGREE OF

DOCTOR OF PHILOSOPHY

IN THE DEPARTMENT

OF

PHYSICS

© Matthew A. Nobes 2004

SIMON FRASER UNIVERSITY

May 2004

APPROVAL

Name: Matthew A. Nobes

Degree: Doctor of Philosophy

Title of Thesis: Automated Lattice Perturbation Theory for Improved
Quark and Gluon Actions

Examining Committee: Robert Frindt (Chair)

Dr. H.D. Trottier
Senior Supervisor
Professor, Department of Physics

Dr. K.S. Viswanathan
Professor, Department of Physics

Dr. R.M. Woloshyn
Research Scientist
TRIUMF

Dr. I.F. Herbut
Internal Examiner
Associate Professor, Department of Physics

Dr. G.W. Kilcup
External Examiner
Associate Professor, Department of Physics
The Ohio State University

Date Approved: May 28th 2004

SIMON FRASER UNIVERSITY

Partial Copyright Licence

Abstract

Many fundamental parameters of the standard model are difficult to extract from measurements because they require an understanding of the strong interaction at low energies. Lattice gauge theories provide a first principles method to compute such effects. Unfortunately with current computational resources, "naive" lattice gauge theories would not give the precision results that the experiments require. Fortunately, there are several field theoretical methods that we can use to improve accuracy at minimal computational cost. One part of this program involves improving the lattice actions, to better approximate the continuum theory.

This improvement can be done order by order in perturbation theory. For several reasons, perturbative calculations in lattice gauge theory are very complicated. To deal with this, we have developed a set of tools to automate the most difficult parts of the calculations.

This thesis introduces the general procedure of perturbatively improving lattice gauge theories, and outlines why perturbative calculations are needed. The calculations are done for the most complex actions currently used by simulations, the Symanzik improved gluon action for the gluons, Fermilab fermions for the heavy quarks, and AsqTad fermions for the light quarks. We report the results of a number of calculations, we have computed various lattice operators (mean link, static quark potential) to second order, and a number of important heavy quark quantities (including matching the clover operator for the Fermilab action) to first order. The latter calculations have the potential to greatly improve lattice QCD determinations of various heavy quark quantities.

To Tiffany

Acknowledgments

Many thanks are due to all who helped me with this work. First and foremost, to Howard Trottier, for proposing the research, guiding me through it, and for teaching me too many things to list. Many thanks also to Richard Woloshyn, for many valuable discussions. Thanks as well to K.S. Viswanathan, for teaching me a considerable amount in my coursework here at SFU.

I have profited from valuable discussions with many colleagues. In particular I thank Peter Lepage, Quentin Mason, Andreas Kronfeld, Paul Mackenzie, Mehmet Oktay, Mark Lamb and Christine Davies. Special thanks to Aida El-Khadra for valuable collaboration on the current matching calculations. Thanks also to Heinz Rothe and World Scientific for permission to reproduce figure 3.1.

Thanks to the grad students at SFU who I have interacted with during my time here. Special thanks to Kit Wong, Sacha Kautsky, Peter Matlock, Dan Vernon and Karn Kallio.

Finally, special thanks to my friends and family for their love and support throughout the writing of this thesis. Most importantly, my parents, Mary and Dana, my Grandmother, and, my wife Tiffany.

Contents

List of Tables

List of Figures

Chapter 1

Introduction

The standard model of particle physics has withstood over twenty-five years of testing. During the 1990s its predictions were tested to very high precision at the Large Electron Positron Collider (LEP), the TeVatron, and B factories (such as BaBar). Today, at the end of the LEP era, it is one of the best tested of our physical theories. The description it provides is the most fundamental picture we have of the physical world. However, as we shall detail in this chapter, the study of the standard model is by no means a closed subject.

1.1 Brief Review of the Standard Model of Particle Physics

There are four known fundamental forces in nature, strong, weak, electromagnetic and gravitational. To describe the interaction of the elementary particles we can ignore the gravitational force. The remaining three forces are described by the standard model (henceforth SM). The SM actually goes one step further, unifying the electromagnetic and weak forces into the electroweak force. Thus the standard model describes two forces.

Each of the forces in the standard model is a gauge theory, with interactions

between fermion fields ("matter") mediated by gauge fields ("force carriers")[1]. The matter fields come in a structure known as a generation, the first generation is the familiar electron, its neutrino, the up (u) quark and the down (d) quark. The u and d quarks are bound by the strong force into protons and neutrons. In this way the particles of the first generation make up all of the matter we see around us.

There are two other generations as well, the second generation contains the muon, its neutrino, and the charm and strange quarks. The particles in the second generation are similar to those in the first, apart from the fact that they are much more massive. The third generation consists of the tau, its neutrino and the top and bottom quarks. Table 1.1 lists the matter particles in the standard model, along with their masses and electric charges[2].

The matter particles interact via the electroweak and strong forces, each force couples to a different type of "charge". For the electroweak force there is the standard photon, which couples to electric charge. As well, there is the Z^0 boson, which acts much like a heavy copy of the photon, and the $W^\pm$ bosons, which couple to, and change, the matter particle type (or flavour).

The strong force couples to another kind of charge; called colour. There are three colour charges (red, green and blue) carried only by quarks. The interaction between colour charge is mediated by gluons, the gauge bosons of the colour $SU(3)$ symmetry. This theory of the strong force is called quantum chromodynamics, or QCD. The Lagrangian for QCD is

$$\mathcal{L} = -\frac{1}{4}F^a_{\mu\nu}F^{\mu\nu}_a + \sum_{q=u,d,c,s,t,b} \bar{\psi}_q(i\gamma_\mu D^\mu - m_q)\psi_q. \qquad (1.1)$$

---

[1]For a pedagogical introduction to gauge theory see [1] and for a overview of the elementary particles and their phenomenology see [2].

[2]The neutrino masses here have been shown as approximately zero, however there is very strong evidence that the neutrinos have a small mass. Additionally, the quark masses listed here are in the $\overline{MS}$ scheme. All values were taken from [3], numbers in brackets are the errors on the last digits, for the e and μ they are negligible. Unless otherwise stated all measured properties (masses, charges, etc.) have been taken from [3].

Particle	Generation	Mass MeV	Charge (e)
electron (e)	1	0.5110	1
electron neutrino (ν_e)	1	≈ 0	0
up quark (u)	1	3.0(1.5)	2/3
down quark (d)	1	6.75(1.75)	$-1/3$
muon (μ)	2	105.7	1
muon neutrino (ν_μ)	2	≈ 0	0
charm quark (c)	2	1200(200)	2/3
strange quark (s)	2	117.5(37.5)	$-1/3$
tau (τ)	3	1776.99(29)	1
tau neutrino (ν_τ)	3	≈ 0	0
top quark (t)	3	174300(5100)	2/3
bottom quark (b)	3	4250(250)	$-1/3$

Table 1.1: The Matter Particles

The notation here is standard and is explained in any introduction to quantum field theory (we're following the conventions of [1]). There are 8 gluon fields A_μ^a with the standard field strength tensor

$$F_{\mu\nu}^a = \partial_\mu A_\nu^a - \partial_\nu A_\mu^a + g f^{abc} A_\mu^b A_\nu^c, \qquad (1.2)$$

and gauge covariant derivative

$$D_\mu = \partial_\mu - i g A_\mu^a T^a. \qquad (1.3)$$

The sum over q is for all six flavours of quark. Using this Lagrangian we can compute the action $S = \int d^4x \mathcal{L}$, and from that compute vacuum expectation values of operators by path integrating

$$\langle \hat{\mathcal{O}}[A, \bar{q}, q] \rangle = \frac{\int DA Dq D\bar{q} \mathcal{O}[A, \bar{q}, q] e^{-iS}}{\int DA Dq D\bar{q} e^{-iS}}. \qquad (1.4)$$

From these expectation values the physical predictions of the theory can be extracted.

For our purposes, the most important thing about QCD is that at low energies the coupling constant, g, is very large and at high energies it's very small. Above energies of about 1 GeV the decrease of the coupling constant can be computed perturbatively. At leading order we have

$$\alpha_s(E^2) = \frac{g^2(E^2)}{4\pi} = \frac{4\pi}{\left(11 - \frac{2}{3} n_f\right) \log\left(\frac{E^2}{\Lambda_{QCD}^2}\right)}, \qquad (1.5)$$

where n_f is the number of quark flavours with $m_q < E$, and Λ_{QCD} is a parameter which depends on n_f. For $n_f = 5$ we have $\Lambda_{QCD} \approx 400$ MeV. Notice that Λ_{QCD} takes the place of the coupling constant in the list of things that need to be fixed from experiment.

The leading order formula for α_s indicates that around $E = 2.25 \Lambda_{QCD} \approx 1$ GeV the coupling constant becomes $\mathcal{O}(1)$ and at $E = \Lambda_{QCD}$ it diverges. This indicates that the energy scale Λ_{QCD} is the rough marker of where QCD perturbation theory,

including the above equation, can be applied. If $E > (\text{few})\Lambda_{QCD}$ then we can use perturbation theory, otherwise we need to look for alternative approaches. Using the conversion factor $\hbar c \approx 200$ MeV fm we can convert the energy scale to a distance. We find that QCD perturbation theory should be useful on scales shorter than about 0.3 fm, at longer distances we need non-perturbative methods. We discuss below that many important experiments require as input predictions from the long distance, non-perturbative, sector of the theory.

1.2 Fundamental parameters of the SM

The electroweak sector of the standard model is considerably more complicated than the QCD part. We will not review it in detail here as we will only be concerned with its most basic properties. Briefly, the electroweak theory is an $SU(2) \times U(1)$ gauge theory. The gauge group is spontaneously broken to $U(1)$ via the Higgs mechanism. The exact form of the Higgs sector has not been determined experimentally, a single real scalar field is the most economic solution.

The symmetry breaking gives mass to three of the four gauge bosons in the unbroken theory. The boson that remains massless is the familiar photon, the massive bosons are the $W^{\pm}$ (mass 80.425(38) GeV) and the Z^0 (mass 91.1876(21) GeV). Of these we will be concerned with the interaction of the W bosons.

The W bosons are very interesting because they change the flavour of the particles they interact with. For example, in the decay of a μ, the μ emits a W^- turning into a ν_{μ}. The (virtual) W then decays into an e and a ν_e. This is illustrated in figure 1.1.

Applying the Feynman rules for the electroweak theory to this decay gives the amplitude for this process (in unitary gauge)

$$\mathcal{M} = \frac{g_w^2}{8} J_{\mu}^{\sigma} \frac{g_{\sigma v} - \frac{q_{\sigma} q_v}{M_W^2}}{q^2 - M_W^2} J_e^v. \tag{1.6}$$

Here $J_{\mu}^{\sigma} = \bar{u}(p_{\nu_{\mu}}) \gamma^{\sigma} u(p_{\mu})$ is the muon weak current, $J_e^v = \bar{u}(p_e) \gamma^v v(p_{\bar{\nu}_e})$ is the
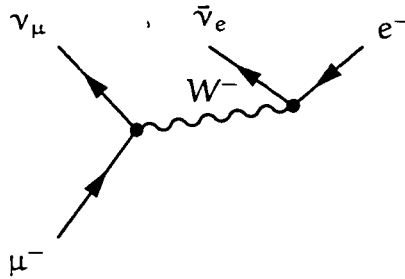
Figure 1.1: The lowest order Feynman diagram for muon decay in the full electroweak theory

electron weak current, and g_w is the weak interaction coupling constant. The momentum transfer (in the muon rest frame) for this process is $q^2 = m_\mu^2 - m_\mu E_{\nu_\mu} < m_\mu^2 \ll M_W^2$. Neglecting the q terms give

$$\mathcal{M} = \frac{G_F}{\sqrt{2}} J_\mu^\nu J_{e,\nu},$$ (1.7)

where we have set $G_F = \frac{\sqrt{2} g_w^2}{8 M_W^2}$. In this form this is the same as the result from the early Fermi theory of β decay [4]. In this theory the W boson is replaced by a four fermion contact interaction. At low energies ($E \ll M_W$) it is an excellent approximation. For the remainder of this discussion we will use this "four-fermion" form.

Quarks have similar interactions with the W bosons. For example, a d quark inside a neutron can decay into a u quark, electron and (electron) antineutrino as shown in figure 1.2. The amplitude for this process will be the same as that for muon decay (1.7) except the weak coupling for the quark current has a different strength, which we will call $V_{ud} g_w$. The net effect is that the amplitude for this process is (1.7), multiplied by V_{ud}. In an exactly analogous way we could consider $c \to s + \ell + \bar{\nu}_\ell$ and $t \to b + \ell + \bar{\nu}_\ell$ decays. We would get extra factors V_{cs} and V_{tb} in each case. Like all couplings, these are fundamental parameters of the standard model, and need to be fixed by experiments.

The situation is actually more complicated than this. The three "V" parameters we've seen so far only couple quarks of the same generation. However, the structure
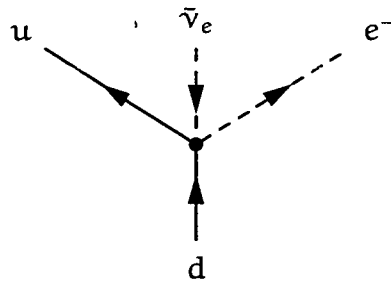
Figure 1.2: The lowest order Feynman diagram for $d \to u + e + \bar{\nu}_e$ in decay in the Fermi effective theory.

of the electroweak theory allows for decays across generations. For example, we can have $s \to u$ decays. All of the couplings are arranged in the Cabibbo–Kobayashi–Maskawa [5],[6] (CKM) matrix,

$$V_{CKM} = \begin{pmatrix} V_{ud} & V_{us} & V_{ub} \\ V_{cd} & V_{cs} & V_{cb} \\ V_{td} & V_{ts} & V_{tb} \end{pmatrix}. \tag{1.8}$$

This matrix appears in the Lagrangian for the standard model, so it must be unitary. This restriction means we can describe this matrix by four parameters, three real angles, and one complex phase. Ignoring the phase, the current world average for the amplitude of this matrix is

$$|V_{CKM}| = \begin{pmatrix} 0.9741 \text{ to } 0.9756 & 0.219 \text{ to } 0.226 & 0.0025 \text{ to } 0.0048 \\ 0.219 \text{ to } 0.226 & 0.9732 \text{ to } 0.9748 & 0.038 \text{ to } 0.044 \\ 0.004 \text{ to } 0.014 & 0.037 \text{ to } 0.044 & 0.9990 \text{ to } 0.9992 \end{pmatrix}. \tag{1.9}$$

There is an obvious pattern to these magnitudes, the diagonals are close to 1, with the off diagonals falling off quickly. A parametrization that takes this into account is the Wolfenstein parametrization [7]

$$V_{CKM} = \begin{pmatrix} 1 - \frac{\lambda^2}{2} & \lambda & A\lambda^3(\rho - i\eta) \\ -\lambda & 1 - \frac{\lambda^2}{2} & A\lambda^2 \\ A\lambda^3(1 - \rho - i\eta) & -A\lambda^2 & 1 \end{pmatrix} + \mathcal{O}(\lambda^4). \tag{1.10}$$

In keeping with the measured values we expect, $\lambda \ll 1$. The other parameters A, ρ and η are $\mathcal{O}(1)$.

These parameters are very important, they are fundamental SM quantities. Without precise knowledge of them many SM predictions have large errors. Related to this, but perhaps of even more interest, is that without good knowledge of these parameters it will be difficult to understand if a measurement has revealed new physics beyond the standard model. So one of the primary goals in contemporary high-energy phenomenology is to understand how these parameters can be accurately extracted from experiments.

1.3 Strong Matrix Elements

The trouble in precisely determining the CKM parameters is not with the electroweak theory. For many processes the lowest order effective Fermi theory would be enough. If not, there is the full theory, and the weak coupling constant g_w is small, so corrections can be computed perturbatively. The trouble is in computing the QCD contribution.

For example, let's consider one of the simplest decays, the purely leptonic decay of a pseudo-scalar meson, P_{Qq} which contains one "heavy" quark Q, and a "light" anti-quark $\bar{q}$ with initial four momentum p. The following analysis actually applies to any pseudo-scalar meson, however later on we will be specifically dealing with heavy–light mesons, so we introduce the notation and language here. This sort of meson can decay into a lepton and antineutrino. Naively this takes place via the diagram of figure 1.3. However, there is a problem with this. Figure 1.3 shows the amplitude $\langle \ell \bar{\nu}_\ell | \hat{V} | Q\bar{q} \rangle$ where Q and q are being treated as free quarks. This is not the case, the quarks are strongly interacting so the external quark lines are dressed by the strong interactions. The situation is even more complicated since the quarks are bound in the meson we really want $\langle \ell \bar{\nu}_\ell | \hat{V} | P_{Qq}(p) \rangle$. The former amplitude neglects the bound state properties of the quarks, which are permanently
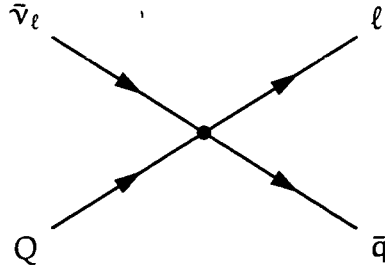
Figure 1.3: The lowest order Feynman diagram for $Q + \bar{q} \to \ell + \bar{\nu}_\ell$

confined within the meson.

The weak interaction operator in this case is the four fermion interaction

$$\hat{V} = \left[\hat{\bar{\ell}} \gamma_\mu (1 - \gamma^5) \hat{\nu}_\ell \right]^* V_{qQ} \sqrt{2} G_F \left[\hat{\bar{q}} \gamma_\mu (1 - \gamma^5) \hat{Q} \right]. \tag{1.11}$$

Since the initial state has negative parity this reduces to

$$\hat{V} = -\sqrt{2} V_{qQ} G_F \hat{J}_\ell^\mu \left[\hat{\bar{q}} \gamma_\mu \gamma^5 \hat{Q} \right]. \tag{1.12}$$

We've set

$$\hat{J}_\ell^\mu = \left[\hat{\bar{\ell}} \gamma_\mu (1 - \gamma^5) \hat{\nu}_\ell \right]$$

here. To compute $\langle \ell \bar{\nu}_\ell | \hat{V} | P_{Qq}(p) \rangle$ we insert a complete set of states, and note that

$$\langle \ell \bar{\nu}_\ell | \hat{J}_\ell^\mu | 0 \rangle = L^\mu$$

is the only non-zero possibility. The rules of the electroweak theory allow calculation of L^μ, we will not need its exact expression here. With this notation, we have

$$\langle \ell \bar{\nu}_\ell | \hat{V} | P_{Qq}(p) \rangle = -\sqrt{2} V_{qQ} G_F L^\mu \langle 0 | \hat{\bar{q}} \gamma_\mu \gamma^5 \hat{Q} | P_{Qq}(p) \rangle \tag{1.13}$$

as our expression for the matrix element.

We can calculate the leptonic part L_μ of equation 1.13, in principle to any order in perturbation theory. It is the hadronic part

$$\langle 0 | \hat{\bar{q}} \gamma_\mu \gamma^5 \hat{Q} | P_{Qq}(p) \rangle \tag{1.14}$$

which is hard to handle. To simplify matters somewhat, we note that the initial momentum p is the only four-vector in this hadronic matrix element. Therefore we can write

$$\langle 0|\hat{\bar{q}}\gamma_\mu\gamma^5\hat{Q}|P_{Qq}(p)\rangle = if_P p_\mu \tag{1.15}$$

with f_P a constant, known as the pseudo-scalar meson decay constant (the i is conventional, and ensures that f_P will be real). With this notation we have the final expression

$$\langle \ell\bar{\nu}_\ell|\hat{V}|P_{Qq}(p)\rangle = -i\sqrt{2}V_{qQ}f_P G_F L^\mu p_\mu. \tag{1.16}$$

Squaring this expression, and integrating over the final state phase space gives the decay rate for the P meson

$$\Gamma(P_{Qq} \to \ell\bar{\nu}_\ell) = |V_{qQ}|^2 f_P^2 \left[\frac{G_F^2 m_\ell^2 m_P}{8\pi} \left(1 - \frac{m_\ell^2}{m_P^2}\right)^2 \right]. \tag{1.17}$$

Everything in square brackets has only small, calculable, perturbative corrections.

The problem is now clear, even assuming that we have an accurate measurement of the decay rate (not always an easy thing to measure) we still cannot determine $|V_{qQ}|$ since it is multiplied by the unknown constant f_P.

This problem is not specific to purely leptonic decays either. For example, in the semi-leptonic decay $P_{Qq} \to P'_{Q'q} + \ell + \bar{\nu}_\ell$ the CKM element $|V_{QQ'}|$ comes out multiplied by a function f of the momentum transfer q which is related to the strong interaction matrix element

$$\langle P'(p')|\gamma^\mu|P(p)\rangle \propto f(q^2)(p' + p)^\mu. \tag{1.18}$$

Even with accurate measurements of the decay rates, without reliable calculations of these matrix elements the fundamental CKM parameters cannot be extracted.

The strong interaction matrix elements required to fully predict these processes cannot, in general, be computed with perturbative QCD. The reason is that the meson state $|P\rangle$ is a bound state. Bound states are non-perturbative in nature, so even if the coupling were weak we would need non-perturbative methods to

determine the matrix elements we need. This is not to say the QCD perturbation theory is not useful. Perturbative QCD effects can be important, however, the experiments work with mesons and baryons, so we need to understand how the quarks are bound, and how to compute the bound state matrix elements.

1.4 Lattice QCD

There are a number of ways to attack the problem of determining what the QCD matrix elements are. The problem that has plagued them all has been that none give high precision results for a broad range of QCD processes.

For example, it is relatively straightforward to build models inspired by QCD and make predictions (see [8] for one example and references to many more) but, as these models have large and mostly uncontrolled systematic errors they rarely give results that have better than 10% precision. Most other methods have similar limitations, all of which essentially stem from the fact that they are not reliable ways to compute low energy QCD matrix elements.

What is needed then is a way of computing directly from QCD the quantities we want, using some sort of controlled approximation. This would allow for calculations to be done with small errors. Furthermore, the systematic errors should be understood, and a means of reducing them must be available. These two features are absolutely crucial to the larger high-energy physics community: they want numbers with errors that are low, well understood and that can be trusted. Such an approximation has actually been known for close to thirty years. It is Wilson's formulation of QCD on a finite lattice [9].

Wilson's idea was to discretize a volume of space-time, turning it into a hypercubic lattice with grid spacing a and total volume L^4. A two-dimensional example of this is shown in figure 1.4. This has the advantage of turning a problem with an infinite number of variables into one with a finite number. This opens up the possibility of numerically evaluating the path integral.
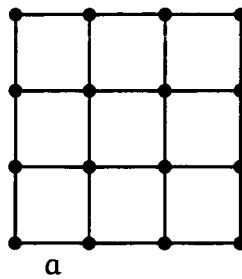
Figure 1.4: A two dimensional lattice

A technical note: QCD is described by a path integral in Minkowski space

$$\mathcal{Z} = \int D \, [\text{fields}] \, e^{iS}. \qquad (1.19)$$

If we wanted to evaluate this numerically we'd run into serious problems, due to the oscillating exponential. This makes numerical integration very difficult. It's much easier to Wick rotate into four dimensional Euclidean space, this takes $S \to iS$ which gives an exponential damping

$$\mathcal{Z} = \int D \, [\text{fields}] \, e^{-S}. \qquad (1.20)$$

This is the formalism we will use for the remainder of this report. Henceforth, unless otherwise noted, all fields, coordinate and momenta will be Euclidean. Minkowski space results can still be extracted from lattice theories. For example, the fourth component of the lattice momentum p_4 is $p_4 = iE(\vec{p})$, where E is the Minkowski space energy. Masses can be extracted by determining this energy at zero three-momentum.

Obviously, putting a continuum theory on a lattice will break the four dimensional Euclidean symmetry which will introduce errors into numerical results. Breaking this symmetry is unavoidable, however it is not a fundamental concern as it is naturally restored in the $a \to 0$ limit. QCD has other symmetries which are important. The most important is gauge symmetry. If we break it, a large number of couplings have to be fine-tuned in order to recover gauge symmetry to the desired approximation in the continuum limit. Fortunately Wilson's formulation of

Lattice QCD preserves gauge invariance.

1.4.1 Gauge Fields on the Lattice

The key to Wilson's action for the gauge fields is to use group elements of $SU(3)$ rather than the Lie algebra elements. The group elements have a natural interpretation in terms of directed paths. Thus, to each link of the lattice we assign a group element $U_\mu(x)$. Pictorially this is

$$U_\mu(x) = \quad x \bullet\!\!\xrightarrow{\hat{\mu}}\!\!\bullet (x + a\hat{\mu}). \tag{1.21}$$

Under an $SU(3)$ transformation $S(x)$ we have $U(x) \rightarrow S(x)U_\mu(x)S^\dagger(x + a\hat{\mu})$. To build up a gauge invariant operator, we can consider the trace of any product of links forming a closed curve.

Consider the shortest such path, a 1×1 square, or plaquette,

$$U_\mu(x)U_\nu(x + a\hat{\mu})U_\mu^\dagger(x + a\hat{\nu})U_\nu^\dagger(x). \tag{1.22}$$

Under a local $SU(3)$ transformation we have,

$$S(x)U_\mu(x)S^\dagger(x + a\hat{\mu})S(x + a\hat{\mu})U_\nu(x + a\hat{\mu})S^\dagger(x + a\hat{\mu} + a\hat{\nu})$$
$$\times S(x + a\hat{\nu})U_\mu^\dagger(x + a\hat{\nu})S^\dagger(x + a\hat{\mu})S(x + a\hat{\mu})U_\nu^\dagger(x)S^\dagger(x). \tag{1.23}$$

Using $S^\dagger(x)S(x) = 1$ this becomes,

$$S(x)U_\mu(x)U_\nu(x + a\hat{\mu})U_\mu^\dagger(x + a\hat{\nu})U_\nu^\dagger(x)S^\dagger(x). \tag{1.24}$$

Taking the trace of this, and permuting the end link around to the front cancels the last gauge variant part. It is clear that this procedure will hold for the trace of any more general closed curve.

We can use these objects to build up an action for the group elements. The simplest thing to do is use the plaquette operator

$$P_{\mu\nu} = \frac{1}{3}\text{ReTr}\left[U_\mu(x)U_\nu(x + a\hat{\mu})U_\mu^\dagger(x + a\hat{\nu})U_\nu^\dagger(x)\right] \tag{1.25}$$

to construct an action for the gauge group elements

$$S_W = \beta \sum_x \sum_{\mu < \nu} [1 - P_{\mu\nu}].$$ (1.26)

This action was first constructed by Wilson [9] and is known as the Wilson gauge action. We expect that the constant β will be related to the QCD coupling g.

To determine the nature of this relationship we will look at the small a expansion of the Wilson action. We want to recover the limit where we can neglect the extremely short distance effects associated with the lattice spacing. Introduce the elements of the Lie algebra $su(3)$, $A_\mu(x)$, with the standard connection between group and algebra elements

$$U_\mu(x) = e^{iga A_\mu(x)}.$$ (1.27)

Expanding to $\mathcal{O}(a^6)$, and using $\text{Tr}[A_\mu] = 0$, we find

$$P_{\mu\nu} = 1 - \frac{a^4}{6}\text{Tr}\left[g^2 F^{\mu\nu}F_{\mu\nu}\right] + \mathcal{O}(a^6).$$ (1.28)

If we set $\beta - 6/g^2$ we recover the continuum action up to spacing errors,

$$S_W = -\frac{1}{2}\int dx \text{Tr}[F_{\mu\nu}F^{\mu\nu}] + \mathcal{O}(a^2),$$ (1.29)

where we have used,

$$a^4 \sum_x \to \int dx \quad \text{and} \quad \sum_{\mu<\nu} = \frac{1}{2}\sum_{\mu,\nu}.$$ (1.30)

From the preceding formulas it is clear that powers of the lattice spacing clutter things up. To simplify the notation we will henceforth use units where $a = 1$ unless otherwise noted.

1.4.2 Fermions on the lattice

Naively putting fermions on the lattice should be straightforward. The fermion fields transform as $\psi(x) \to S(x)\psi(x)$ so the mass term $\bar{\psi}(x)\psi(x)$ is automatically

gauge invariant[3]. The term,

$$\bar{\psi}(x)U_\mu(x)\psi(x+\hat{\mu})$$

is also gauge invariant. We can use this sort of operator to construct a gauge invariant kinetic term,

$$\bar{\psi}(x)D_\mu\psi(x) = \frac{1}{2}\left(\bar{\psi}(x)U_\mu(x)\psi(x+\hat{\mu}) - \bar{\psi}(x)U_\mu^\dagger(x-\hat{\mu})\psi(x-\hat{\mu})\right). \qquad (1.31)$$

With these two operators we propose the following fermion action

$$S_N = \sum_x \bar{\psi}(x)\left(\gamma^\mu D_\mu + m\right)\psi(x). \qquad (1.32)$$

This is known as the naive fermion action. In the $a \to 0$ limit it reproduces the continuum (Dirac) action with $\mathcal{O}(a^2)$ errors.

The naive fermion action has a very unfortunate property that limits its usefulness for numerical work. To see this problem we consider the weak coupling limit, $g \to 0$, which means we can take $U_\mu(x) = 1$. This gives,

$$S_N \approx \sum_x \left[\sum_{\mu=1}^4 \frac{\left(\bar{\psi}(x)\gamma^\mu\psi(x+\hat{\mu}) - \bar{\psi}(x)\gamma^\mu\psi(x-\hat{\mu})\right)}{2} + m\bar{\psi}(x)\psi(x)\right]. \qquad (1.33)$$

Going to momentum space this becomes, with $\bar{p}_\mu = \sin(p_\mu a)$,

$$S_N = \frac{1}{L^4}\sum_p \bar{\psi}(-p)\left[i\gamma^\mu\bar{p}_\mu + m\right]\psi(p). \qquad (1.34)$$

From equation 1.34 we can read off the momentum space propagator

$$S(p) = \frac{-i\gamma_\mu\bar{p}^\mu + m}{\bar{p}^2 + m^2}. \qquad (1.35)$$

The mass shell for these fermions is given by solving

$$\sin(p_4) = im. \qquad (1.36)$$

---

[3]Recall that $\bar{\psi} = \psi^\dagger\gamma_0$.

Naively, this has the solution $p_4 = \sin^{-1}(im)$ which in the continuum limit gives $p_4 = im$, the correct Euclidean mass shell. The problem is that (restoring the lattice spacing)

$$p_4 a = \sin^{-1}(ima) + \pi \tag{1.37}$$

is also a solution. Thus a lattice quark with *high* energy close to the cutoff π/a will become a low energy quark, nearly at rest, in the continuum limit. This is clearly a big problem, as numerical simulations will give 16 degenerate types (or "tastes") of quarks. There are few ways of dealing with this problem. We will outline one of them here, and touch on another in the next section.

The most straightforward solution to this problem is to add an irrelevant operator to the quark action, which modifies the small a behavior of the "doubler" quarks. An operator which does this is the lattice Laplacian

$$\triangle\psi(x) = \sum_{\mu=1}^{4} \left(U_\mu(x)\psi(x+\hat{\mu}) + U_\mu^\dagger(x-\hat{\mu})\psi(x-\hat{\mu}) - 2\psi(x) \right). \tag{1.38}$$

We add this into the action, with an arbitrary coefficient r,

$$S_{W_q} = \sum_x \bar{\psi}(x) \left(\gamma^\mu D_\mu - \frac{ar}{2}\triangle + m\bar{\psi}(x) \right)\psi(x). \tag{1.39}$$

This changes the mass shell condition to (again restoring a)

$$\sin^2(p_4 a) + \left[ma + 2r\sin^2\left(\frac{p_4 a}{2}\right) \right]. \tag{1.40}$$

In this case $p_4 a = \sin^{-1}(ima)$ gives the correct continuum limit but, due to the $\sin(p/2)$ term, $p_4 a = \sin^{-1}(ima) + \pi$ is no longer a solution. This solves the fermion doubler problem by driving the energy of the doublers up near the cutoff.

This solution to the doubling problem was first proposed by Wilson [10]. It is widely used in the lattice field theory community. It does suffer from two serious drawbacks. First, the Laplacian operator is dimension five. This introduces a $\mathcal{O}(a)$ error, whereas the naive action had $\mathcal{O}(a^2)$ errors. Furthermore, and more seriously, the Wilson action does not have the chiral symmetry that QCD exhibits in the

limit of massless quarks. This means that fermion masses receive large additive mass renormalization and calculating any quantity which is sensitive to the chiral properties of QCD is very difficult.

Full QCD

We can put these two actions together into a full approximate action for QCD,

$$S = S_W + \sum_q S_{W_q}. \qquad (1.41)$$

This action reproduces full QCD up to linear errors in the spacing. We can use this to evaluate QCD matrix elements. For example,

$$\langle 0|Q\gamma^\mu \bar{q}|P_{Qq}\rangle = \langle 0|Q\gamma^\mu \bar{q}Q\bar{q}|0\rangle = \int DU D\psi D\bar{\psi} Q\gamma^\mu \bar{q}Q\bar{q}e^{-S}. \qquad (1.42)$$

In principle there are a finite number of integrals, so one could just do them all. However, even on a moderately sized lattice there are too many integrals to evaluate. Fortunately the weighting e^{-S} makes these path integrals amenable to Monte Carlo methods.

1.4.3 Dynamical Fermions

The techniques of Monte Carlo simulations are not the direct subject of this report. We are more concerned with the errors that they report. As we have discussed above, we would like to have small errors for QCD matrix elements. Before discussing small, controllable errors we have to address the one approximation in lattice QCD that does not meet the controlled criteria: the quenched approximation.

Fermionic variables cannot be represented in a computer so we have to find another way to deal with the fermion integral. This is not hard to do, at least conceptually. We can write the Wilson quark action as

$$S = \bar{\psi}(x)\mathcal{M}[U]\psi(x) \qquad (1.43)$$

where $\mathcal{M}$ has the derivative and mass operators, which depend on U. This action is bilinear in the quark fields, so we can integrate them out,

$$\int D\bar{\psi}D\psi e^{-S_{W_q}} = \det(\mathcal{M}[U]).$$

(1.44)

Therefore the general path integral can be represented as

$$\mathcal{Z} = \int DU \det(\mathcal{M}[U]) e^{-S_W}.$$

(1.45)

This allows us to use purely gluonic variables in the computer. To compute matrix elements involving quarks we can use the propagator formula

$$S_F = \mathcal{M}^{-1}[U].$$

(1.46)

The trouble is that the fermionic matrix $\mathcal{M}[U]$ is very large and sparse. This makes it computationally very expensive to invert. In the past many people doing large scale Monte Carlo simulations would simply set $\det \mathcal{M} = 1$, neglecting the dynamical quarks altogether. This is known as the quenched approximation.

For many years computing power was such that there was no way to avoid the quenched approximation. In spite of this rather extreme approximation, many interesting results were obtained with quenched simulations. However, even the best quenched results contained uncontrolled, and often not well understood, systematic errors. This means that lattice QCD results could not provide the high precision QCD results needed to understand experiments.

Fortunately the quenched approximation is going away. Modern teraflop scale computers are allowing high statistics results for unquenched simulations. With this source of error being removed it is even more important to look at other sources of systematic errors, and how to control them.

One technical detail worth pointing out here is that one of the main reasons that unquenched simulations are becoming more feasible is the use of so-called improved staggered (or AsqTad) fermions introduced in [11]. In the interests of completeness we give an outline of how one constructs a staggered quark action. In chapter 2 we will discuss the improvement.

We begin with the naive fermion action

$$S_N = \sum_x \bar{\psi}(x) \left(\gamma^\mu D_\mu + m \right) \psi(x). \tag{1.47}$$

As we discussed above, this action describes 16 different tastes of quark. One way to get rid of these extra tastes is to introduce a Laplacian term as we did previously, and another is to "stagger" the fermions. This means we spin diagonalize the naive fermion action. This is accomplished via the transformation

$$\psi(x) = T(x)\chi(x), \quad \bar{\psi}(x) = \bar{\chi}(x)T^\dagger(x), \tag{1.48}$$

where we demand that

$$T^\dagger(x)\gamma_\mu T(x+\hat{\mu}) = \eta_\mu(x)I. \tag{1.49}$$

This transformation will produce an action diagonal in the spin indices.

A explicit matrix that implements (1.49) is

$$T(x) = \gamma_1^{x_1} \gamma_2^{x_2} \gamma_3^{x_3} \gamma_4^{x_4}. \tag{1.50}$$

With this choice the factor $\eta(x)$ is

$$\eta_\mu(x) = (-1)^{x_1 + \cdots + x_{\mu-1}}, \quad \eta_1(x) = 1. \tag{1.51}$$

Implementing this transforms the naive fermion action to

$$S_N = \sum_x \sum_{\alpha=1}^4 \bar{\chi}_\alpha(x) \left(\eta_\mu(x)D^\mu + m \right) \chi_\alpha(x), \tag{1.52}$$

where we've shown the sum over the single spin index. It's clear that in this form the naive fermion action is just four copies of the same thing; each term in the sum over α is identical. This suggests that we can "stagger" the fermions by simply dropping the sum over α.

Dropping the sum over α gives the unimproved staggered quark action

$$S_{St} = \sum_x \bar{\chi}(x) \left(\eta_\mu(x)D^\mu + m \right) \chi(x). \tag{1.53}$$

This action will describe four tastes of quarks, rather than sixteen. There are techniques which can be used to define an effective number of flavours, and hence to further reduce taste doubling, but we will not discuss them here.

Recall that for the Wilson fermion action we introduced a term $\bar{\psi}\triangle\psi$ to the action which removed the doublers. However, such a term breaks the chiral symmetry of QCD, leading to large additive mass renormalizations. This greatly slows down matrix inversions, as the large renormalizations introduce unphysical "exceptional" configurations.

The staggered formalism has a remnant chiral symmetry, which protects against any additive mass renormalizations. This greatly speeds up the matrix inversions. A further factor in favour of staggered fermions is that they have 1/4 the number of spin degrees of freedom, resulting in a smaller matrix to invert. Overall, the savings from these fermions are a factor of 20 or more [12].

1.4.4 HPQCD

With the quenched approximation going away there is a tremendous opportunity for lattice QCD to make a major impact on the experimental high-energy physics program. If lattice QCD is to be relevant to experimentalists, we need to deliver results with low errors that are under control.

This is the goal of the High Precision QCD (HPQCD) collaboration. A loose collaboration of researchers from North America and the UK, HPQCD seeks to apply the many innovations in lattice QCD developed over the last ten years to quantities of interest to the broader high-energy physics community.

In order to do this, we need to make use of highly improved actions in order to reduce the lattice spacing errors which dominate. The following two chapters outline the technical details behind the perturbative improvement program. These techniques, and the calculations performed with them, are absolutely crucial to this program.

Given the size of the HPQCD collaboration and the number of authors listed

on its papers, it is appropriate to emphasize that the work presented here was performed by the author, under the supervision of Howard Trottier. The calculations of various link operators, presented in chapter 4, and the matching calculations in chapter 6 represent the author's original contributions to the multi-authored works of HPQCD. These calculations have impacted on several of HPQCD's papers (perturbation theory for Wilson loops [13], improved staggered quark action [14], and the determination of α_s [15]).

Chapter 2

Improving Lattice QCD

The current experimental situation requires precision lattice calculations in order to extract standard model parameters, or resolve possible signals of new physics. Despite many impressive successes (for example, the calculation of the light hadron spectrum in the quenched approximation [16]) the lattice QCD community has not delivered the precision calculations that are needed.

There are a number of reasons for this. The first is that, until recently the cost of doing unquenched simulations was prohibitively expensive. With modern computers, removing the quenched approximation is now possible. The MILC collaboration [17] has generated large numbers of gauge field configurations with light dynamical quarks, removing this major source of lattice errors.

In fact, the removal of the quenched approximation is particularly important since it removes an *uncontrolled* systematic error from lattice results. With this error removed we can investigate the remaining, controllable, errors in lattice calculations, and try to find ways of reducing them.

2.1   Errors in Lattice QCD Simulations

Lattice QCD simulations use Monte-Carlo methods, so there are unavoidable statistical errors associated with them. These errors are well understood and, with

modern computers, generating sufficient statistics is not usually the major source of error.

Another source of error, which plagues both quenched and unquenched simulations, is quark mass errors. These stem from the need to invert the lattice Dirac operator $\gamma \cdot D + m$ (or some modification of it, like addition of the Laplacian term). As m goes to zero (which is the limit we want to consider for up and down quarks) the algorithms for inverting this matrix critically slow down. There is a well-known "wall" at which simulation with lower m_q becomes effectively impossible. In order to circumvent this problem, simulations must be done at unphysical quark masses, and extrapolated to the physical limit.

These extrapolations can introduce large errors. Often, simple polynomial extrapolations are not adequate. The $m \to 0$ limit of QCD is described by chiral perturbation theory [18] (χPT). Often these chiral expansions have non-analytic terms, for example the tree level χPT prediction for the pion mass is $m_\pi \propto \sqrt{m_u + m_d}$, and the one loop χPT correction to the pseudoscalar B meson decay constant contains a term that is logarithmic in the quark mass. These types of terms can substantially alter the extrapolation at small quark masses [19].

Ideally one would like to do lattice simulations at quark masses that are in the region where chiral perturbation theory is applicable and reliable. Most lattice simulations are probably not in this region [20] however the MILC collaboration has simulated at sea quark masses three to five times smaller than the strange quark mass, and reports reliable chiral extrapolations [17]. There are other technical issues with chiral extrapolations beyond the scope of this report [21], [22].

2.1.1   Spacing Errors

The dominant errors in most modern lattice simulations are the errors associated with the finite lattice spacing (a). The Wilson actions we outlined in chapter 1 have $\mathcal{O}(a)$ errors for the quarks and $\mathcal{O}(a^2)$ errors for the gluons. Of course, simulations can be run at multiple values of a and extrapolations performed, but the errors are

still large.

The obvious solution to this problem is to simply run at smaller values of the lattice spacing. This is, unfortunately, not feasible. The number of points that are needed to simulate on an L^4 lattice is $\frac{L^4}{a^4}$ so naively, one would expect that the computer time needed would scale as a^{-4}. This is not the case. The Monte-Carlo simulation routines used to generate gauge field configurations critically slow down for small a. For this reason the computer time scales at least as a^{-6} instead of a^{-4}. This limitation exceeds what would allow for a reasonable time to wait for brute force reduction of a. Of course, increases in computing power are vitally important, but they will not be enough to deliver high precision results in a timely manner.

2.2 Improvement

Fortunately there is another way to address this problem. Rather than brute force reduction of the lattice spacing, we might look for a better discretization of the QCD action; one which has lower spacing errors to start with.

A simple example illustrates the general technique. Assume we wished to compute a numerical derivative. We might use the simple forward difference

$$\frac{df(x)}{dx} = \frac{f(x+\epsilon) - f(x)}{\epsilon} + \mathcal{O}(\epsilon), \tag{2.1}$$

but this has linear errors. For no extra cost we can use a symmetric derivative,

$$\frac{df(x)}{dx} = \frac{f(x+\epsilon) - f(x-\epsilon)}{2\epsilon} + \mathcal{O}(\epsilon^2), \tag{2.2}$$

which has quadratic errors.

The situation is similar in lattice field theory. Rather than using the simple Wilson actions presented in the chapter 1, we can use "improved" versions of actions that have lower errors. Unlike the simple numerical example this has some additional cost, but it is much faster than trying a brute force reduction.

There are many approaches to improvement, and improved actions are almost universally used in lattice simulations. The approach we will discuss in this report
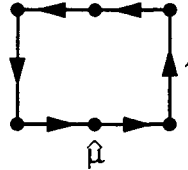
is known as Symanzik improvement [23]. For the gluon action this approach is fairly straightforward. Recall from the previous chapter that the small a expansion of the plaquette term in the Wilson action is

$$P_{\mu\nu} = 1 - \frac{a^4}{6}\text{Tr}\left[g^2 F^{\mu\nu}F_{\mu\nu}\right] + \mathcal{O}(a^6). \qquad (2.3)$$

The next term in this expansion is

$$-\frac{a^6}{72}\text{Tr}\left[gF_{\mu\nu}(D_\mu^2 + D_\nu^2)gF_{\mu\nu}\right] \qquad (2.4)$$

Now we look at the expansion of the following operator

$$R_{\mu\nu} = \quad \hat{\nu} \qquad (2.5)$$

we have

$$R_{\mu\nu} + R_{\nu\mu} = 1 - \frac{8}{6}a^4\text{Tr}\left[g^2 F^{\mu\nu}F_{\mu\nu}\right] - \frac{20}{72}a^6\text{Tr}\left[gF_{\mu\nu}(D_\mu^2 + D_\nu^2)gF_{\mu\nu}\right] + \mathcal{O}(a^8). \quad (2.6)$$

If we take,

$$\mathcal{L} = \frac{5}{3}(1 - P_{\mu\nu}) - \frac{1}{12}[1 - (R_{\mu\nu} + R_{\nu\mu})] \qquad (2.7)$$

we recover the continuum action up to $\mathcal{O}(a^4)$ errors. By adding a new operator into the action we have managed to subtract out the $\mathcal{O}(a^2)$ error. The computational cost of this improvement is orders of magnitude lower than brute force reduction of the lattice spacing [24].

2.2.1 Symanzik Improvement of the Wilson Quark Action

Recall the Wilson gluon action

$$S = \sum_x \bar{\psi}(x)\left(m_0 + \gamma_\mu D^\mu - \frac{r}{2}\Delta\right)\psi(x). \qquad (2.8)$$

The Laplacian term, needed to solve the fermion doubling problem, induces an $\mathcal{O}(a)$ error. We would like to cancel this error by adding another operator to the

action. Noting that the Laplacian operator has dimension five, we look for another dimension five operator. There is only one,

$$\mathcal{O} = \bar{\psi}\sigma_{\mu\nu}F^{\mu\nu}\psi.$$

Here $F^{\mu\nu}$ is a lattice approximant to the continuum field strength tensor. We use the clover approximation

$$F_{\mu\nu} = \frac{1}{8}\sum_{\bar{\mu}=\pm\mu, \bar{\nu}=\pm\nu} \text{sign}(\bar{\mu}\bar{\nu})U_{\bar{\mu}}U_{\bar{\nu}}U_{\bar{\mu}}^{\dagger}U_{\bar{\nu}}^{\dagger} + \text{H.C.}$$

which is accurate to $\mathcal{O}(a^2)$.

We add this operator into the action with an arbitrary coefficient

$$S_{SW} = \sum_{x} \bar{\psi}(x)\left(m_0 + \gamma_{\mu}D^{\mu} - \frac{r}{2}\triangle + c_{SW}\sigma_{\mu\nu}F^{\mu\nu}\right)\psi(x). \tag{2.9}$$

This is known as the Sheikholeslami-Wolhert [25] or clover action. If we can determine the coefficient c_{SW} we should be able to cancel the $\mathcal{O}(a)$ errors. The problem is to determine c_{SW}.

One way of proceeding is to look at the Feynman rules generated by this action. Taking $U_{\mu} = e^{-ig a A_{\mu}}$ and expanding to first order in a we find the quark–gluon vertex for the action (2.9) is

$$\Gamma_{\mu} = -g_0 t^a \left[\gamma_{\mu} - \frac{i}{2}a(1 - c_{SW})(p + p')_{\mu}\right] + \mathcal{O}(a^2). \tag{2.10}$$

Clearly setting $c_{SW} = 1$ will ensure that this vertex agrees with the continuum one to $\mathcal{O}(a^2)$.

Of course this is not the full story, as there are further lattice spacing errors that can turn out to be uncomfortably large. As well, our determination was done in free field theory, interactions between quarks and gluons will surely modify this result. Indeed the calculation of the leading interaction effects will be one of the main focuses of this thesis. To understand these effects, it pays to think a bit more carefully about the way we determined c_{SW}.

2.3   The Physics of Improvement

In order to understand spacing errors and the improvement program better, it is instructive to consider the physical origin of the lattice spacing errors and what is accomplished by the addition of improvement operators. This discussion will make it clearer why the naive improvement considered above is not sufficient.

The discussion up to now has treated the lattice field theory as some numerical approximation to a continuum field theory. That is, we took some field theory we wanted to study and constructed some numerical approximation to it. This is of course a correct point of view, but it is not the most useful one for discussing improvement.

It is far more useful to think of our lattice field theory as a continuum euclidean field theory with a hard spatial cutoff of a. That is, any field mode with wavelength less than a is simply thrown out of the theory. In momentum space this idea translates into the statement that field modes with momenta greater than $\frac{\pi}{a}$ are excluded.

In this way of thinking, lattice QCD becomes an effective field theory, one which agrees with full QCD at long distances, but disagrees on short distances. The spacing errors, from this perspective, reflect this short distance disagreement. Adding improvement operators becomes a systematic procedure, just like in any other effective field theory. There is a tower of terms, organized by some "small" expansion parameter (in this case $\Lambda_{QCD} a \approx 0.2$), and one expands to a desired order in it. Once one has these terms, they are each added to the action with a separate coefficient.

These coefficients can be fixed by matching to the full theory. In our case, we started with the Wilson quark action. It contains the dimension four operators, and this matches the low-energy, long-wavelength dispersion relation for quarks in the underlying continuum theory. In this action the Laplacian term is redundant and can be removed by a field transformation, but we keep it to solve the doubling

problem. Unfortunately it induces an $\mathcal{O}(a)$ error that can be very large.

To correct the $\mathcal{O}(a)$ error (the Λ_{QCD} is implicit) in the Wilson action we added the next set of operators from the tower. In this case, there was only one $\sigma_{\mu\nu}F^{\mu\nu}$. The coefficient was fixed by demanding that the quark-gluon vertex agree with continuum QCD. In the effective field theory view, we were really demanding that the tree level scattering of a quark off of a gluon is the same in both theories to $\mathcal{O}(a^2)$. This is best illustrated graphically. Consider quark-quark scattering off of a chromo-magnetic field, there will be tree level diagrams for both the lattice and continuum,

$$\left(\begin{array}{c} \text{diagram} \end{array} \right)_{l,c} = \text{tree}_{l,c}. \tag{2.11}$$

With $c_{SW} = 1$ our calculation above shows that

$$\text{tree}_c - \text{tree}_l = 0.$$

However there are one-loop corrections to the continuum amplitude, and the lattice amplitude. To insure that they are not mismatched we must have a one-loop contribution to c_{SW} (we'll call the one-loop part $c_{SW}^{[1]}$) such that

$$\text{one-loop}_c - \text{one-loop}_l - c_{SW}^{[1]} \times \text{tree}_l = 0.$$

Solving for $c_{SW}^{[1]}$ gives, graphically,

$$c_{SW}^{[1]} = \frac{\left(\begin{array}{c} \text{diagram} \end{array} \right)_l - \left(\begin{array}{c} \text{diagram} \end{array} \right)_c}{\left(\begin{array}{c} \text{diagram} \end{array} \right)_l}. \tag{2.12}$$

The hatched blobs represent the sum of all the one-loop corrections.

From this perspective it is easy to understand why the naive "numerical improvement" presented above doesn't work to remove all of the $\mathcal{O}(a)$ errors. We know that in QCD (or any QFT) scattering amplitudes get radiative corrections. Our simple matching didn't take these into account, so we expect that in addition to $\mathcal{O}(a^2)$ errors we will have $\mathcal{O}(\alpha_s a)$ errors. In a "typical" lattice simulation $a \approx 0.1$ fm, $\alpha_s \approx 0.2$ and $\Lambda_{QCD} \approx 300\text{MeV} = 1.5\text{fm}^{-1}$. With these parameters the error from the one-loop corrections is 0.015, comparable to the estimated $\mathcal{O}(a^2)$ errors of 0.0225. Furthermore, if we are to achieve high precision results, we really must cancel the $\mathcal{O}(a^2)$ errors as well, making it absolutely crucial to remove the one-loop errors.

The situation is actually worse than this in some cases. Owing to the nature of the lattice regulated theory there are so-called lattice tadpole graphs, which can give errors that are not suppressed by powers of a. As we shall see in chapter 3 for some quantities (such as the mean link) the leading perturbative error is really $\mathcal{O}(\alpha_s) = 0.2$. We will see how to deal with these errors later in this report.

Due to the lattice cutoff, the Feynman rules in these theories are very hard to work with. We have developed a set of tools which allow perturbative calculations to be automated. These tools, and how we use them in lattice perturbation theory, will be the subject of chapter 3.

The HPQCD collaboration has set a goal of achieving high precision results from lattice QCD. We want to compute a broad range of physical quantities with errors of a few percent. In order to do this we need all lattice spacing errors of $\mathcal{O}(a^4, \alpha^2 a^2)$. This means that we need all of the action improvement parameters to either one or two loops of perturbation theory. This requires an ambitious perturbative matching program, which is now in progress.

2.3.1 Improvement of the Staggered Quark Action

The unimproved staggered action (1.53) has large $\mathcal{O}(a^2)$ errors, so it is desirable to improve it. Such an action was constructed in [11], and is given, in the regular spin

basis, by

$$S_{\text{AsqTad}} = \sum_x \bar{\psi}(x) \left(\gamma^\mu D'_\mu - \frac{1}{6} \gamma^\mu (D_\mu)^3 + m \right) \psi(x), \qquad (2.13)$$

where

$$D'_\mu \psi(x) = \frac{1}{2u_0} \left(V'_\mu(x)\psi(x+\hat{\mu}) - V'^\dagger_\mu(x-\hat{\mu})\psi(x-\hat{\mu}) \right), \qquad (2.14)$$

$$V'_\mu(x) = V_\mu - \sum_{\rho \neq \mu} \frac{\Delta^2_\rho U_\mu(x)}{4}, \qquad (2.15)$$

$$
\begin{aligned}
\Delta^2_\rho U_\mu(x) = {} & \frac{1}{4u_0^2} \left(U_\rho(x)U_\rho(x+\hat{\rho})U_\mu(x+2\hat{\rho})U_\rho^\dagger(x+\hat{\rho}+\hat{\mu})U_\rho^\dagger(x+\hat{\mu}) \right. \\
& - 2U_\mu(x) \qquad\qquad\qquad\qquad\qquad\qquad\qquad\qquad (2.16) \\
& + \left. U_\rho^\dagger(x-\hat{\rho})U_\rho^\dagger(x-2\hat{\rho})U_\mu(x-2\hat{\rho})U_\rho(x-2\hat{\rho}+\hat{\mu})U_\rho(x-\hat{\rho}+\hat{\mu}) \right)
\end{aligned}
$$

$$V_\mu(x) = \prod_{\rho \neq \mu} \left(1 + \frac{\Delta_\rho}{4} \right)_{\text{symm}} U_\mu(x), \qquad (2.17)$$

and

$$
\begin{aligned}
\Delta_\rho U_\mu(x) = {} & \frac{1}{u_0^2} \left(U_\rho(x)U_\mu(x+\hat{\rho})U_\rho^\dagger(x+\hat{\mu}) \right. \\
& - 2u_0^2 U_\mu(x) \qquad\qquad\qquad\qquad\qquad (2.18) \\
& + \left. U_\rho^\dagger(x-\hat{\rho})U_\mu(x-\hat{\rho})U_\rho(x-\hat{\rho}+\hat{\mu}) \right).
\end{aligned}
$$

Here u_0 is a mean field improvement factor, which will be discussed at length in chapter 3. This action has errors of $\mathcal{O}(a^4, \alpha_s a^2)$.

2.3.2 Other uses of lattice perturbation theory

Beyond matching of action parameters, there are many other uses of lattice perturbation theory. We discuss two relevant examples here.

Operator matching

Consider some lattice operator $\hat{O}_{\text{latt}}$, it will only agree with the continuum operator $\hat{O}_c$ up to some order in the lattice spacing. That is we will have

$$\hat{O}_{\text{latt}} = \hat{O}_c + \mathcal{O}(a^n).$$

We can make this a bit more precise. Consider the case where there is one lattice operator $\hat{O}_0$ with the same dimension as the continuum operator. There will also be a tower of operators, $\hat{O}_n$ with the same quantum numbers, but higher dimensions. These will be suppressed by powers of the lattice spacing. This allows us to write the connection between the lattice and continuum operators as (restoring the lattice spacing)

$$\hat{O}_c = Z(g,\ldots)\left\{\hat{O}_0 + \sum_n a^{d_n} C_n(g,\ldots)\hat{O}_n\right\}, \qquad (2.19)$$

where $(g,\ldots)$ indicates the dependence on all the couplings in the action, masses, the Wilson parameter r, etc, and d_n is the dimension of the operator $\hat{O}_n$. The overall factor of Z is conventional.

The situation with the currents is the same as with the action parameters. The coefficients are calculable in perturbation theory, and can be tuned to remove errors to any desired order in $\alpha^m a^n$. Often the coefficients C_n are expanded further in some mass expansion. For example, if the mass is very large, we expect that C_n will produce a set of corrections suppressed by powers of the quark mass.

Determining α_s

Another very important use for lattice perturbation theory is in determining the strong coupling constant from non-perturbative simulations. This is a three-stage procedure.

The first stage is to fix the QCD constants non-perturbatively. We need to fix the quark masses and a, the lattice spacing. This can be done by demanding that

the lattice simulation reproduce five experimental numbers. For example, we tune the light quark mass until the pion mass comes out right.

Once we know all the inputs we measure some extremely short distance quantity on the lattice. The simplest thing to do is to measure the average plaquette P. Now, the need for perturbation theory comes in. Assume we have a perturbative expansion for P,

$$P = 1 + P_1 \alpha_s(q^*) + P_2 \alpha_s^2(q^*) + \cdots$$

Since we have a measurement of the left hand side of this equation, we can solve for $\alpha_s(q^*)$. Naively we expect the scale $q^* \sim \pi/a$, that is the plaquette is evaluated at a scale near the cutoff. A precise method for determining q^* will be given in chapter 3.

Finally we can use the conversion between the lattice coupling, and the $\overline{MS}$ to get a value for $\alpha_{\overline{MS}}(\pi/a)$. This result is usually scaled up to $E = M_Z$ and compared to other determinations of α. The lattice result compares favourably with the world average. The lattice determination of α_s is particularly interesting since it involves input from both perturbative and non-perturbative calculations. The agreement between this and other methods of determining α_s is a very powerful argument in favour of QCD. Of course this whole program depends on being able to do the perturbation theory for a number of short distance quantities. We will address some of these calculations in chapter 4.

Chapter 3

Methods for lattice perturbation theory

3.1 The need for automation of bare perturbation theory

As we mentioned in chapter 2 lattice perturbation theory is technically more complicated than standard continuum perturbation theory. The reasons for this are straightforward, the breaking of four dimensional Euclidean symmetry by the lattice regulator, and the non-linear connection between the link fields U_μ and the gauge fields A_μ.

The breaking of Euclidean symmetry has a number of unfortunate effects. First, as we observed in chapter 1, the Feynman rules are trigonometric functions of the momenta, rather than polynomial ones. Clearly this makes manipulation, and simplification, more difficult. Furthermore, there are corrections to the vertices that vanish in the continuum limit, but are present in the lattice theory. These additional terms, along with the trigonometric functions, makes deriving and calculating with these large vertices very error prone. The number of terms in a vertex

is naively given by [26]

$$n_{r,\ell} = \frac{2}{(r-1)!} \ell(\ell+1)\cdots(\ell+r-1) \tag{3.1}$$

where r is the number of gluons, and ℓ is the length of the curve in the action. This formula grows very quickly. For example, the 2 gluon vertex ($r = 2$) from the Wilson plaquette action ($\ell = 4$) only has 40 terms, however the six gluon vertex from the rectangular improvement term ($\ell = 6$) has 5544 terms. We will address the problems that this growth presents below.

Another issue is the hard cutoffs of π/a on momentum integrals. This means that the traditional "textbook" tricks for loop integrals do not work. Of course, before one even thinks about evaluating the loop integrals, one must have a reliable way to generate the vertex functions.

For striking example of the troubles that these issues can cause, we look at the four gluon vertex. In the continuum theory we have

$$\begin{aligned}
\frac{i}{g^2}\Gamma^{abcd}_{\mu\nu\rho\sigma} &= f^{abe}f^{cde}(\delta_{\mu\rho}\delta_{\nu\sigma} - \delta_{\mu\sigma}\delta_{\nu\rho}) \\
&+ f^{abe}f^{cde}(\delta_{\mu\rho}\delta_{\nu\sigma} - \delta_{\mu\sigma}\delta_{\nu\rho}) \\
&+ f^{abe}f^{cde}(\delta_{\mu\rho}\delta_{\nu\sigma} - \delta_{\mu\sigma}\delta_{\nu\rho}).
\end{aligned}$$

This is already a rather complicated expression. If we derive the four gluon vertex from the Wilson gauge action, we get the result shown in figure 3.1 (used with permission from [27]). Notice that the vertex is much more complicated than the continuum version, and this is just the simplest gauge action. Other actions, such as the improved gauge action, would generate rules that would fill many pages. The need for some more automatic method of dealing with such expressions is hinted at in the footnote shown on figure 3.1. The expression for Γ is a corrected version! The original paper had an error. Even further, the page reproduced here has another error. The argument of the vertex on the left hand side is given as p, and on the right hand side it is k. This seems a minor point, but such errors are easy to make when typing complicated vertex functions into a text editor. Clearly then if we

want to perform perturbative calculations with improved actions we will need to automate the generation of these vertices.

The non-linear connection between the gauge field and the link field

$$U_\mu(x) = e^{igaA_\mu(x)} \tag{3.2}$$

is the origin of the complexity of the Feynman rules. Consider the part of the rule coming from $\bar{\psi}(x)U_\mu(x)\psi(x + a\hat{\mu})$. Expanding the link field will give a tower of vertices. There will be a quark–gluon vertex, a quark two-gluon vertex, etc. The first three terms in this tower are shown in figure 3.2. The same issue arises with the gluon action. In addition to the regular three- and four-gluon vertices, which are already very complicated, there is an infinite tower of higher order vertices, all of which get progressively more complicated.

The situation is not totally hopeless. These vertices come with progressively more powers of α, so at a given order in perturbation theory we only need to consider a few of them. Nonetheless, given their complexity, it is essential to be able to automatically generate them.

There is one further difficulty with the perturbative improvement program. The number of actions that have been proposed for use in lattice QCD studies is very large. Just for simulating fermions we have NRQCD, Fermilab, D234, clover, AsqTad, HYP, FLIC, domain wall, overlap, and more. Given this large, and increasing, number of actions we would like to have a method of generating Feynman rules that makes switching actions easy. In this way, once we set up a calculation it is relatively straightforward to change the action. This allows for a detailed study of the improvement properties of various actions.

3.1.1 The Lüscher–Weisz Algorithm

Fortunately an algorithm exists which has most of the desirable properties we need. This is the Lüscher–Weisz algorithm, first outlined in [26] (see also [28],[29] and [30]). The description of the algorithm given in [26] paper is somewhat opaque. In

242 *Lattice Gauge Theories*

where*

$$\Gamma_{\mu\nu\lambda\rho}^{ABCD}(p,q,r,s) =$$

$$-g_0^2\Big[\sum_E f_{ABE}f_{CDE}\Big\{\delta_{\mu\lambda}\delta_{\nu\rho}[\cos\tfrac{1}{2}a(q-s)_\mu\cos\tfrac{1}{2}a(k-r)_\nu - \tfrac{a^4}{12}\tilde{k}_\nu\tilde{q}_\mu\tilde{r}_\nu\tilde{s}_\mu]$$

$$-\delta_{\mu\rho}\delta_{\nu\lambda}[\cos\tfrac{1}{2}a(q-r)_\mu\cos\tfrac{1}{2}a(k-s)_\nu - \tfrac{a^4}{12}\tilde{k}_\nu\tilde{q}_\mu\tilde{r}_\mu\tilde{s}_\nu]$$

$$+\tfrac{1}{6}\delta_{\nu\lambda}\delta_{\nu\rho}a^2\widetilde{(s-r)}_\mu\tilde{k}_\nu\cos(\tfrac{1}{2}aq_\mu)$$

$$-\tfrac{1}{6}\delta_{\mu\lambda}\delta_{\mu\rho}a^2\widetilde{(s-r)}_\nu\tilde{q}_\mu\cos(\tfrac{1}{2}ak_\nu)$$

$$+\tfrac{1}{6}\delta_{\mu\nu}\delta_{\mu\rho}a^2\widetilde{(q-k)}_\lambda\tilde{r}_\rho\cos(\tfrac{1}{2}as_\lambda)$$

$$-\tfrac{1}{6}\delta_{\mu\nu}\delta_{\mu\lambda}a^2\widetilde{(q-k)}_\rho\tilde{s}_\lambda\cos(\tfrac{1}{2}ar_\rho)$$

$$+\tfrac{1}{12}\delta_{\mu\nu}\delta_{\mu\lambda}\delta_{\mu\rho}a^2\sum_\sigma\widetilde{(q-k)}_\sigma\widetilde{(s-r)}_\sigma\Big\}$$

$$+(B\leftrightarrow C,\nu\leftrightarrow\lambda,q\leftrightarrow r)+(B\leftrightarrow D,\nu\leftrightarrow\rho,q\leftrightarrow s)\Big]$$

$$+\tfrac{g_0^2}{12}a^4\Big\{\tfrac{2}{3}(\delta_{AB}\delta_{CD}+\delta_{AC}\delta_{BD}+\delta_{AD}\delta_{BC})$$

$$+\sum_E(d_{ABE}d_{CDE}+d_{ACE}d_{BDE}+d_{ADE}d_{BCE})\Big\}$$

$$\times\Big\{\delta_{\mu\nu}\delta_{\mu\lambda}\delta_{\mu\rho}\sum_\sigma\tilde{k}_\sigma\tilde{q}_\sigma\tilde{r}_\sigma\tilde{s}_\sigma - \delta_{\mu\nu}\delta_{\mu\lambda}\tilde{k}_\rho\tilde{q}_\rho\tilde{r}_\rho\tilde{s}_\rho$$

$$-\delta_{\mu\nu}\delta_{\mu\rho}\tilde{k}_\lambda\tilde{q}_\lambda\tilde{s}_\lambda\tilde{r}_\mu - \delta_{\mu\lambda}\delta_{\mu\rho}\tilde{k}_\nu\tilde{r}_\nu\tilde{s}_\nu\tilde{q}_\mu - \delta_{\nu\lambda}\delta_{\nu\rho}\tilde{q}_\mu\tilde{r}_\mu\tilde{s}_\mu\tilde{k}_\nu$$

$$+\delta_{\mu\nu}\delta_{\lambda\rho}\tilde{k}_\lambda\tilde{q}_\lambda\tilde{r}_\mu\tilde{s}_\mu + \delta_{\mu\lambda}\delta_{\nu\rho}\tilde{k}_\nu\tilde{r}_\nu\tilde{q}_\mu\tilde{s}_\mu + \delta_{\mu\rho}\delta_{\nu\lambda}\tilde{k}_\nu\tilde{s}_\nu\tilde{q}_\mu\tilde{r}_\mu\Big\}$$

(15.53b)

This concludes our discussion of the pure gluonic sector. We now proceed to the analysis of the fermionic and ghost sectors.

iv) *Fermionic and ghost contributions*

Consider first the contribution to (15.22b) arising from $S_F^{(W)}[A,\hat\psi,\bar\psi]$. For Wilson fermions it is given by (6.4), where the link variables are replaced by (15.1a). Expanding these in powers of ϕ_μ, and introducing the dimensional fermion fields and gauge potentials according to (4.3a) and (15.36), one obtains up to

---

* This is a corrected version of the expression given by Kawai et al. (1981).

Figure 3.1: The four-gluon vertex, and an instructive footnote.
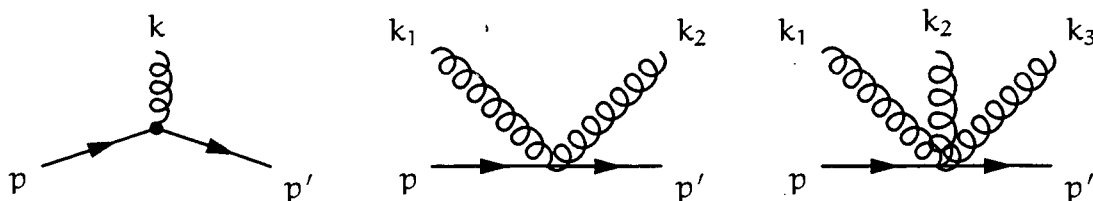
Figure 3.2: Terms in the tower of vertices generate by $\bar{\psi}(x)e^{ig_0 A_\mu(x)}\psi(x)$.

light of the central role it will play in what follows we will give a more detailed description here. Following that we will outline the implementation of the algorithm in the object oriented scripting language Python[1].

In general, a lattice gluon action is the sum of a number of "sub-actions", each containing a sum over the trace of some closed curve of links. That is,

$$S = \sum_{\mathcal{C}} S(\mathcal{C}).$$

For example, for the Wilson gluon action there are six curves, corresponding to the plaquettes in various planes. Clearly it is sufficient to consider the problem of generating the Feynman rules for a single curve at a time. Our problem then is to generate the rules for the action,

$$S(\mathcal{C}) = \sum_x \mathcal{L}(\mathcal{C}), \tag{3.3}$$

where

$$\mathcal{L}(\mathcal{C}) = (\text{constant}) \times \text{ReTr}\,[1 - \mathcal{C}]\,.$$

The vertex functions V will be given by expanding in g_0

$$S(\mathcal{C}) = \sum_{r=2}^{\infty} \frac{(ig_0)^r}{r!} \left(\sum_{a_1,\mu_1} \int \frac{d^4k_1}{(2\pi)^4} \cdots \sum_{a_r,\mu_r} \int \frac{d^4k_r}{(2\pi)^4} \right) (2\pi)^4 \delta(\sum_{i=1}^{r} k_i)$$
$$\times \left(A^{a_1}_{\mu_1}(k_1) \cdots A^{a_r}_{\mu_r}(k_r) \right) V^{\mu_1 \cdots \mu_r}_{a_1 \cdots a_r}(k_1, \cdots, k_r). \tag{3.4}$$

One further requirement is that the vertex functions be totally symmetric under permutations of any two gluon labels.

---

[1]For an introduction to Python see [31]. Python is free software, available at the Python website http://www.python.org.

The problem is now clearly defined. We want an algorithm that takes a given link path C and returns the vertex functions V to some specified order r. The return should be in the form of a subroutine that represents the vertex in some convenient language (Fortran in this report, though any modern compiled language would work). These subroutines are subsequently used by another program which codes a given Feynman diagram out of the vertex functions, and which performs the loop integrations.

The path C is given by a set of points on the lattice, starting at $n(1)$ and ending at $n(\ell)$. For a plaquette in the xy plane these are

$$
\begin{aligned}
n(1) &= [0,0,0,0] \\
n(2) &= [1,0,0,0] \\
n(3) &= [1,1,0,0] \\
n(4) &= [0,1,0,0]
\end{aligned}
$$

Clearly knowing these allows us to specify the direction of any link. We write these as a sign s times a direction $\hat{\mu}$ as follows,

$$
n(i-1) - n(i) = s(i)\hat{\mu}(i), \quad n(0) = n(\ell). \tag{3.5}
$$

The list of signs allows us to tell if the link in the path is a daggered or undaggered one. This allows us to write the curve as

$$
C = e^{ig_0 X_1} \cdots e^{ig_0 X_\ell}, \tag{3.6}
$$

with

$$
X_i = A_{\mu[i]}(n[i]) \text{ if } s[i] = +1, \text{ and } X_i = -A_{\mu[i]}(n[i-1]) \text{ if } s[i] = -1.
$$

Finally setting

$$
\text{Re}(1-C) = -\frac{1}{2}(C + C^\dagger - 2)
$$

we find

$$
\mathcal{L} = -\frac{1}{2}\text{Tr}\left(e^{ig_0 X_\ell} \cdots e^{ig_0 X_1} + e^{-ig_0 X_1} \cdots e^{-ig_0 X_\ell} - 2\right). \tag{3.7}
$$

We want to expand this expression in g_0. The trouble is that the link fields are non-abelian, so the ordering matters.

The solution of Lüscher and Wiesz is quite simple. We start by picking one ordering of links, then sum over all the distinct orderings. To do the ordering we start at the origin of the curve, and move along it until we get to the first term ig_0X that contributes, this could be the first link, the last link, or any one in between. We label it by u_1, so the first term in our product $ig_0X_{u_1}$. The index u_1 is going to run over all the links in the path $1, \ldots, \ell$ since the first contribution to the vertex function could have come from the expansion of any one of the links.

We continue, looking for the next contribution. It could be from the same link (i.e. from an X^2 contribution to the Taylor expansion of the exponential), or at another link, further along the path. We'll denote this contribution $ig_0X_{u_2}$, where $u_2 \geq u_1$. We proceed in this manner, until we have r gluons, arranged in an order,

$$(ig_0)^r X_{u_1} X_{u_2} \cdots X_{u_r}, \quad 1 \leq u_1 \leq u_2 \leq \cdots \leq u_r \leq \ell. \tag{3.8}$$

Finally, we sum over all possible orderings of this type, which gives the r gluon contribution

$$\sum_{1 \leq u_1 \leq u_2 \leq \cdots \leq u_r \leq \ell} \frac{(-1)^{r+1}}{2} \frac{(ig_0)^r}{\text{factor}} \text{Tr} \left[X_{u_1} \cdots X_{u_r} + (-1)^r X_{u_r} \cdots X_{u_1} \right]. \tag{3.9}$$

This solves the ordering issue. We can write the full Lagrangian as,

$$\mathcal{L} = \sum_{r=2}^{\infty} \frac{(ig_0)^r}{r!} \mathcal{L}_r, \tag{3.10}$$

with,

$$\mathcal{L}_r = \sum_{1 \leq u_1 \leq u_2 \leq \cdots \leq u_r \leq \ell} \frac{(-1)^{r+1}}{2} \frac{r!}{\text{factor}} \text{Tr} \left[X_{u_1} \cdots X_{u_r} + (-1)^r X_{u_r} \cdots X_{u_1} \right]. \tag{3.11}$$

We have to specify the factor in (3.11). This counts the number of times a single link contributes. A simple expression for the factor is obtained by counting the number of gluons coming from each link

$$\alpha_i = \sum_{a=1}^{r} \delta_{i,u_a}. \tag{3.12}$$

With this expression, we can write the full expression for the r gluon contribution

$$\mathcal{L}_r = \sum_{1 \leq u_1 \leq u_2 \leq \cdots \leq u_r \leq \ell} \frac{(-1)^{r+1}}{2} \frac{r!}{\alpha_1! \cdots \alpha_\ell!} \operatorname{Tr} [X_{u_1} \cdots X_{u_r} + (-1)^r X_{u_r} \cdots X_{u_1}]. \quad (3.13)$$

We want the momentum space vertex functions, so we Fourier transform

$$X_i = \sum_{a,\mu} \int \frac{d^4 k}{(2\pi)^4} s[i] e^{ik \cdot x + ik \cdot a[i]/2} \delta_{\mu\mu[i]} T^a A_\mu^a(k). \quad (3.14)$$

There are a few things about this expression worth detailing. The location of the field is given by the starting point of the curve x plus the position along the curve

$$\frac{a[i]}{2} = \frac{n[i] + n[i-1]}{2}. \quad (3.15)$$

The factor of 1/2 reflects the fact that the link connects the points x and $x + a$, so it makes sense to use the midpoint of that path as the transform point. The delta function ensures that the gauge field A will be polarized in the same direction as the link field. Finally, T^a is the element of the SU(3) algebra. This is the only part that doesn't commute.

We use the expression for the Fourier transform in (3.13), which gives

$$\begin{aligned}
\mathcal{L}_r &= \sum_{a_1,\mu_1} \int \frac{d^4 k_1}{(2\pi)^4} \cdots \sum_{a_r,\mu_r} \int \frac{d^4 k_r}{(2\pi)^4} \sum_{1 \leq u_1 \leq u_2 \leq \cdots \leq u_r \leq \ell} \frac{(-1)^{r+1}}{2} \frac{r!}{\alpha_1! \cdots \alpha_\ell!} \\
&\times \ e^{i(k_1 + \cdots + k_r) \cdot x} s[1]^{\alpha_1} \cdots s[\ell]^{\alpha_\ell} \operatorname{Tr} (T^{a_1} \cdots T^{a_r} + (-1)^r T^{a_r} \cdots T^{a_1}) \\
&\times \ \left(\delta_{\mu_1 \mu[u_1]} e^{ik_1 \cdot a[u_1]} \cdots \delta_{\mu_r \mu[u_r]} e^{ik_r \cdot a[u_r]} \right) A_{\mu_1}^{a_1}(k_1) \cdots A_{\mu_r}^{a_r}(k_r). \quad (3.16)
\end{aligned}$$

To clean this up a bit we write the colour factor as

$$C_r^{a_1 \cdots a_r} = \operatorname{Tr} (T^{a_1} \cdots T^{a_r} + (-1)^r T^{a_r} \cdots T^{a_1}), \quad (3.17)$$

and we extract the function

$$\begin{aligned}
Y_{\mu_1 \cdots \mu_r}^r (k_1, \cdots, k_r) &= \sum_{1 \leq u_1 \leq u_2 \leq \cdots \leq u_r \leq \ell} \frac{(-1)^{r+1}}{2} \frac{r!}{\alpha_1! \cdots \alpha_\ell!} \quad (3.18) \\
&\times \ s[1]^{\alpha_1} \cdots s[\ell]^{\alpha_\ell} \left(\delta_{\mu_1 \mu[u_1]} e^{ik_1 \cdot a[u_1]} \cdots \delta_{\mu_r \mu[u_r]} e^{ik_r \cdot a[u_r]} \right).
\end{aligned}$$

Using these expressions in (3.3), along with,

$$\sum_x e^{i(k_1+\cdots+k_r)\cdot x} = (2\pi)^4\delta(k_1+\cdots+k_r),$$

gives

$$\begin{aligned}
S(\mathcal{C}) &= \sum_{r=2}^{\infty} \frac{(ig_0)^r}{r!} \left(\sum_{a_1,\mu_1} \int \frac{d^4k_1}{(2\pi)^4} \cdots \sum_{a_r,\mu_r} \int \frac{d^4k_r}{(2\pi)^4} \right) (2\pi)^4\delta(\sum_{i=1}^{r} k_i) \\
&\times \left(A_{\mu_1}^{a_1}(k_1) \cdots A_{\mu_r}^{a_r}(k_r) \right) C_r^{a_1\cdots a_r} Y_{\mu_1\cdots\mu_r}^r(k_1,\cdots,k_r).
\end{aligned} \tag{3.19}$$

The final step in the derivation is to symmetrize under permutation of any two gluon indices, as follows

$$V_{\mu_1\cdots\mu_r}^{a_1\cdots a_r}(k_1,\cdots,k_r) = \frac{1}{r!}\sum_{\mathcal{P}_r} C_r^{a_1\cdots a_r} Y_{\mu_1\cdots\mu_r}^r(k_1,\cdots,k_r). \tag{3.20}$$

Here $\mathcal{P}_r$ represents the sum over all permutations of the labels

$$1,\cdots,r.$$

For example, if $r=3$ we have

$$\begin{aligned}
V_{\mu_1\mu_2\mu_3}^{a_1 a_2 a_3}(k_1,k_2,k_3) &= C^{a_1 a_2 a_3} Y_{\mu_1\mu_2\mu_3}(k_1,k_2,k_3) \\
&+ C^{a_1 a_3 a_2} Y_{\mu_1\mu_3\mu_2}(k_1,k_3,k_2) \\
&+ C^{a_2 a_3 a_1} Y_{\mu_2\mu_3\mu_1}(k_2,k_3,k_1) \\
&+ C^{a_2 a_1 a_3} Y_{\mu_2\mu_1\mu_3}(k_2,k_1,k_3) \\
&+ C^{a_3 a_1 a_2} Y_{\mu_3\mu_1\mu_2}(k_3,k_1,k_2) \\
&+ C^{a_3 a_2 a_1} Y_{\mu_3\mu_2\mu_1}(k_3,k_2,k_1).
\end{aligned}$$

All that we need to automate is the generation of the unsymmetrized parts of the vertices Y^r, the colour factors and symmetrization are trivial to implement, by hand.

To automatically generate the function Y we rewrite it as

$$Y_{\mu_1\cdots\mu_r}^r(k_1,\cdots,k_r) = \sum_{1\le u_1\le u_2\le\cdots\le u_r\le\ell} f(\mu_1,k_1;\cdots;\mu_r,k_r)e^{ik_1\cdot a[u_1]/2+\cdots+ik_r\cdot a[u_r]/2},$$

$$\tag{3.21}$$

i	n[i]	s[i]	û[i]	µ[i]	a[i]
1	[0, 0, 0, 0]	+1	[0, 1, 0, 0]	2	[0, 1, 0, 0]
2	[1, 0, 0, 0]	−1	[1, 0, 0, 0]	1	[1, 0, 0, 0]
3	[1, 1, 0, 0]	−1	[0, 1, 0, 0]	2	[2, 1, 0, 0]
4	[0, 1, 0, 0]	+1	[1, 0, 0, 0]	1	[1, 2, 0, 0]

Table 3.1: Curve parameters for a plaquette in the xy plane.

where

$$f(\mu_1, k_1; \cdots; \mu_r, k_r) = \frac{(-1)^{r+1}}{2} \frac{r!}{\alpha_1! \cdots \alpha_\ell!} s[1]^{\alpha_1} \cdots s[\ell]^{\alpha_\ell} \delta_{\mu_1 \mu[u_1]} \cdots \delta_{\mu_r \mu[u_r]}. \quad (3.22)$$

These expressions entirely are determined by the indices $u_1, \cdots, u_r$. This fact allows us to construct a dictionary, indexed by $\mu_1, \cdots, \mu_r$, with entries $f, a[u_1], \cdots, a[u_\ell]$. Then, to build up the vertex we sum up all the terms which contribute to each orientation, for a given set of input momenta.

Example

To make these ideas clear, we will construct $Y^2_{\mu_1 \mu_2}(k_1, k_2)$ for a plaquette in the xy plane. The input to the algorithm is a list of points, specifying the curve. From these we can construct the lists s, $\hat{\mu}$, μ and a, using (3.5) and (3.15). These values are enumerated in table 3.1.

These values allow us to compute the values for the α constants, which count the number of gluons from a single link, and, with those, write down the f factors defined in (3.22). These are enumerated in table 3.2. With the a vectors from table 3.1 and the f factors and delta functions from table 3.2 we can assemble the dictionary for the $Y_{\mu_1 \mu_2}$ vertex. For example, the entry for $\mu_1 = \mu_2 = 2$ has three terms associated with it, which are listed in table 3.3. With these values we can construct

$$Y_{22}(k, q) = -\frac{1}{2} e^{i(k_2 + q_2)/2} + e^{i(k_2 + 2q_1 + q_2)/2} - \frac{1}{2} e^{i(2k_1 + k_2 + 2q_1 + q_2)/2}.$$

u_1	u_2	α_1	α_2	α_3	α_4	f
1	1	2	0	0	0	$-\frac{1}{2}\delta_{\mu_1 2}\delta_{\mu_2 2}$
1	2	1	1	0	0	$\delta_{\mu_1 2}\delta_{\mu_2 1}$
1	3	1	0	1	0	$\delta_{\mu_1 2}\delta_{\mu_2 2}$
1	4	1	0	0	1	$-\delta_{\mu_1 2}\delta_{\mu_2 1}$
2	2	0	2	0	0	$-\frac{1}{2}\delta_{\mu_1 1}\delta_{\mu_2 1}$
2	3	0	1	1	0	$-\delta_{\mu_1 1}\delta_{\mu_2 2}$
2	4	0	1	0	1	$\delta_{\mu_1 1}\delta_{\mu_2 1}$
3	3	0	0	2	0	$-\frac{1}{2}\delta_{\mu_1 2}\delta_{\mu_2 2}$
3	4	0	0	1	1	$\delta_{\mu_1 2}\delta_{\mu_2 1}$
4	4	0	0	0	2	$-\frac{1}{2}\delta_{\mu_1 1}\delta_{\mu_2 1}$

Table 3.2: Front factors for the two gluon expansion of plaquette in the xy plane.

front factor	$a[1]$	$a[2]$
$-\frac{1}{2}$	$[0,1,0,0]$	$[0,1,0,0]$
$+1$	$[0,1,0,0]$	$[2,1,0,0]$
$-\frac{1}{2}$	$[2,1,0,0]$	$[2,1,0,0]$

Table 3.3: Terms in the $(2,2)$ dictionary entry.

Clearly, if we had the contents of tables 3.1 and 3.2 we could write out a Fortran source file that would compute Y_{22} for given input momenta. We could clearly do the same for all of the other directions, we won't write them all out. This method is clearly quite labour intensive, even for this simple case. Once again this illustrates the need to automate the generation of the vertex rules. The algorithm described in this section is easily implemented in a symbolic computer language, as described next.

Implementation in Python

The implementation of this algorithm in Python is straightforward. We start with a path

$$\text{path} = [(0,0,0,0), \cdots, (\text{endpoint})] \tag{3.23}$$

and assign the n's, moving around it. Once we have the ns, a subroutine computes the signs s, direction vectors $\hat{\mu}$, directions μ and gluon positions a. With these we can construct the factors f.

The delta functions in the f factors are used to figure out which entry a term belongs with. For example

$$f = f_0 \delta_{\mu_1 1} \delta_{\mu_2 3} \delta_{\mu_3 4} \tag{3.24}$$

means that an term

$$[f_0, a[u_1], a[u_2], a[u_3]] \tag{3.25}$$

gets put in the entry indexed by $(1,3,4)$. To save a bit of space, if the entry already has a term

$$[f'_0, a[u_1], a[u_2], a[u_3]] \tag{3.26}$$

we just add the two front factors, so the two terms get replaced by

$$[f'_0 + f_0, a[u_1], a[u_2], a[u_3]]. \tag{3.27}$$

Note that for any term with $f = 0$, either by this addition or the delta functions, we don't write into the dictionary.

The end result of this procedure is a dictionary (hash table) with entries indexed by the Lorentz indices. From this point it is easy to construct a source code (e.g. in Fortran) which implements this table in a form for later use in evaluating Feynman diagrams. We use a template to write a standard file, which defines a subroutine that takes the momenta as arguments and outputs the unsymmetrized vertex

$$Y_{\mu_1 \cdots \mu_l}. \tag{3.28}$$

Note that compared to the cost of performing the loop integrations the cost of generating the Feynman rules is trivial. For the most complicated case considered here, the two gluon vertex generated by the improved staggered fermion action, it takes a few minutes to generate the vertex tables.

Pick one entry, say (1,3,4) for a three gluon vertex. This entry will have a number of terms of the form

$$f, a_1, a_2, a_3.$$

The vertex writer steps through each of these terms, writing (in the first version of this code, "writing" meant literally writing a term of this form into the Fortran subroutine)

$$Y(1,3,4) = Y(1,3,4) + f e^{\frac{i}{2}(k_1 \cdot a_1 + k_2 \cdot a_2 + k_3 \cdot a_3)} \tag{3.29}$$

for each one. In this way we build up the vertex. Actually, to save more space, we write only the non-zero parts of the dot products. For example, with

$$a_1 = [1,0,0,0]$$
$$a_2 = [0,0,0,1]$$
$$a_3 = [0,0,2,0],$$

we write

$$Y(1,3,4) = Y(1,3,4) + f e^{\frac{i}{2}(k_1^x + k_2^t + 2k_3^z)}.$$

After all the entries have been summed over we have the unsymmetrized vertex, we can easily take the product with the colour factor, and symmetrize the result.

Clearly the procedure we have just outlined satisfies our requirements, it automatically generates the Feynman rules without any human intervention at all. Furthermore, the only inputs are link paths, so generating new sets of rules is easy. By breaking the action S up into a sum over the various curves it is clear how to add new operators to the action.

3.1.2 Adding Quarks

It is also straightforward to extend this algorithm to quark actions; we just have to make three small changes. The structure of a quark operator on the lattice is a bit different than a gluon one. Whereas a gluon operator is the trace of a closed curve, a quark operator is a line of links joining two quark fields. For example, we might want to consider

$$\bar{\psi}(x)U_\mu(x)U_\mu(x+\hat{\mu})\psi(x+\hat{\mu}). \tag{3.30}$$

This highlights the three changes we have to make, taking the displacement of the quark field into account, changing the colour factor, and allowing for open paths.

To take the displacement of the quark field into account we note that the Fourier transform of the field displaced by some distance d is

$$\psi(x+d) = \int \frac{d^4k}{(2\pi)^4} e^{ik\cdot d} e^{ik\cdot x} \psi(k) \tag{3.31}$$

This shows that the the only effect, in momentum space, of the displacement of the quark field is to multiply each term in the vertex by the factor $e^{ik\cdot d}$. From an implementation perspective this is a trivial thing. For quark vertices we check the endpoint of the path of links $(n[\ell] = x_e)$ and multiply each term by $\exp(ik \cdot x_e)$. This also reproduces the correct "no–gluon" vertices that we need for the quark propagator.

Changing the colour factor is just as straightforward. There are two major changes, since the action is now

$$\bar{\psi}(x)U_{\mu_1}(x)\cdots U_{\mu_\ell}(x+n[\ell-1])\psi(x+n[\ell]) \tag{3.32}$$

we don't have the trace over the colour matrices T, and there is no real part of the trace. So the colour "factor" in this case becomes

$$C_f^{a_1\cdots a_r} = T^{a_1} \cdot T^{a_r}. \tag{3.33}$$

Working with these matrix products typically involves working out the colour factor for a diagram in advance, and only keeping certain parts.

Finally we have to slightly change the way we define the path. For a closed path we stopped one point away from the initial point, and imposed the condition $n(0) = n(\ell)$ (see (3.5)). With an open path, we set $n[0]$ to the initial point, and go up to $n[\ell]$. That is, (3.5) gets rewritten as

$$n[i-1] - n[i] = s[i]\hat{\mu}[i], \quad i = 1, \cdots, \ell. \tag{3.34}$$

This is the only change, after that everything proceeds in the same way.

One further issue comes up with quark paths. Unlike gluon paths, quark operators typically have a direction. For example, the link operator is

$$\bar{\psi}(x)U_\mu(x)\psi(x + \hat{\mu}). \tag{3.35}$$

This is a component of the operator $\gamma^\mu D_\mu$ so in order to deal with quark vertices we need to keep track of the spin indices. For example, for $\gamma^\mu D_\mu$ we use the automatic vertex generator four times to get rules for D_x, D_y, etc. Then, in the Fortran code, multiply each vertex rule by the appropriate gamma matrix. For this work we just keep track of these by hand, however they could be automated as well.

3.1.3 Large vertices and performance

One of the key problems with the LW algorithm is that the vertices it generates grow very rapidly as they get more complex. As we mentioned above the growth is factorial in the size of the input path and in the number of gluons, that is

$$n_{r,\ell} = \frac{2}{(r-1)!}\ell(\ell+1)\cdots(\ell+r-1). \tag{3.36}$$

This can result in very large Fortran source files, which are slow to compile and produce extremely large object files.

There is a simple way to fix this problem, at least for the actions we will be considering here. The key is that every term has the exact same form (3.29). The
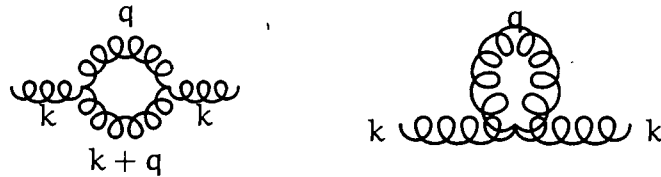
Figure 3.3: Gluon loop contributions to the gluon self energy.

various quantities $(f, \{a_i\})$ change from term to term, but the form of the terms do not change. We can avoid the large source files by writing the varying parameters into a text file, and reading them in at run time. This avoids needless compilation of thousands of instructions.

Of course, we cannot avoid the double factorial growth altogether; this is inherent in the complexity of the Feynman rules, and there is only so much reduction we can do. By reading in text files we trade the problems of large source and object files into a problem with large arrays. That is, after reading in the text files we have large arrays in memory. Now assume that we want to calculate a diagram with this array. We have to run the whole array in from memory, through the CPU's cache, multiplying by the momenta. This returns the values for Y, but, for large arrays it gets very slow.

3.1.4 Bare perturbation theory

Once we have generated the Feynman rules, the remainder of our perturbative calculations are done in a very straightforward manner. We use our Python scripts to generate the Feynman rules that we need. For example, let's say we wanted to compute the one–loop contributions to the gluon self energy from diagrams involving gluons. There are two diagrams, shown in figure 3.3. For these diagrams we need three different Feynman rules, the two-gluon vertex (which gets inverted to make the propagator) $V_{\mu\nu}^{ab}(k, -k)$, the three-gluon vertex $V_{\mu\nu\sigma}^{abc}(k_1, k_2, k_3)$ and the four-gluon vertex $V_{\mu\nu\sigma\rho}^{abcd}(k_1, k_2, k_3, k_4)$. These are the symmetrized rules, built from the automatically generated unsymmetrized ones.

Gauge fixing and measure terms

Just like in the continuum theory we need to do gauge fixing in order to remove the redundant gauge degrees of freedom from the path integral. This is just the usual Faddeev–Popov method outlined in any QFT textbook applied to the discretized action.

Another issue for lattice perturbation theory is the conversion of the lattice path integral measure $D[U]$, which integrates over link fields, into the gauge field integration measure $D[A]$. The connection between U and A is non-linear, so we expect that we cannot just substitute

$$D[U] \to D[A].$$

This is indeed the case, and we need to properly derive the connection between the two integration measures. This is a standard exercise in group theory, though fairly long. We refer the interested reader to [27] and merely quote the result here,

$$D[U] = D[A]e^{-S_M[A]} \tag{3.37}$$

where

$$S_M[A] = -\frac{1}{2}\sum_{x,\mu} \text{Tr}\log\left[1 + 2\sum_{\ell=1}^{\infty} \frac{(-1)^\ell}{(2\ell+2)!}(g_0 A_\mu^a T^a)\right]. \tag{3.38}$$

In this report we will only need the first term in this series, so for our purposes we can use

$$D[U] = D[A]e^{-S_M^1[A]} \tag{3.39}$$

where

$$S_M^1[A] = \frac{g_0^2}{48}\sum_{x,\mu} \delta^{ab}\delta_{\mu\nu}A_\mu^a(x)A_\nu^b(x). \tag{3.40}$$

In addition to the measure terms, we need to fix the gauge in the path integral. To do this we will use the Faddeev–Popov procedure. Once again this is a standard result, and we provide a brief summary of the development in [32].

We start with the path integral for the gauge field[2]

$$Z = \int D[U] e^{-S_W[A]}. \tag{3.41}$$

Here $D[U]$ is the (gauge invariant) measure we discussed above, and $S_W[A]$ is the Wilson gluon action (or any other gauge invariant improved action). On the lattice, a gauge transformation is represented as

$$\Lambda(x) = e^{iT_b \omega^b(x)}.$$

It is sufficient to consider gauge transformations infinitesimally close to the unit transformation, so we write

$$\Lambda(x) = 1 + iT_b \delta\omega^b(x) \tag{3.42}$$

dropping all higher order terms. Under such a transformation, the gauge field A transforms as follows

$$\delta A^c_\mu(x) = \frac{1}{g} \left[E^{-1}_{bc}(\overline{A_\mu(x)}) \delta\omega^b(x + \hat{\mu}) - E^{-1}_{cb}(\overline{A_\mu(x)}) \delta\omega^b(x) \right] \tag{3.43}$$

where

$$E^{-1}(x) = \frac{x}{1 - e^{-x}}, \tag{3.44}$$

and

$$\overline{A_\mu(x)}_{bc} = g f_{bcd} A^d_\mu(x). \tag{3.45}$$

We wish to use a covariant gauge fixing, so we introduce the gauge fixing function

$$f^c(A(x)) = \Delta^\mu A^c_\mu(x) = \sum_{\mu=1}^{4} \left(A^c_\mu(x) - A^c_\mu(x - \hat{\mu}) \right). \tag{3.46}$$

Under an infinitesimal gauge transformation we find, using (3.43)

$$\delta f^c(A(x)) = \sum_y \mathcal{M}_{cx,by} \delta\omega^b(y) \tag{3.47}$$

---

[2]We omit the fermion action in this discussion, so long as it is gauge invariant, nothing changes, just replace $S_W[A]$ by $S_W[A] + S_F[\bar\psi, \psi, A]$.

where we have introduced the Faddeev–Popov operator

$$
\begin{aligned}
\mathcal{M}_{cx,by}[A] &= \frac{1}{g} \sum_{\mu=1}^{4} \left[E_{bc}^{-1}(\overline{A_\mu(x)}) \delta_{x+\hat{\mu},y} - E^{-1}(\overline{A_\mu(x)}) \delta_{x,y} \right. \\
&\quad \left. - E^{-1}(\overline{A_\mu(x-\hat{\mu})}) \delta_{x,y} - E^{-1}(\overline{A_\mu(x-\hat{\mu})}) \delta_{x-\hat{\mu},y} \right].
\end{aligned}
\tag{3.48}
$$

We denote the gauge transformed field by $A^\wedge(x)$. Equation (3.47) shows that if we transform from the variables $f^c(A^\wedge(x))$ to $\omega^b(x)$ the Jacobian is just $\mathcal{M}$. Defining the determinant of the Jacobian, or the Faddeev–Popov determinant, as

$$
\Delta_f[A] = \det \mathcal{M}[A]
\tag{3.49}
$$

we see that the integral

$$
\int \prod_{x,b} d\omega^b(x) \prod_{y,c} \delta \left(f^c(A^\wedge(y)) - g_y^c \right) \Delta_f[A^\wedge]
\tag{3.50}
$$

is a constant.

Returning to the original path integral, we have

$$
Z = \int D[U] e^{-S_W[A]} = \int D[U^\wedge] e^{-S_W[A^\wedge]}
\tag{3.51}
$$

since everything in this expression is gauge invariant. Now we are free to multiply this by the constant (3.50)

$$
Z = \int D[U^\wedge] \prod_{x,b} d\omega^b(x) \prod_{y,c} \delta \left(f^c(A^\wedge(y)) - g_y^c \right) \Delta_f[A^\wedge] e^{-S_W[A^\wedge]}.
\tag{3.52}
$$

Transforming to A gives

$$
Z = \left(\int \prod_{x,b} d\omega^b(x) \right) \int D[U] \prod_{y,c} \delta \left(f^c(A(y)) - g_y^c \right) \Delta_f[A] e^{-S_W[A]}.
\tag{3.53}
$$

We can drop the integral over ω as it is an uninteresting constant.

Next we integrate over g with a Gaussian weight $e^{\frac{g^2}{2\xi}}$, which gives

$$
Z = \int D[U] \Delta_f[A] e^{-S_W[A] - S_{gf}[A]}, \qquad S_{gf} = \frac{1}{2\xi} \sum_y [f^c(A(y))]^2.
\tag{3.54}
$$

Finally, we express the Faddeev–Popov determinant as an integral over ghost fields

$$\Delta_f[A] = \int D\eta D\bar{\eta} e^{-S_{FP}[A,\eta,\bar{\eta}]}, \tag{3.55}$$

$$S_{FP} = \sum_{x,\mu} \left(\bar{\eta}_c(x+\hat{\mu}) - \bar{\eta}_c(x)\right) \left(E_{cb}^{-1}(\overline{A_\mu(x)})\eta_b(x) - E_{bc}^{-1}(\overline{A_\mu(x)})\eta_b(x+\hat{\mu})\right). \tag{3.56}$$

This expression can be expanded in the gauge coupling to generate Feynman rules for gauge field-ghost interactions. This can be done by hand, the explicit expression is well-known [26].

With the gauge fixing accomplished there we can easily implement the diagrams shown in figure 3.3. For example the tadpole diagram is

$$T(p) = \int \frac{d^4k}{(2\pi)^4} V_{\mu\nu\rho\mu}^{abca}(p,k,-k,-p) D_{bc}^{\nu\rho}(k). \tag{3.57}$$

We assemble the diagrams by hand, and then numerically integrate them. To do the numerical integrations we use the VEGAS routine [33]. In this way we have performed all of the calculations in this report. Many other calculations have also been performed by the HPQCD perturbation theory group, using this same basic approach.

The numerical integrations are typically well-behaved, however we can run into problems when the integrands have contributions from widely separate scales. We will discuss these issues as they arise in the forthcoming chapters.

3.2   Issues with bare perturbation theory

The general Lüscher–Weisz algorithm has been understood since 1985. Why, then, has lattice perturbation theory not been applied widely? One reason is that even with the Lüscher–Weisz algorithm, these perturbative calculations are very difficult. Another reason is that for many years the predictions of lattice perturbation theory disagreed substantially with non-perturbative calculations of short distance quantities.

As an illustration, we consider the perturbative versus non-perturbative determinations of the mean link. Working at $\beta = 6/g_0^2 \approx 6$ the one-loop perturbative value for the mean link in Landau gauge is ≈ 0.078, compared to the non-perturbatively determined value 0.139. At this β we have $\alpha_s = g^2/4\pi \approx 0.08$. Such disagreements were typical of any comparison between perturbative and non-perturbative results for short distance quantities. According to our quick estimates in chapter 1, perturbation theory ought to work very well in this case. This failure of lattice perturbation theory meant that the perturbative improvement of actions could not be trusted, and hence doomed lattice field theory to waiting for computers to become powerful enough to work "brute force" at very small a. Alternatively, symmetry considerations can be used in some cases to design improved actions and operators without recourse to perturbation theory. These non-perturbative techniques are beyond the scope of this report, for an up to date review see [34].

In a groundbreaking 1993 paper [35] Lepage and Mackenzie solved this issue. They showed why perturbation theory was disagreeing with the non-perturbative calculations, and suggested ways to improve the agreement. It takes three different techniques to fix the perturbative series, we review them here. Of the three, two (better expansion parameter and scale setting) are well-known in continuum perturbation theory, and one (tadpole improvement) is unique to the lattice.

3.2.1 α_V

The first problem with pre-Lepage–Mackenzie lattice perturbation theory was that perturbative expansions were typically done with the bare lattice coupling. This is a bad choice of expansion parameter. In general, using a bad expansion parameter can result in perturbative series that are technically correct, but practically useless. To see this, lets assume we have a well behaved perturbative series,

$$f(x_{good}) = f_0 + f_1 x_{good} + f_2 x_{good}^2$$

where all the coefficients are $\mathcal{O}(1)$ and $x \ll 1$. If we then make a transformation

$$x_{bad} = x_{good}(1 - 1000x_{good})$$

The second order coefficients become very large. If we look only at the power of x the two series are equally good, but in practice the series in x_{bad} will badly disagree with data.

The solution to this problem is fairly clear; use a good coupling. There is no unique choice for what to use as a good coupling. Lepage and Mackenzie suggested using a physically motivated choice. For example, we can define a coupling α_V such that the short distance $Q\bar{Q}$ potential has the form

$$V(q) = -\frac{4}{3}\frac{\alpha_V(q)}{q^2} \tag{3.58}$$

to all orders.

Equation 3.58 gives us a means to convert α_0 to α_V. We compute $V(q)$ as a series in α_0,

$$V(q) = -\frac{4}{3}\frac{\alpha_0(1 - V_1\alpha_0 + \dots)}{q^2}. \tag{3.59}$$

The connection can be read off,

$$\alpha_V = \alpha_0(1 - V_1\alpha_0 + \cdots). \tag{3.60}$$

Perturbative series that are expressed in terms of α_V have much better convergence properties than those expressed in terms of α_0. We will discuss the computation of the connection between the two couplings later in this report, for now we simply quote the long known result for the Wilson gluon action

$$\alpha_0(q) = \alpha_V\left[1 - \alpha_V\left(\frac{11}{4\pi}\log\left(\frac{\pi^2}{q^2}\right) + 4.702\right) + \mathcal{O}(\alpha_V^2)\right]. \tag{3.61}$$

It is the large constant term 4.702 which is causing the problems with series expressed in terms of α_0. We would like to understand the origin of these large terms, and if possible arrange perturbation theory such that they don't occur.

3.2.2 Tadpole improvement

The large terms are due to so-called lattice tadpole diagrams in perturbation theory. Consider the perturbative expansion of the link variable,

$$U_\mu(x) = 1 - igaA_\mu(x) - \frac{g^2a^2}{2}A_\mu(x)A_\mu(x) + \cdots.$$

Taking the expectation value we find

$$\langle U_\mu(x) \rangle = 1 - \frac{g^2a^2}{2}\langle A_\mu(x)A_\mu(x)\rangle + \cdots,$$

so naively we expect that perturbative series will reproduce the continuum prediction (1) up to $\mathcal{O}((ga)^2)$ errors.

Unfortunately this naive expectation is not correct. The reason is that the correction term

$$\langle A_\mu(x)A_\mu(x)\rangle = \underset{\text{---}}{\overset{\text{\large\textcircled{}}}{\longrightarrow}}$$

can be written (in Feynman gauge)

$$\langle A_\mu(x)A_\mu(x)\rangle = \int_{-\frac{\pi}{a}}^{\frac{\pi}{a}} \frac{dk}{\sum_{\mu=1}^4 \left[\frac{2}{a}\sin\left(\frac{k_\mu a}{2}\right)\right]^2} \propto \frac{1}{a^2}.$$

When multiplied into $(ga)^2$ this cancels the a dependence, giving only a suppression of $\mathcal{O}(g^2)$. Note that this problem is not present in the continuum, these power divergent diagrams vanish in dimensional regularization.

Impact for high precision lattice QCD

These tadpole diagrams are disastrous for improving lattice QCD. Recall the improved quark action of chapter 2,

$$S_{SW} = \bar\psi(x)\left[\gamma_\mu D^\mu - \frac{r}{2}\triangle + c_{SW}\sigma_{\mu\nu}F^{\mu\nu} + m_0\right]\psi(x).$$

We argued that with $c_{SW} = 1$ this action would be correct to $\mathcal{O}(a^2, \alpha a)$. In improvement coefficients they cause the perturbative errors to be much larger than

expected. For example a correction that is expected to be $1 \times \alpha_s$ might turn out to be $6 \times \alpha_s$ due to the large tadpole contribution.

Fortunately there is a way to at least partially remove these errors without perturbative calculations. Rather than using the bare link variable U_μ in non-perturbative simulations, one uses a "tadpole–improved" link, $\tilde{U}_\mu(x) = \frac{U_\mu(x)}{u_0}$. Here u_0 is some measure of the average value of the link variable (common choices are the mean link in Landau gauge, or the fourth root of the average plaquette).

Recall the original Wilson gauge action,

$$S_W = \frac{1}{g^2} \sum_{\mu < \nu} [1 - P_{\mu\nu}] .$$ (3.62)

Multiplying and dividing by u_0^4, and setting $\tilde{g} = g/u_0^2$ we find,

$$S_W = \frac{1}{\tilde{g}^2 u_0^4} \sum_{\mu < \nu} [1 - P_{\mu\nu}] .$$ (3.63)

Using the action in this form results in much lower errors, and perturbation theory in $\tilde{g}$ is much better behaved. In fact the relationship between $\tilde{\alpha} = \frac{\tilde{g}^2}{4\pi}$ and α_V has no large constants. Evidently $\tilde{\alpha}$ is another "good" expansion parameter.

3.2.3 Scale setting

A final issue for lattice perturbation theory is determining what energy scale to use in the strong coupling. Recall from chapter 1 that the strong coupling constant varied with energy. At lowest order in perturbation theory we have,

$$\alpha_V(E^2) = \frac{g^2(E^2)}{4\pi} = \frac{4\pi}{\left(11 - \frac{2}{3}n_f\right) \log\left(\frac{E^2}{\Lambda^2}\right)} .$$ (3.64)

The issue for lattice perturbation theory is to determine what value we should use for E. For the purpose of this section, a more convenient expression for α is

$$\alpha_V(E^2) = \frac{\alpha_V(\mu)}{1 + \alpha_V(\mu)\beta_0 \log(E^2/\mu^2)}, \qquad \beta_0 = \frac{11 - \frac{2}{3}n_f}{4\pi} .$$ (3.65)

We are trying to correct for physics that has been excluded by the UV cutoff, so we might try using $E = q^* = \pi/a$ as our energy scale. While this reasoning is correct, it is not a particularly precise way of determining the ideal q^*. We would like to have a more precise way of setting the scale.

A general one-loop term in a perturbative series has the form

$$T_1 = \alpha_V(q^*) \int d^4 q f(q).$$

We might try to determine q^* by setting

$$\alpha_V(q^*) \int d^4 q f(q) = \int d^4 q \, \alpha_V(q) f(q). \tag{3.66}$$

This will produce an average value for q^*, but we must be careful about using equation 3.65. As we've written it, it will produce a divergent integral. The key is to expand 3.65 to the correct order in α

$$\alpha_V(q) = \alpha_V(q^*) \left[1 - \beta_0 \alpha_V(q^*) \log\left(\frac{q^2}{q^{*2}}\right) + \cdots \right]. \tag{3.67}$$

Using (3.67) in (3.66) and solving for $\log(q^{*2})$ gives

$$\log(q^{*2}) = \frac{\int d^4 q f(q) \log(q^2)}{\int d^4 q f(q)}. \tag{3.68}$$

Using $\alpha_V(q^*)$ rather than $\alpha_V(\pi/a)$ in perturbative series can result in still better agreement with non-perturbative simulations, there are examples of this in [35].

Troubles with q^*

The simple definition of q^* outlined above suffices for many lattice calculations. However, it can fail in some cases of interest. For example when the denominator

$$\int d^4 q f(q)$$

vanishes (or gets anomalously small) the formula (3.68) clearly doesn't apply (or gives anomalously large values for q^*). The solution to this problem is to use a higher order expansion for $\alpha_V(q)$. This procedure is outlined in [36], along with detailed examples of its use.

Chapter 4

Link operator results

In this chapter we will consider the perturbative expansion of various operators built out of links. There are four operators we wish to consider. The first, and simplest, is the mean link. That is the expectation value of a single-link operator $\langle U_\mu \rangle$. This is a gauge dependent quantity.

Another simple gauge dependent quantity we can consider is the expectation value of a line of links in some direction. This is known as a Wilson line of length L, where L is the number of links in the line. We will denote this as P(L). Again, this quantity is gauge dependent, except when the length of the line is equal to the length of the lattice. The Wilson line is a important quantity, because the self-energy of a static quark can be extracted from the Wilson line's overlap with the ground state. That is,

$$\lim_{L \to \infty} \langle P(L)|0 \rangle = ce^{-E_0 L}. \tag{4.1}$$

The static quark self-energy E_0 is gauge invariant, but the overlap c is not.

From the Wilson lines, the next most complicated quantity is the static quark potential. By computing the correlation function of two Wilson lines, we can extract the potential. We outline this in more detail below. We work in the $L \to \infty$ limit, which gives gauge invariant results.

Finally we would like to compute the expectation values for various small closed

paths. The simplest of these are Wilson loops, that is rectangles of length R and width T in a plane. These quantities are gauge invariant and will be denoted as $W(R, T)$.

All of these quantities are important to know in perturbation theory. The mean link is an input into tadpole improved lattice simulations so it is useful to know. Typically it is measured non-perturbatively, however the perturbative result could be used. The Wilson lines and static quark potential are needed to compute the relationship between α_0 and α_V as discussed in chapter 3. In addition, if we have a calculation for the static quark potential in the continuum theory we can use the lattice calculation to relate α_V to α_0. Finally, as outlined in chapter 2, perturbative expansions for small Wilson loops play a vital role in extracting the strong coupling α from lattice simulations.

4.1 Gauge field actions

It is desirable to consider as wide a range of gauge field actions as we can. To that end, we report results in this chapter for three different gauge field actions. The first is the unimproved Wilson gauge action. That is,

$$S_W = \beta \sum_{x;\mu<\nu} [1 - P_{\mu\nu}].$$ (4.2)

where $P_{\mu\nu}$ is the trace of the plaquette, as detailed in chapter 1 and $\beta = \frac{6}{g^2}$. Most of the things we calculate using the Wilson action have already been computed, so we can use this action to test our methods.

We also consider the Symanzik improved action of chapter 2,

$$S_I = \beta_{pl} \sum_{x;\mu<\nu} [1 - P_{\mu\nu}] + \beta_{rt}^0 \sum_{x;\mu<\nu} [1 - R_{\mu\nu}],$$ (4.3)

where

$$\beta_{pl} = \frac{10}{g^2}, \qquad \beta_{rt}^0 = \frac{\beta_{pl}}{20}.$$

At this point, there are a number of ways to go about tadpole improving this action. We choose to only consider the additional tadpole factors generated by the rectangle terms, since there are two additional links in the rectangle we get two powers of the average link. That is, our action is

$$S_I = \beta_{pl} \sum_{x;\mu<\nu} [1 - P_{\mu\nu}] + \beta_{rt}^0 \sum_{x;\mu<\nu} [1 - R_{\mu\nu}], \tag{4.4}$$

where

$$\beta_{pl} = \frac{10}{g^2}, \qquad \beta_{rt}^0 = \frac{\beta_{pl}}{20u_0^2}.$$

The counterterm generated by the $1/u_0^2$ factor will cancel some, but not all, of the large second order coefficients. The remainder will be dealt with by converting to α_V.

Both of the previous actions have uncorrected $\mathcal{O}(\alpha a^2)$ errors. An action which removes these is [37],

$$\begin{aligned} S_G &= \beta_{pl} \sum_{x;\mu<\nu} (1 - P_{\mu\nu}) + \beta_{rt} \sum_{x;\mu\neq\nu} (1 - R_{\mu\nu}) \\ &\quad + \beta_{pg} \sum_{x;\mu<\nu<\sigma} (1 - C_{\mu\nu\sigma}), \end{aligned} \tag{4.5}$$

where

$$\begin{aligned} \beta_{pl} &= \frac{10}{g^2}, \qquad \beta_{rt} = -\frac{\beta_{pl}}{20u_0^2}(1 + 0.4805\alpha_{latt}) \\ \beta_{pg} &= -\frac{\beta_{pl}}{u_0^2}0.03325\alpha_{latt}, \qquad \alpha_{latt} = \frac{g^2}{4\pi}. \end{aligned}$$

This action is is highly improved, it's errors are $\mathcal{O}(a^4, \alpha^2 a^2)$. The term $C_{\mu\nu\sigma}$ is a six link "chair term" defined by

$$C_{\mu\nu\sigma} = \frac{1}{3}\text{Tr}\left[U_\mu(x)U_\nu(x + \hat{\mu})U_\sigma(x + \hat{\mu} + \hat{\nu})U_\mu^\dagger(x + \hat{\nu} + \hat{\sigma})U_\nu^\dagger(x + \hat{\sigma})U_\sigma^\dagger(x)\right].$$

Note that this prescription for improvement is not unique. There are other redundant operators that can be used instead that would also remove the errors. Our perturbative methods could be applied to them as well.

We present our results for an expansion in the bare lattice coupling $\alpha_{latt} = g^2/(4\pi)$. We include tadpole counterterms for (4.5), which are generated by the first order expansion of the mean-field in the rectangle terms. In this chapter we use the mean-field, u_0, defined by the average plaquette which, for the action of (4.5), is given to first order by $u_0 \approx 1 - 0.7671\alpha_{latt}$. Our second order results also included the counterterm generated by the $1 \times 1 \times 1$ paths in (4.5).

4.2 Twisted periodic boundary conditions

A problem that comes up repeatedly in doing perturbative calculations is that most of the quantities we wish to compute are infrared divergent. In a matching calculation these divergences must cancel, since the lattice and continuum theories are the same at long ($\gg a$) distances. For this cancellation to work we must use the same infrared regulator for both theories, we will return to this point in chapter 6.

We would like to have a gauge invariant infrared regulator. We need this because we are doing second order calculations, so a gluon mass (which is a more traditional IR regulator) could destroy the gauge invariance. Another infrared issue that comes up occurs when we compute on a finite lattice with periodic boundary conditions. In this case, integrals over the lattice momentum

$$\int_{-\pi}^{\pi} \frac{d^4k}{(2\pi)^4} \frac{1}{\sum_{\mu=1}^{4} \left(2\sin\left[\frac{k_\mu}{2}\right]\right)^2} = 0.1549326(6),$$

which are well behaved, become badly behaved lattice sums

$$\left(\prod_{\mu=1}^{4} \sum_{n_\mu=-L/2}^{L/2}\right) \frac{1}{\sum_{\mu=1}^{4} \left(2\sin\left[\frac{\pi n_\mu}{L}\right]\right)^2}. \tag{4.6}$$

The trouble is that the zero-mode $n_1 = n_2 = n_3 = n_4 = 0$ is only properly treated in the $L \to \infty$ limit.

There is an infrared regulator that is both gauge invariant and removes this zero-mode problem, twisted periodic boundary conditions [38]. We review twisted boundary conditions here in some detail; even more technical detail can be found in [26].

We consider a lattice with volume L^4, with regular periodic boundary conditions

$$U_\sigma(x + L\hat{\mu}) = U_\sigma(x), \quad \mu = z, t, \tag{4.7}$$

in two directions (zt), and twisted periodic boundary conditions

$$U_\sigma(x + L\hat{\nu}) = \Omega_\nu U_\sigma(x)\Omega_\nu^\dagger, \quad \mu = x, y, \tag{4.8}$$

in the other two. The twist matrices Ω are constant elements of $SU(N)$. We can solve for the twist matrices by considering the effect of a crossing both the x and y boundaries. There are two ways of doing this, applying (4.8) in the x then y directions,

$$U_x(1 + L, 1 + L, z, t) = \Omega_x\Omega_y U_x(1, 1, z, t)\Omega_y^\dagger\Omega_x^\dagger, \tag{4.9}$$

or applying (4.8) in the y then x directions,

$$U_x(1 + L, 1 + L, z, t) = \Omega_y\Omega_x U_x(1, 1, z, t)\Omega_x^\dagger\Omega_y^\dagger. \tag{4.10}$$

These two possibilities must be equal. Enforcing this, right multiplying both sides by $(\Omega_y\Omega_x)^\dagger$ and left multiplying both sides by $\Omega_x\Omega_y$, gives

$$(\Omega_y\Omega_x)^\dagger\Omega_x\Omega_y U_x = U_x(\Omega_y\Omega_x)^\dagger\Omega_x\Omega_y, \tag{4.11}$$

or

$$\left[(\Omega_y\Omega_x)^\dagger\Omega_x\Omega_y, U_x\right] = 0. \tag{4.12}$$

In order for (4.12) to hold for an arbitrary link element $(\Omega_y\Omega_x)^\dagger\Omega_x\Omega_y$ must be an element of the centre group of $SU(N)$, $Z(N)$. We define $z = e^{2\pi i/N}$, to get

$$(\Omega_y\Omega_x)^\dagger\Omega_x\Omega_y = z$$
$$\Omega_x\Omega_y = z\Omega_y\Omega_x. \tag{4.13}$$

This equation can be solved for an explicit set of twist matrices, however we do not need to do this for perturbative calculations. Instead we consider the effect of twists on the gauge fields $A_\mu(x)$.

The gauge fields are related to the link fields via

$$U_\mu(x) = e^{igA_\mu(x)}.$$

We find that the gauge field must satisfy

$$A_\mu(x + L\hat{\nu}) = \Omega_\nu A_\mu(x)\Omega_\nu^\dagger. \qquad (4.14)$$

We wish to have an expression for the momentum space gauge field, so we try the Fourier decomposition

$$A_\mu(x) = \frac{1}{NL^4} \sum_k \Gamma_k e^{ik\cdot x + i\frac{k_\mu}{2}} A_\mu(k). \qquad (4.15)$$

Rather than expanding in the traditional colour matrices T^a, we have expanded in a set of twisted colour matrices Γ_k which we take to be momentum dependent. We will derive conditions on these matrices below, but one important point is that we have traded the traditional colour degrees of freedom $a = 1, \ldots, 8$ for additional momentum degrees of freedom.

Fourier expanding both sides of (4.14) we find the condition on the twisted colour matrices

$$\Omega_\nu \Gamma_k \Omega_\nu^\dagger = e^{ik_\nu L} \Gamma_k. \qquad (4.16)$$

We left multiply both sides of this with $N - 1$ more Ω_ν's and right multiply with $N - 1$ more $\Omega_\nu^\dagger$'s. This gives

$$\Omega_\nu^N \Gamma_k (\Omega_\nu^\dagger)^N = e^{ik_\nu L} \Omega_\nu^{N-1} \Gamma_k (\Omega_\nu^\dagger)^{N-1}. \qquad (4.17)$$

Using (4.16) repeatedly on the right hand side, and $\Omega_\nu^N = (-1)^{N-1}$ on the left we find

$$\Gamma_k = (-1)^{N-1} e^{iNk_\nu L} \Gamma_k. \qquad (4.18)$$

This is solved, up to an arbitrary phase factor, by

$$k_\nu = \frac{2\pi}{NL} n_\nu, \quad n_\nu = 1, 2, \ldots \tag{4.19}$$

That is, in the twisted directions there are three times as many momentum modes as there would be for periodic boundary conditions. An explicit solution of (4.18) with a convenient choice of phase [39] is

$$\Gamma_k = \Omega_x^{-n_y} \Omega_y^{n_x} z^{-n_x n_y}. \tag{4.20}$$

The twisted momenta, for the purposes of solving (4.18), are defined modulo N. This means that there appears to be N^2 choices for the n_x and n_y values in our solution for Γ_k. This is not quite the case. Consider the $n_x = n_y = 0$ mode, which gives the $N \times N$ identity matrix $I_{N \times N}$. Note that we must have

$$\text{Tr}(A_\mu(x)) = 0. \tag{4.21}$$

Since $\text{Tr}(I_{N \times N}) = N$ we must have

$$A(k_x = 0(\text{mod}N), k_y = 0(\text{mod}N), k_z, k_t) = 0. \tag{4.22}$$

This is the crucial property which makes twisted boundary conditions appealing. The zero-mode $k_x = k_y = k_z = k_t = 0$ is excluded from the theory. The bad lattice sum (4.6) becomes

$$\left(\prod_{\mu=1}^{2} \sum_{n_\mu = -3L/2}^{3L/2} \right) \left(\prod_{\mu=3}^{4} \sum_{n_\mu = -3L/2}^{3L/2} \right) \frac{\chi_k}{\sum_{\mu=1}^{4} \left(2 \sin \left[\frac{\pi n_\mu}{L} \right] \right)^2}, \tag{4.23}$$

where $\chi_k = 0$ if $k_T = 0(\text{mod}N)$, and $\chi_k = 1$ otherwise. We've introduced the notation

$$k_T = 0(\text{mod}N),$$

which means

$$n_x = 0(\text{mod}N), \quad \text{and} \quad n_y = 0(\text{mod}N).$$

The sum (4.23) has no zero-mode, so it is well behaved.

There are a few other properties of the Γ_ks that we will need. First, the $N^2 - 1$ remaining matrices must be traceless

$$\text{Tr}\Gamma_k = 0, \text{ if } k_T \neq 0. \tag{4.24}$$

Notice that there are $N^2 - 1$ remaining matrices, which is the same as for more traditional colour basis. Two other properties of these matrices we will need are

$$\Gamma_k^\dagger = \Gamma_{-k}, \tag{4.25}$$

and

$$\Gamma_{k'}\Gamma_k = z^{-(n_x' n_y - n_x n_y')}\Gamma_{k'+k} = Z(n, n')\Gamma_{k'+k}, \tag{4.26}$$

which trivially follow from (4.20) with our choice of phase.

Twisted colour factors and smell

Using the twisted colour basis in the automatic vertex generator doesn't require many changes. For gluon actions we just replace

$$C^{a_1 \cdots a_r} = \text{Tr}\left[T^{a_1} \cdots T^{a_r} + (-1)^r T^{a_r} \cdots T^{a_1}\right],$$

by

$$C(k_1, \cdots, k_r) = \frac{1}{N}\text{Tr}\left[\Gamma_{k_1} \cdots \Gamma_{k_r} + (-1)^r \Gamma_{k_r} \cdots \Gamma_{k_1}\right]. \tag{4.27}$$

It is actually easier to work with this sort of colour factor. Repeated use of (4.26) allows all of these colour factors to be reduced to the form

$$C(k_1, \cdots, k_r) = \frac{f(k_1, \cdots, k_r)}{N}\text{Tr}\left[\Gamma_{k_1 + k_2 + \cdots + k_r}\right]. \tag{4.28}$$

The trace will be zero unless we have

$$(k_1 + k_2 + \cdots + k_r)_{\text{twisteddirections}} = 0(\text{mod}N), \tag{4.29}$$

which enforces momentum conservation on the twisted momentum modes. Assume that the momentum conservation condition is met; we have $\text{Tr}\Gamma_0 = N$, so the colour factor is

$$C(k_1, \cdots, k_r) = f(k_1, \cdots, k_r). \tag{4.30}$$

An example should make this clear. We consider the three-gluon colour factor,

$$
\begin{aligned}
C(k_1, k_2, k_3) &= \frac{1}{N}\text{Tr}\left[\Gamma_{k_1}\Gamma_{k_2}\Gamma_{k_3} - \Gamma_{k_3}\Gamma_{k_2}\Gamma_{k_1}\right] \\
&= \frac{1}{N}\text{Tr}\left[Z(n_1, n_2)\Gamma_{k_1+k_2}\Gamma_{k_3} - Z(n_3, n_2)\Gamma_{k_3+k_2}\Gamma_{k_1}\right] \\
&= \left[Z(n_1, n_2)Z(n_1 + n_2, n_3) - Z(n_3, n_2)Z(n_3 + n_2, n_1)\right]\frac{\text{Tr}\Gamma_0}{N} \\
&= \left[Z(n_1, n_2)Z(n_1 + n_2, n_3) - Z(n_3, n_2)Z(n_3 + n_2, n_1)\right]. \quad (4.31)
\end{aligned}
$$

Clearly this is the sort of procedure which lends itself to automation very well.

In order to treat quarks in this formulation, we must express them in this new colour basis [40]. This is most easily done by introducing an additional $SU(N')$ symmetry group for the quarks, this is known as the smell group [41]. Here we take $N' = N$. We must modify the quark action to take this into account. Take the mass term (MT) as an example. In the ordinary colour basis we write

$$MT = \sum_{c=1}^{N} \bar{\psi}_c(x)\psi_c(x). \tag{4.32}$$

We introduce N copies of this, one for each smell,

$$MT = \sum_{c,s=1}^{N} \frac{1}{N}\bar{\psi}_{sc}(x)\psi_{cs}(x), \tag{4.33}$$

where the quarks are now $N \times N$ matrices in colour–smell space, and we have used

$$\overline{\psi_{cs}(x)} = \bar{\psi}_{sc}(x). \tag{4.34}$$

The sums now just give the trace, so we have

$$MT = \frac{1}{N}\text{Tr}\bar{\psi}(x)\psi(x). \tag{4.35}$$

This is general, for any term in the quark action, we replace the quark fields by colour–smell matrix fields, and take the trace. Analogous to (4.15) we have the Fourier expansion of the quark field

$$\psi_{sc}(x) = \frac{1}{NL^4} \sum_k (\Gamma_k)_{sc} e^{ik\cdot x} \psi(p).$$

(4.36)

With this modification, the colour factors for the quark actions are just

$$C^f(\bar{p}, k_1, \cdots, k_r, p) = \frac{1}{N} \text{Tr} \left[\Gamma_{\bar{p}}^\dagger \Gamma_{k_1} \cdots \Gamma_{k_r} \Gamma_p \right],$$

(4.37)

where p ($\bar{p}$) is the incoming (outgoing) quark momentum. These factors can be worked out by using (4.25) and (4.26). Again, they are easy to automate.

Triple Twists

One can take these boundary conditions one step further and twist in the z direction as well. By going through the derivations of the Ω twist matrices again, one finds that all of our previous results hold, with one further condition [42]

$$n_3 = (n_2 - n_1)(\text{mod} N).$$

(4.38)

So in addition to the zero-mode being eliminated by $n_1 = n_2 = 0$, all modes that do not satisfy this new condition are gone. This eliminates many momenta from sums.

4.3 Results in α_0

We return to the results of our perturbative calculations. All of the results in this section have been derived using triple twisted periodic boundary conditions. To perform the mode sums we used the following identity:

$$\sum_{n=0}^{N-1} f(n) = \int_0^N f(\text{INT}(x)) dx,$$

(4.39)

where $\mathrm{INT}(x)$ is x truncated to an integer. This allows us to evaluate sums over lattice momentum using the VEGAS numerical integration routine.

We start by considering the static quark potential. We can use it to define a renormalized coupling α_V, which can be used as the expansion parameter for other quantities. To compute the static quark potential we take the correlator of two Wilson lines of length L_T, separated by a distance R, $< \Theta(R, L_T) >$. The static quark potential is then given by

$$V(R) + 2E_0 = \lim_{L_T \to \infty} \frac{-1}{L_T} \ln < \Theta(R, L_T) >, \tag{4.40}$$

where E_0 is the self-energy of an isolated quark (see below for our calculation of this quantity). Expanded in the bare coupling the static quark potential should have the following form [35]

$$
\begin{aligned}
V(R) &= -\frac{4}{3} \frac{\alpha_{\text{latt}}}{R} \\
&\times \{1 + \alpha_{\text{latt}} (2\beta_0 \ln(\pi R) + C(R))\},
\end{aligned}
\tag{4.41}
$$

where $\beta_0 = (11 - 2/3 n_f)/(4\pi)$ and $C(R)$ is a function of R which goes to a constant as $R \to \infty$.

As mentioned in chapter 2, the static quark potential is used to define a renormalized coupling. This is done by demanding that the Fourier transform of (4.41) have the form

$$V(q) = -\frac{4}{3} \frac{4\pi}{q^2} \alpha_V(q). \tag{4.42}$$

Using this definition, we obtain the expansion for the bare coupling in terms of the physical one,

$$
\begin{aligned}
\alpha_{\text{latt}} &= \alpha_V \left\{ 1 - \alpha_V \left(2\beta_0 \ln \left(\frac{\pi}{q} \right) + \tilde{C} \right) \right. \\
&\left. + \mathcal{O}(\alpha_V^2) \right\}.
\end{aligned}
\tag{4.43}
$$

Note that by explicitly doing the Fourier transform, we have

$$\tilde{C} = C(R \to \infty) + 2\beta_0 \gamma_E, \tag{4.44}$$

where $\gamma_E = 0.57722\ldots$ is Euler's constant.
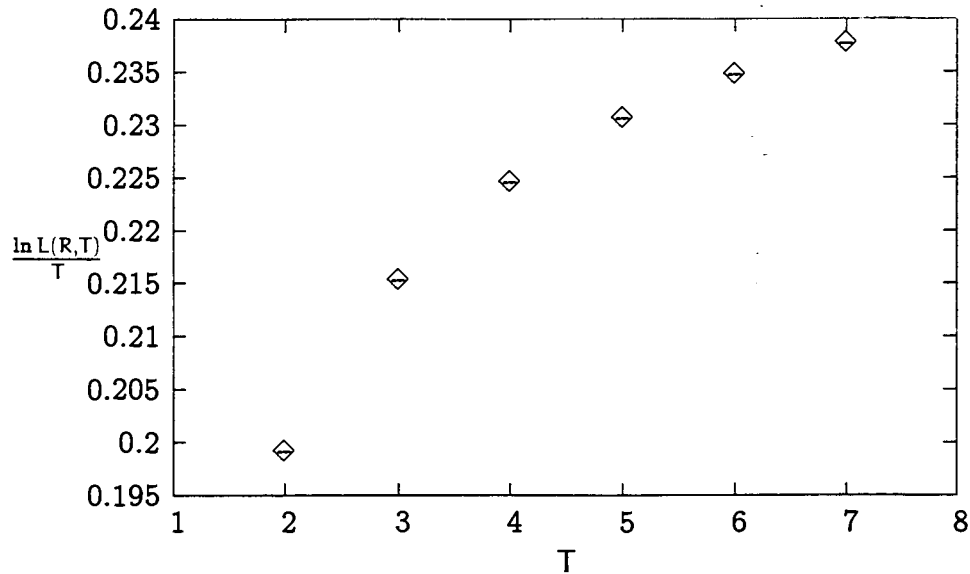
Figure 4.1: Leading order correlator of Wilson lines for R = 3, using (4.3).

Fitting V(R)

Extracting V(R) from the correlations is quite difficult, we will outline the procedures in some detail. The central problem is that we are computing

$$V(R) + 2E_0 = \lim_{T \to \infty} \frac{-1}{T} \ln < \Theta(R, T) > . \tag{4.45}$$

The trouble is that $V(R) \approx \frac{1}{R}$ and $E_0 =$ constant, so the signal we want is swamped as we increase R. As we shall see, this problem is very hard to surmount.

To extract V(R) we start by taking the $T \to \infty$ of a number of correlators, $\frac{-1}{T} \ln \langle \Theta(R, T) \rangle$, at a number of fixed R values. Figures 4.1 and 4.2 show the correlators at R = 3. We fit functions of the form $a + b/T + c/T^2$ to them and keep only the constant part a. We do this for 9 values of R from 1 to 9. This gives values for $V(R) + 2E_0$. The NLO piece is shown in figure 4.3, the "swamping" of the 1/R potential is clear.

We can do somewhat better by globally fitting all of the data to a function of the two variables R and T. We can use Bayesian fitting methods [43]. In this
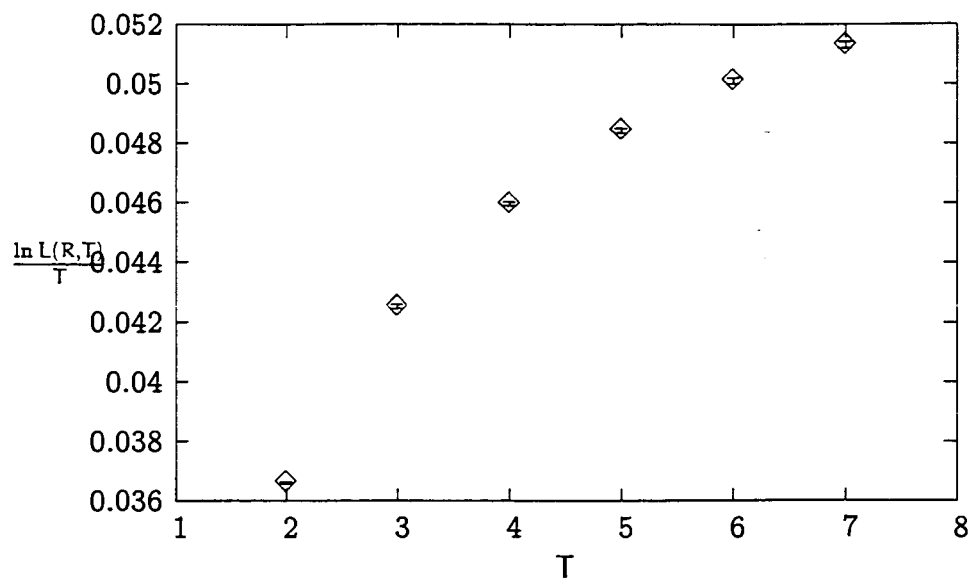
Figure 4.2: Next to leading order correlator of Wilson lines for R = 3, using (4.3).
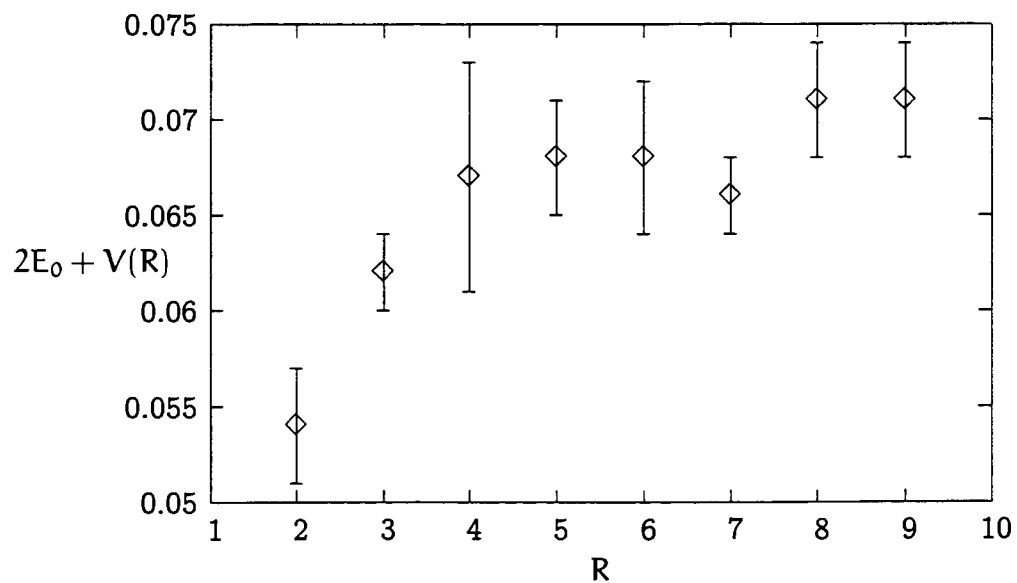
Figure 4.3: Next to leading order potential and self-energy, using (4.3).

approach we try a fitting function with many parameters

$$f(R, T) = f_0 + \frac{f_1}{R} + \frac{f_2}{T} + \frac{f_3}{RT} + \cdots. \tag{4.46}$$

The Bayesian fitting routine allows us to use a large number of parameters, increasing the quality of the fits. We can also make use of the known form of the potential, and independent determinations of the self-energy (see below) to fix some of the terms in the fitting function. For example we can fix $f_0 = 2E_0$, using our calculation of E_0 reported below. Even with these techniques, the results are still hard to extract, and the fundamental problem of suppression with $1/R$ is hard to surmount.

As a test of our calculations we reproduced the known result for the Wilson gluon action, $\tilde{C} = 4.70$. We have also determined $\tilde{C}$ for the improved gluon actions. Using (4.3) we fine

$$\tilde{C}_{I1} = 2.94(77), \tag{4.47}$$

and with (4.5) we have

$$\tilde{C}_{I2} = 3.537(2). \tag{4.48}$$

We could easily recompute $\tilde{C}$ for other gluon (and quark) actions, and with other definitions of u_0.

In addition to the static quark potential, we have computed a number of other quantities. Tables 4.1, 4.2, and 4.3 give results for the logarithms of small Wilson loops, whose perturbative expansion is defined by,

$$-\frac{1}{2(R+T)} \ln W(R, T) = \sum_n w_n(R, T)\alpha_{\text{latt}}^n. \tag{4.49}$$

We also give results for the scale q^* in table 4.1 and 4.2, the scales for the one loop improved action (4.5) are the same as those reported in table 4.2 for the tree level action (4.3). The results for the Wilson action agree with those of [44].

We have also computed the static quark self-energy E_0 through second order. We define the self-energy $E_0(L)$ on a finite lattice according to

$$E_0(L) = -\frac{1}{L} \ln[P_t(L)] = \sum_n c_n(L)\alpha_{\text{latt}}^n. \tag{4.50}$$

R	T	w_1	w_2	q^*
1	1	1.0471(4)	3.548(7)	3.358(8)
1	2	1.2041(2)	4.460(5)	3.014(8)
1	3	1.2589(2)	4.816(6)	2.931(9)
2	2	1.4342(3)	5.841(7)	2.591(8)
2	3	1.5177(3)	6.41(1)	2.525(8)
3	3	1.610(1)	7.09(4)	2.446(8)

Table 4.1: Perturbative Wilson loops evaluated using Wilson glue, errors are from the VEGAS integrations.

R	T	w_1	w_2	q^*
1	1	0.7673(2)	1.562(4)	3.322(7)
1	2	0.9255(2)	2.059(8)	3.031(8)
1	3	0.9849(2)	2.28(2)	2.851(8)
2	2	1.1503(3)	2.85(2)	2.595(8)
2	3	1.2342(3)	3.22(4)	2.48(1)
3	3	1.3231(4)	3.55(6)	2.31(1)

Table 4.2: Perturbative Wilson loops evaluated using (4.3).

R	T	w_1	w_2
1	1	0.7673(2)	2.070(4)
1	2	0.9255(2)	2.796(8)
1	3	0.9849(2)	3.11(2)
2	2	1.1503(3)	3.93(2)
2	3	1.2342(3)	4.43(4)
3	3	1.3231(4)	4.91(6)

Table 4.3: Perturbative Wilson loops evaluated using (4.5).

Here $P_t(L)$ is the Wilson line on a lattice of size L^4. For an infinite volume lattice, we consider lines of length L, which are gauge variant, and extrapolate $L \to \infty$. The infinite volume extrapolation agrees with earlier estimates, $E_0 = 2.1172\alpha_{\text{latt}} + 11.152\alpha_{\text{latt}}^2$. The finite volume results were used in a determination of the third order self-energy, using Monte-Carlo methods [42].

Finally, we have computed the mean link in Landau gauge. In agreement with earlier determinations we have for the Wilson action,

$$u_0 = 1 - 0.9738(2)\alpha_{\text{latt}} - 3.33(1)\alpha_{\text{latt}}^2. \tag{4.51}$$

For the tree level Symanzik improved action (4.3) we have the new result

$$u_0 = 1 - 0.7501(1)\alpha_{\text{latt}} - 1.5(1)\alpha_{\text{latt}}^2, \tag{4.52}$$

and for the one-loop Symanzik improved action (4.5) we report,

$$u_0 = 1 - 0.7501(1)\alpha_{\text{latt}} - 2.19(1)\alpha_{\text{latt}}^2. \tag{4.53}$$

The methods for automatic vertex generation can also be readily applied to complicated fermionic actions. For example, we computed the n_f part of the average plaquette at second order for improved staggered fermions [11]. We find: $w_2(1,1) = 1.958(2) - 0.06969(4)n_f$.

4.3.1 Application of these results

As we outlined at the end of chapter 2 the results in this chapter can be used in conjunction with non-perturbative simulations to extract the strong coupling constant, α_s. In practice, the methods outlined here do not provide the most practical way of doing the perturbation theory for the connection between α_V and α_{latt}. Other methods have been used, to rederive these results with lower errors, and to higher orders[45].

The results presented in this chapter came before [45], and provided very valuable independent checks of these newer results, which use a background field technique for the matching, rather than the static potential.

Another use for the perturbative potential reported here is to provide another, independent, determination of α_s from Monte Carlo simulations, using measured values of the static potential at short distances, instead of small Wilson loops. The perturbation theory will eventually be used to correct the simulation results of the static potential for lattice discretization errors.

Chapter 5

Fermilab Quarks

As we discussed in chapter 1, a central problem in high-energy phenomenology is to determine the elements of the CKM matrix. Looking at (1.9) it's clear that those involving heavy quarks are not known very well. Furthermore, the complex phase of the matrix, related to the parameters ρ and η in the Wolfenstein parametrization (1.10), are only accessible via the heavy quark sector of this matrix.

This alone makes heavy quark physics a relevant subject for study. Combined with the active experimental program in this field, heavy quark physics has been and continues to be a very active area. Clearly we would like to be able to attack problems in this field with lattice field theory techniques.

5.1   Heavy quarks on the lattice

There is a problem with doing heavy quark physics on the lattice. The scale $m_Q a$ is not much less than one (at least at currently used, and foreseeable, lattice spacings). Practically what this means is that heavy quarks have a Compton wavelength $1/m_Q$ that is comparable to the lattice spacing a. This means that the heavy quark's dynamics do not get resolved by the simulations. There are a large number of ways that have been proposed to deal with this. In this report we will be focused on the Fermilab approach to heavy quark physics. However it will be very useful to review

a more traditional approach; the heavy quark effective theory. This approach shares common themes and language with the Fermilab method.

The heavy quark effective theory method is to explicitly integrate the heavy quarks out of the theory, treating their dynamics in some systematic expansion. This approach has been widely used in the continuum [46] to address problems in heavy quark physics.

To use this approach, one needs an expansion parameter. In systems with one heavy, and one light, quark, the expansion parameter is $1/M_Q$. By taking the $M_Q \to \infty$ limit of QCD one constructs the heavy quark effective theory[1](HQET)

$$S_{\text{HQET}} = \int d^4 x \bar{Q}_v(x) i D_t Q_v(x) + \mathcal{O}\left(\frac{1}{M_Q}\right). \tag{5.1}$$

This the continuum Minkowski space version of the theory. The heavy quark fields Q_v are related to the continuum fields Q, at tree level, by

$$Q_v(x) = e^{i M_Q t} \frac{1 + \gamma_4}{2} Q(x). \tag{5.2}$$

In the same manner as a lattice theory, HQET can be "improved" by systematically correcting the action. Each correction is suppressed by $\alpha_s^n M_Q^{-m}$, so we can always (in principle) make the theory as close to full QCD as we'd like. Just like the lattice improvement program, tree level corrections (those for which $n = 0$) need to be perturbatively matched to get full agreement.

This program can be implemented on the lattice. At tree level, and to $\mathcal{O}(1/M_Q)$, one has

$$S_{\text{LHQET}} = \sum_x \bar{Q}_v(x) U_4(x) Q_v(x + \hat{\mu}). \tag{5.3}$$

Just like the continuum theory, this action has $1/M_Q$ errors, as well as $\mathcal{O}(a^2)$ errors. These can be systematically corrected for, and perturbative errors removed.

Another approach along these lines is nonrelativistic QCD (NRQCD). NRQCD is used to describe systems with more than one heavy quark. In NRQCD the

---

[1]For the sake of simplicity we are writing all HQET expressions in the rest frame $v = (1, 0, 0, 0)$. More general expressions can be found in [46].

expansion parameter is the relative velocity of the system with two heavy quarks. With this counting the tree level continuum theory to $\mathcal{O}(v^2)$ is

$$S_{\text{NRQCD}} = \int d^4x \psi^\dagger(x) \left[iD_t + \frac{\vec{D}^2}{2M} \right] \psi(x). \tag{5.4}$$

Not surprisingly, this is just the Schrödinger action, with a non-abelian gauge interaction. Just as with HQET, corrections to this action can be considered, and a lattice theory can be developed [47].

5.2   The Fermilab Approach

Heavy quark and nonrelativistic approaches work very well for situations involving a b quark. In this case the scales m_b^{-1} and v_b are typically very small, so lattice versions of HQET and NRQCD can be applied. The situation with the charm quark is more complicated. In this case $m_c a \approx 1$ so expansions in either small or large ma may not be viable [48]. It would be desirable to have a formulation which was valid for all quark masses, large or small. This is provided by the Fermilab approach [49].

The basic idea behind the Fermilab approach is to make all the relevant coefficients in the action mass dependent, rather than fixed to the large mass limit. In addition, the space and time directions are separated in order to allow for a smooth transition from light to heavy quarks. The remainder of this chapter will focus on detailing the Fermilab approach, and in the following chapter we will outline our perturbative calculations using these actions.

The Fermilab action, proposed in [49], is analogous to (2.9) and is given by (with the lattice spacing restored)

$$\begin{aligned} S \;=\; & a^4 \sum_x \bar{\psi}_0(x) \left[m_0 + \frac{1+\gamma_4}{2} D_4^- - \frac{1-\gamma_4}{2} D_4^+ + \zeta_0 \vec{\gamma} \cdot \vec{D} \right. \\ & \left. - \frac{a r_s \zeta_0}{2} \triangle^{(3)} - \frac{i a c_B^0 \zeta_0}{2} \vec{\Sigma} \cdot \vec{B} - \frac{a c_E^0 \zeta_0}{2} \vec{\alpha} \cdot \vec{E} \right] \psi_0(x), \tag{5.5} \end{aligned}$$

where we have put a 0 on all the bare quantities and used the following definitions for the various operators

$$T_\mu \psi(x) = U_\mu(x)\psi(x + a\hat{\mu}),$$

$$T_{-\mu}\psi(x) = U_\mu^\dagger(x - a\hat{\mu})\psi(x),$$

$$D_4^+ \psi(x) = \frac{1}{a}(T_4 - 1)\psi(x),$$

$$D_4^- \psi(x) = \frac{1}{a}(1 - T_{-4})\psi(x),$$

$$D_i \psi(x) = \frac{1}{2a}(T_i - T_{-i})\psi(x),$$

$$\triangle^{(3)}\psi(x) = \frac{1}{a^2}(T_i + T_{-i} - 2)\psi(x),$$

$$B_i = \frac{1}{2}\epsilon_{ijk}F_{jk},$$

$$E_i = F_{0i}, \quad \text{and}$$

$$F_{\mu\nu}\psi(x) = \frac{1}{8a^2}\sum_{\bar{\mu}=\pm\mu,\bar{\nu}=\pm\nu} \text{sign}(\bar{\mu}\bar{\nu})\,(T_{\bar{\mu}}T_{\bar{\nu}}T_{-\bar{\mu}}T_{-\bar{\nu}} + \text{H.C.})\,\psi(x).$$

The key feature of this action is that the couplings (r_s, ζ, c_B and c_F) are mass dependent. In fact *no* assumptions are made, *a priori* about the bare mass m_0. As well, the space and time directions are split apart. We expect that as $m_0 \rightarrow 0$ we should recover the clover action, and for $m_0 \rightarrow \infty$ we should find $\zeta \rightarrow 0$ (with $c_B\zeta$ fixed) to recover the heavy quark limit. The only expansion made here is in pa, the quark momentum, this is why the Fermilab approach works well at any mass.

This action has been used by the group at Fermilab to address many problems in heavy quark physics [50],[51]. Unlike other actions in wide use, it is specifically designed to work for any quark mass. In particular, the region $ma \approx 1$ is a region where many other approaches either fail or require error-prone extrapolations. On typical lattice spacings $ma = 1$ corresponds to roughly the physical charm quark mass, so for D meson studies the Fermilab action is very useful.

The Fermilab action works for heavy quarks because the dominant mass dependence is carried in the coefficients of the action, and not simulated in the computer.

For example, if one tried to simulate a very heavy quark using (2.9), the problems discussed above would apply. The simulation simply would not "catch" the dynamics of the heavy quark. On the other hand, with the Fermilab action, the coefficients are tuned such that one would basically be working with the HQET action (5.1).

Tree level determination

To see how the various coefficients change with the bare mass, we will outline how the tree level determination of ζ, c_B and c_E is done. This follows the discussion in [49], interested readers can find more technical details there.

To begin we note that the operator $\triangle^{(3)}$ is redundant, it can be removed by a field transformation. This means we are free to take its coefficient r_s to be whatever value we want (typically we take $r_s = 1$). As well, the bare mass m_0 is an input parameter, so it is fixed. We want to determine how ζ, c_B and c_E depend on it.

The coefficient ζ can be determined by looking at the propagator for the free fermion field. This will actually tell us a lot about the way the Fermilab theory works. By setting all the interactions in (5.5) to zero, and going to p space it is straightforward to derive the propagator

$$S_F^{-1}(p_0, \vec{p}) = i\gamma_0 \sin(p_0 a) + ia\vec{\gamma} \cdot \vec{S} - \cos(p_0 a) + \mu(\vec{p}), \qquad (5.6)$$

with

$$S_i = \zeta \frac{\sin(p_i a)}{a}, \quad \mu(\vec{p}) = 1 + m_0 a + \frac{r_s \zeta a^2}{2} \hat{\vec{p}}^2, \quad \hat{p}_i = \frac{2}{a} \sin\left(\frac{p_i a}{2}\right).$$

We rewrite S_F as

$$S_F(p_0, \vec{p}) = \frac{-i\gamma_0 \sin(p_0 a) - ia\vec{\gamma} \cdot \vec{S} - \cos(p_0 a) + \mu(\vec{p})}{\sin^2(p_0 a) + a^2 \vec{S}^2 + [\mu(\vec{p}) - \cos(p_0 a)]^2}. \qquad (5.7)$$

Using (5.7) we can determine the dispersion relation for these fermions. To do this, we set $p_0 = iE(\vec{p})$ and solve for the point where the denominator vanishes.

Doing this, we find that the energy is given by

$$\cosh(Ea) = \frac{1 + a^2 \vec{S}^2 + \mu^2(\vec{p})}{2\mu(\vec{p})}. \tag{5.8}$$

One of the important distinctions between Fermilab fermions and clover fermions is that $m_0 a$ is not assumed to be small. Accordingly we expand (5.8) in powers of $p_i a$. This gives

$$E^2(\vec{p}) = M_1^2(m_0 a) + \frac{M_1(m_0 a)}{M_2(m_0 a)} \vec{p}^2 + \mathcal{O}(p^4 a^2), \tag{5.9}$$

where

$$M_1 a = \log(1 + m_0 a), \quad M_2 a = \left[\frac{2\zeta^2}{m_0 a(2 + m_0 a)} + \frac{r_s \zeta}{1 + m_0 a} \right]^{-1}. \tag{5.10}$$

We can impose conditions on (5.9) to determine ζ. The most obvious case would be to duplicate the continuum dispersion relationship, up to the spacing errors. This would require setting $M_1 = M_2$. Doing this, and solving for ζ gives (in $a = 1$ units, here and henceforth)

$$\zeta_{M_1 = M_2} = \sqrt{\left(\frac{r_c m_0(2 + m_0)}{4(1 + m_0)} \right)^2 + \frac{m_0(2 + m_0)}{2 \log(1 + m_0)}} - \frac{r_c m_0(2 + m_0)}{4(1 + m_0)}. \tag{5.11}$$

This gives

$$E^2 = M_1^2 + \vec{p}^2 + \mathcal{O}(p^2 a^4)$$

which is the continuum dispersion relationship for a quark of mass M_1.

Enforcing $M_1 = M_2$ is the most obvious way to set ζ but it is perhaps not the most useful. Assume we want to simulate a heavy quark, at some fixed (not necessarily small or large) $m_0 a$. Taking the square root of (5.9) gives

$$E = M_1 + \frac{\vec{p}^2}{2M_2} + \mathcal{O}(p^4 a^2). \tag{5.12}$$

For simulating a nonrelativistic quark with physical mass m_q we would demand $M_2 = m_q$ and forget about M_1, since the rest mass only produces an overall energy shift. This gives

$$\zeta_{m_q = M_2} = f(m_0) \left[\sqrt{1 + \frac{2}{m_q f(m_0)}} - 1 \right], \quad f(x) = \frac{r_s x(2 + x)}{4(1 + x)}. \tag{5.13}$$

This is appealing, since for large m_q, $\zeta \approx 0$, which would give the HQET action if we varied r_s to keep $r_s \zeta$ constant.

A third approach to setting ζ, the one used in practice, is to once again forget about M_1, but fix $\zeta = 1$. Then the physical quark mass is give by $M_2(m_0) = m_q$. This has technical advantages in the simulations, and is conceptually simple. In this case (5.10) provides the connection between m_0 and M_2 with $\zeta, r_s = 1$. On a a $= 0.1$ fm lattice, to simulate $m_q = 2$ GeV (approximately the charm quark mass) means that we need to take $m_0 a = 1.17$, which is right in the intermediate region. As this is the approach used in simulations, all of our numerical results will be presented with $\zeta = 1$. However all of the expressions in this report will be for general ζ so other methods can be used.

There is one more important quantity to be considered related to (5.7), the fermion wavefunction renormalization factor Z_2. To find this we consider the residue of the propagator (5.7) at $p_0 = iE(\vec{p})$. Using the full dispersion relation (5.8) the residue is

$$Z_2(\vec{p}) = \mu^{-1}(\vec{p}) = \frac{1}{1 + m_0 + \frac{r_s \zeta_0}{2}\vec{p}^2}. \tag{5.14}$$

Unlike the continuum theory, this is dependent on the three momentum. To define a wavefunction renormalization we use the $\vec{p} = 0$ value,

$$Z_2 = \frac{1}{1 + m_0} = e^{-M_1}.$$

For processes with external particles not at rest, we need to use the full Z. This definition has been chosen to conform to the conventions of [49], we will introduce a slightly different convention in the following chapter.

Fixing c_B and c_E

With zeta fixed at tree level, we turn to the improvement terms. Just as with the improvement discussed in chapter 2, we compute the scattering of a quark off of some background gluon field and demand that the $O(a)$ difference from the

continuum result vanish, by tuning c_B and c_E. This procedure will reproduce the results from [49], valid for all bare masses,

$$c_B = r_s, \quad c_E = \frac{\zeta^2 - 1}{m_0(2 + m_0)} + \frac{r_s\zeta}{1 + m_0} + \frac{r_s^2 m_0(2 + m_0)}{4(1 + m_0)^2}. \tag{5.15}$$

We will not reproduce the derivation of these here, as in the following chapter an automatic method will be presented. The analytic derivation of these results (using a different method) is presented in [49]. There is a minor subtlety concerning c_E which bears discussing. The Fermilab action we have been working with is correct only up to $\mathcal{O}(pa)$. If we wanted to correct to the next order we would need to add a number of new operators to the action [52], one of which is the spin–orbit term

$$\frac{c_{so}\zeta}{2}\bar{\psi}\gamma_0 \left[\vec{\gamma} \cdot \vec{D}, \vec{\gamma} \cdot \vec{E}\right] \psi. \tag{5.16}$$

This additional operator will affect the matching of c_E at tree level, giving

$$c_E = \frac{\zeta^2 - 1}{m_0(2 + m_0)} + \frac{r_s\zeta}{1 + m_0} + \frac{r_s^2 m_0(2 + m_0)}{4(1 + m_0)^2} + \frac{c_{so}m_0(2 + m_0)}{\zeta(1 + m_0)}. \tag{5.17}$$

Our results will correspond to $c_{so} = 0$.

5.2.1 Tadpole improvement of the Fermilab action

We saw in chapter 3 that tadpole diagrams can ruin the naive estimates of perturbative errors. The examples that we considered there all pertained to gluon actions, however the same issues plague us here. For example, the one loop diagrams for the fermion self energy are shown in figure 5.1. The second diagram is the tadpole, which has no continuum analogue. Calculation of the self energy [53] (and chapter 6) reveals that the tadpole diagram, in Feynman gauge, is very large.

Once again, if we hope to have accurate perturbative determinations of the Fermilab action parameters, we need to remove these large tadpoles. As we saw in chapter 2 one way to do this is to tadpole improve the action.

To tadpole improve the Fermilab action we write all links U as

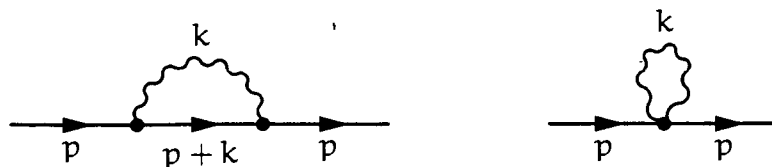$$U = \frac{u_0 U}{u_0} = u_0\tilde{U}.$$

Figure 5.1: Self energy diagrams for lattice fermions

Here u_0 is some estimate of the average value of a link field. Rewriting the action in terms of $\tilde{U}$, we find

$$S = u_0 \sum_x \bar{\psi}_0(x) \left[\tilde{m}_0 + \frac{1+\gamma_4}{2} D_4^- - \frac{1-\gamma_4}{2} D_4^+ + \zeta_0 \vec{\gamma} \cdot \vec{D} \right.$$
$$\left. - \frac{r_s \zeta_0}{2} \triangle^{(3)} - \frac{i \tilde{c}_B^0 \zeta_0}{2} \vec{\Sigma} \cdot \vec{B} - \frac{\tilde{c}_E^0 \zeta_0}{2} \vec{\alpha} \cdot \vec{E} \right] \psi_0(x), \qquad (5.18)$$

where all the derivatives are now written using the $\tilde{U}$ link, and

$$\tilde{m}_0 = \frac{m_0}{u_0} + \{1 + 3 r_s \zeta\} (u_0^{-1} - 1), \quad \tilde{c}_{B,E} = u_0^3 c_{B,E}. \qquad (5.19)$$

Perturbative calculations with this action are straightforward. We compute in bare perturbation theory, and then use (5.19) with a u_0 taken either from the mean link, or the fourth root of the plaquette. We can use the values for u_0 from chapter 4 to compute the tadpole improved couplings.

5.3 Lattice calculations of hyperfine splittings

The calculations we will outline in the next section will have a broad impact on a number of areas in high energy phenomenology, there is one area that we want to highlight here.

One of the easiest things to measure in a heavy quark simulation is the hyperfine splitting

$$\Delta_M = M_{J/\psi} - M_{\eta_c}.$$

The experimental value for this quantity is

$$\Delta_M = 117.7(1.3) \text{ MeV}.$$

The hyperfine splitting is important, because it impacts upon determinations of the bound state wavefunction at the origin. The bound state wavefunction at the origin is related to decay constants (for example, f_B), so if we are to have confidence in lattice QCD determinations these important quantities it is important to understand the hyperfine splittings, and get good agreement with experiments.

The trouble is that lattice simulations all seem to significantly underestimate this quantity. For many years quenched simulations ([54], [55]) found results that were up to $\approx 50\%$ lower than the measured number. It was suspected that this discrepancy was due to the quenched approximation, however early results with the unquenched MILC configurations [56] showed that this problem remained. A more recent unquenched simulation gives [50]

$$\Delta_M = 97(2) \text{ MeV},$$

which is around 20% off. The various determinations of this quantity have been done by different groups using very different actions, so the disagreement is not a consequence of using a particular formulation of lattice fermions.

This sort of hyperfine splitting is a fairly easy thing to calculate in lattice QCD, so the statistical errors are not a factor. As the discussion of chapter 2 makes clear, it is likely that there are uncorrected systematic errors we should look for. The results of [50] do not show any strong dependence on the light sea quark masses, suggesting that the chiral extrapolation of this quantity is well-behaved. This leaves only lattice spacing errors, and perturbative errors as the most likely sources.

The coefficients of the Fermilab action used in [50] are only mean field tadpole improved. This leaves $(\alpha_s a \Lambda_{QCD})$ errors. This can easily give 10% or larger corrections. The operators that directly affect the hyperfine splittings are

$$\vec{\gamma} \cdot \vec{D} \quad \text{and} \quad \vec{\sigma} \cdot \vec{B}.$$

This means that we need to compute the perturbative corrections to ζ and c_B in order to determine the effect perturbative corrections have on the hyperfine splitting.

The other source of error is due to the finite lattice spacing. With $\Lambda_{QCD} \approx 300$ MeV, $(\Lambda_{QCD}a)^2 \approx 0.04$ so at least some of the error is due to lattice spacing effects. The full dimension 6 Fermilab action will fix this. The situation is better in NRQCD, since a fully $\mathcal{O}(a^2)$ action is known, however the coefficients are only mean-field tadpole improved in this case as well.

Chapter 6

Matching Calculations for Fermilab Quarks

6.1 Renormalization of the Fermilab action

For the tree level matching we discussed in the previous chapter we worked with the bare parameters of the Fermilab action. This is, of course, acceptable, since any differences between the bare and renormalized theories would occur at $\mathcal{O}(\alpha)$. For matching at one loop order, however, it will be important to understand how the Fermilab action gets renormalized. We start with the bare action

$$
\begin{aligned}
S \; = \; & \sum_x \bar{\psi}_0(x) \left[m_0 + \frac{1+\gamma_4}{2} D_4^- - \frac{1-\gamma_4}{2} D_4^+ + \zeta_0 \vec{\gamma} \cdot \vec{D} \right. \\
& \left. - \; \frac{r_s \zeta_0}{2} \triangle^{(3)} - \frac{i c_{B,0} \zeta_0}{2} \vec{\Sigma} \cdot \vec{B} - \frac{c_{E,0} \zeta_0}{2} \vec{\alpha} \cdot \vec{E} \right] \psi_0(x),
\end{aligned}
\tag{6.1}
$$

and investigate the transition to a renormalized action[1].

We digress here briefly on our notation. We are computing the perturbation series for a number of quantities. Consider a general quantity, denoted by Δ. We

---

[1]We do not use subscripts to denote the renormalized parameters, however we have been careful to always use a 0 subscript on all bare parameters.

will write the perturbation expansion of this as

$$\Delta = \Delta^{[0]} + g_0^2 \Delta^{[1]} + \cdots. \tag{6.2}$$

So $\Delta^{[n]}$ is the n-loop contribution, using the bare coupling g_0 as the expansion parameter.

We begin with the field renormalization, which requires some care. Recall from the previous chapter, we found the full residue of the Fermilab propagator, at tree level, to be

$$\mathcal{Z}_2(\vec{p}) = \frac{1}{1 + m_0 + \frac{r_s \zeta}{2} \vec{p}^2}. \tag{6.3}$$

More generally, we write the residue as a function of the renormalized quantities as

$$\mathcal{Z}_2 = \mathcal{Z}(m, \zeta, \vec{p}) Z_2, \tag{6.4}$$

where

$$\mathcal{Z}(m, \zeta, \vec{p}) = \frac{1}{1 + m + \frac{r_s \zeta}{2} \vec{p}^2}, \tag{6.5}$$

and the wavefunction renormalization is

$$Z_2 = 1 + g_0^2 Z_2^{[1]} + \cdots. \tag{6.6}$$

Care must be taken to properly track the factors generated by $\mathcal{Z}$. At tree level, and with $\vec{p} = 0$ this is just the factor

$$\frac{1}{1 + m} = e^{-M_1^{[0]}}$$

which will multiply all zero-momentum external lines. This split emphasizes that external field lines obey the free field equations of motion, expressed in terms of the renormalized parameters. Then there are perturbative corrections to this, given by the series (6.6).

Next we consider the renormalization of the bare mass m_0 and Fermilab parameter ζ_0. We have no conditions on the bare mass, so we simply write

$$m = m_0 + g_0^2 m^{[1]}. \tag{6.7}$$

We also have

$$\zeta = \zeta_0 + g_0^2 \zeta^{[1]}.$$
(6.8)

To determine $\zeta^{[1]}$ we look at the tree level expression for the kinetic mass (5.10)

$$M_2^{[0]} = \left[\frac{1}{m_0(2 + m_0)} + \frac{r_s \zeta_0}{1 + m_0} \right]^{-1}.$$
(6.9)

It's convenient [53] to rewrite this as

$$M_2^{[0]} = m_2(\zeta_0, M_1^{[0]}), \quad m_2(x, y) = \frac{e^y \sinh y}{x^2 + r_s x \sinh y}, \quad M_1^{[0]} = \log(1 + m_0), \quad (6.10)$$

and define the full expression for the mass as

$$M_2 = Z_{M_2}(m_0, \zeta_0) m_2(\zeta_0, M_1).$$
(6.11)

This contains two perturbative factors; the full expression for

$$M_1 = \log(1 + m_0) + g_0^2 M_1^{[1]} + \cdots,$$

and an "intermediate" renormalization factor,

$$Z_{M_2}(m_0, \zeta) = 1 + g_0^2 Z_{M_2}^{[1]} + \cdots.$$

The latter factor captures the renormalizations of M_2 not shared by M_1.

Using this notation we *define* the renormalized parameter ζ according to

$$M_2 = m_2(\zeta, M_1).$$
(6.12)

That is, the *physical* kinetic mass must be the same expressed in terms of the renormalized and bare parameters. The renormalized quantities M_1, M_2 and ζ are connected by the same relation (6.12) as the tree-level quantities $M_1^{[0]}$, $M_2^{[0]}$ and ζ_0 in (6.10). This will prove to be very convenient when computing radiative corrections to a scattering amplitude in renormalized perturbation theory; equation (6.12) will ensure that the leading-order amplitude in the lattice effective theory remains properly matched to the leading-order amplitude in the continuum theory,

when both are evaluated at the same renormalized quark mass. The $O(g^2)$ radiative correction to an action parameter such as c_B will then come entirely from one-loop Feynman diagrams.

The condition on M_2 fixes $\zeta^{[1]}$, to get an explicit expression we expand both (6.11) and (6.12) out to $O(g_0^2)$. For (6.11) we have

$$M_2 = m_2(\zeta_0, M_1^{[0]}) + g_0^2 Z_{M_2}(\zeta_0, m_0) + g_0^2 M_1^{[1]} \frac{\partial m_2(\zeta_0, M_1^{[0]})}{\partial M_1^{[0]}},$$

and for (6.12) using $\zeta = \zeta_0 + g_0^2 \zeta^{[1]}$,

$$M_2 = m_2(\zeta_0, M_1^{[0]}) + g_0^2 \zeta^{[1]} \frac{\partial m_2(\zeta_0, M_1^{[0]})}{\partial \zeta_0} + M_1^{[1]} \frac{\partial m_2(\zeta_0, M_1^{[0]})}{\partial M_1^{[0]}}.$$

Solving these for $\zeta^{[1]}$ gives

$$\zeta^{[1]} = Z_{M_2}(\zeta_0, m_0) \frac{m_2(\zeta_0, M_1^{[0]})}{\frac{\partial m_2(\zeta_0, M_1^{[0]})}{\partial \zeta_0}}. \tag{6.13}$$

For completeness, we compute the derivative, obtaining the final expression for the one-loop contribution to ζ

$$\zeta^{[1]} = -Z_{M_2}(\zeta_0, m_0) \frac{\zeta_0^2 + r_s \zeta_0 \sinh M_1^{[0]}}{2\zeta_0 + r_s \sinh M_1^{[0]}}. \tag{6.14}$$

Finally we need to address the renormalizations of c_B and c_E. We will be computing the one loop corrections to these parameters by matching scattering amplitudes between the continuum theory and our lattice theory. The scattering amplitudes will involve physical (i.e. renormalized) quarks and gluons, so it makes sense to set up a renormalized perturbation theory, and work in that. However, at the end we want the one loop correction to the *bare* quantities, as these are what will be input to lattice simulations.

We can expand the bare couplings as

$$c_{B,0}(\zeta_0, m_0) = c_{B,0}^{[0]}(\zeta_0, m_0) + g_0^2 c_B^{[1]}(\zeta_0, m_0) \tag{6.15}$$

and

$$c_{E,0}(\zeta_0, m_0) = c_{E,0}^{[0]}(\zeta_0, m_0) + g_0^2 c_E^{[1]}(\zeta_0, m_0). \tag{6.16}$$

Now we define the renormalized couplings as

$$c_B(\zeta, m) = c_B^{[0]}(\zeta, m), \quad c_E(\zeta, m) = c_E^{[0]}(\zeta, m). \tag{6.17}$$

Therefore at one loop we have,

$$c_{B,0}(\zeta_0, m_0) = c_B(\zeta, m) + g_0^2 c_B^{[1]}(\zeta_0, m_0), \tag{6.18}$$

and

$$c_{E,0}(\zeta_0, m_0) = c_E^{[0]}(\zeta, m) - g_0^2 \zeta_0 \left[\zeta_{[1]} \frac{\partial}{\partial \zeta_0} + \frac{M_1^{[1]}}{1 + m_0} \frac{\partial}{\partial m_0} \right] c_E^{[0]}(m_0, \zeta_0) + c_E^{[1]}(\zeta_0, m_0). \tag{6.19}$$

The derivative terms take into account the implicit difference between $c_E^{[0]}(m_0, \zeta_0)$ and $c_E^{[0]}(m, \zeta)$ that occur at one loop order. These terms are not present for c_B, since at tree level

$$c_B^{[0]}(m_0, \zeta_0) = c_B^{[0]}(m, \zeta) = r_s = \text{constant}. \tag{6.20}$$

We now have a complete set of renormalization factors

$$\psi_0 = \sqrt{1 + g_0^2 Z_2^{[1]}} \psi$$

$$m_0 = m - g_0^2 m^{[1]}$$

$$\zeta_0(m_0) = \zeta(m) - g_0^2 \zeta^{[1]}(m_0)$$

$$c_{B,0}(\zeta_0, m_0) = c_B(\zeta, m) + g_0^2 c_B^{[1]}(\zeta_0, m_0)$$

$$c_{E,0}(\zeta_0, m_0) = c_E^{[0]}(\zeta, m) - g_0^2 \zeta_0 \left[\zeta_{[1]} \frac{\partial}{\partial \zeta_0} + \frac{M_1^{[1]}}{1 + m_0} \frac{\partial}{\partial m_0} \right] c_E^{[0]}(m_0, \zeta_0) + c_E^{[1]}(\zeta_0, m_0).$$

The terms on the left hand side here are the original functions of the bare parameters. On the right hand side they are expressed as renormalized functions of the renormalized parameters, plus the one loop counterterms. This allows to write the Fermilab action as

$$S_0 = \left(1 + g_0^2 Z_2^{[1]} \right) S_r + g_0^2 \delta S, \tag{6.21}$$

where the renormalized action is

$$
\begin{aligned}
S_r \;=\; \sum_x \bar\psi(x) & \left[m + \frac{1+\gamma_4}{2} D_4^- - \frac{1-\gamma_4}{2} D_4^+ + \zeta \vec\gamma \cdot \vec{D} \right. \\
& \left. - \frac{r_s \zeta}{2} \triangle^{(3)} - \frac{i c_B \zeta}{2} \vec\Sigma \cdot \vec{B} - \frac{c_E \zeta}{2} \vec\alpha \cdot \vec{E} \right] \psi(x),
\end{aligned}
\tag{6.22}
$$

and the counterterms are

$$
\begin{aligned}
\delta S \;=\; a^4 \sum_x \bar\psi(x) & \left[-m^{[1]} - \zeta^{[1]} \left(\vec\gamma \cdot \vec{D} - \frac{r_s}{2} \triangle^{(3)} \right) \right. \tag{6.23} \\
& \left. - \frac{i \delta_B}{2} \vec\Sigma \cdot \vec{B} - \frac{\delta_E}{2} \vec\alpha \cdot \vec{E} \right] \psi(x).
\end{aligned}
$$

We have defined

$$
\delta_B = \zeta_0 c_B^{[1]}(m_0, \zeta_0) - \zeta^{[1]} c_B(\zeta_0, m_0)
\tag{6.24}
$$

and

$$
\delta_E = g_0^2 \zeta_0 c_E^{[1]}(m_0, \zeta_0) - \zeta^{[1]} c_E^{[0]}(m_0, \zeta_0) - \zeta_0 \left[\zeta^{[1]} \frac{\partial}{\partial \zeta_0} + \frac{M_1^{[1]}}{1 + m_0} \frac{\partial}{\partial m_0} \right] c_E^{[0]}(m_0, \zeta_0).
\tag{6.25}
$$

The results of our calculations that will be directly used as input to the simulations are the one-loop corrected values of $c_{E,0}$ and $c_{B,0}$ in the bare action (6.1), given by e.g.

$$
c_{E,0} = c_E^{[0]}(m_0, \zeta_0) + g^2 c_E^{[1]}(m_0, \zeta_0).
\tag{6.26}
$$

The expressions for the counterterms (6.24) and (6.25) are the connection we use to extract these quantities from our renormalized perturbation theory.

Before addressing the one loop results for $c_{B,E}^{[1]}$ we clearly need to compute $\zeta^{[1]}$ and $m^{[1]}$ from the self energy.

6.2   Calculation of the self energy

Equation (6.14) relates the one loop part of ζ to the renormalization of the kinetic mass. The latter quantity can be calculated by looking at the one-loop self energy

for the fermion. The full energy is expected to go as

$$E(\vec{p}) = M_1 + \frac{\vec{p}^2}{2M_2} + \mathcal{O}(\vec{p}^3).$$

Expanding this out to $\mathcal{O}(g_0^2)$ and dropping the higher order momentum corrections gives

$$
\begin{aligned}
E(\vec{p}) &= E^{[0]}(\vec{p}) + g_0^2 E^{[1]}(\vec{p}) \\
E^{[0]}(\vec{p}) &= M_1^{[0]} + \frac{\vec{p}^2}{2M_2^{[0]}} \\
E^{[1]}(\vec{p}) &= M_1^{[1]} - \frac{\vec{p}^2}{2M_2^{[0]}} \frac{M_2^{[1]}}{M_1^{[0]}}.
\end{aligned}
\tag{6.27}
$$

This allows us to solve for $M_2^{[1]}$,

$$M_2^{[1]} = \left\{ M_2^{[0]} \right\}^2 \left(\frac{dE^{[1]}(\vec{p})}{dp_1^2} \right)_{\vec{p}=0}.
\tag{6.28}$$

The derivative on the right hand side can be evaluated from the one-loop corrections to the fermion propagator. From that, we can extract $M_2^{[1]}$, Z_{M_2} and, finally, $\zeta^{[1]}$.

To solve for the self energy, we write the full fermion propagator as

$$S_F^{-1}(p_0, \vec{p}) = i\gamma_0 \sin(p_0) + ia\vec{\gamma} \cdot \vec{S} - \cos(p_0) + \mu(\vec{p}) - \Sigma(p),
\tag{6.29}$$

where we use the same conventions as chapter 5 with

$$S_i = \zeta_0 \sin(p_i), \quad \mu(\vec{p}) = 1 + m_0 + \frac{r_s \zeta_0}{2} \hat{\vec{p}}^2, \quad \hat{p}_i = 2\sin\left(\frac{p_i}{2}\right).$$

The additional function $\Sigma(p)$ is the self-energy correction. It is given by the sum of the two diagrams shown in figure 5.1. We write this correction as

$$\Sigma(p) = \sum_\mu i\gamma_\mu A_\mu(p_0, \vec{p}) + C(p_0, \vec{p}).
\tag{6.30}$$

The extraction of the various quantities of interest from the self-energy correction is fairly tedious. The calculation is well known, so we content ourselves with

restating the one-loop results of [53]. The one loop expression for the rest mass M_1 is needed to separate the factor Z_{M_2} from the full expression for M_2 (6.11). We have

$$M_1^{[1]} = \left[A_0^{[1]}(iM_1^{[0]}, \vec{0}) - C^{[1]}(iM_1^{[0]}, \vec{0}) + C^{[1]}(0, \vec{0}) \right] e^{-M_1^{[0]}}, \qquad (6.31)$$

where the factor $C(0, \vec{0})$ ensures that zero-mass quarks do not get an additive mass shift at one-loop order. This factor is often measured non-perturbatively in simulations, in which case that value can be used in place of the factor $C^{[1]}(0, \vec{0})$.

With the one loop expression for M_1, we can extract the factor Z_{M_2} at one loop. It is given by

$$
\begin{aligned}
Z_{M_2}^{[1]} &= \frac{2\zeta_0 A_1^{[1]}(iM_1^{[0]}, \vec{0}) - \zeta_0^2 A_0^{[1]}(iM_1^{[0]}, \vec{0}) - D^{[1]}(\vec{0}) \sinh M_1^{[0]}}{\zeta_0^2 + r_s \zeta_0 \sinh M_1^{[0]}} \\
&\quad - A_0^{[1]}(iM_1^{[0]}, \vec{0}) \cosh\left[M_1^{[0]}\right] e^{-M_1^{[0]}}.
\end{aligned} \qquad (6.32)
$$

Where

$$D(\vec{0}) = \left(\frac{d^2}{dp_1^2} \left[A_0(iE(\vec{p}), \vec{p}) \sinh M_1^{[0]} - C(iE(\vec{p}), \vec{p}) \right] \right)_{\vec{p}=0}. \qquad (6.33)$$

Finally, we quote the one loop result for Z_2,

$$
\begin{aligned}
Z_2^{[1]} &= \left[A_0^{[1]}(iM_1^{[0]}, \vec{0}) \cosh M_1^{[0]} - \left(\frac{\partial A_0^{[1]}(p_0, \vec{0})}{\partial p_0} \right)_{p_0 = iM_1^{[0]}} \right. \\
&\quad \left. + \left(\frac{\partial C^{[1]}(p_0, \vec{0})}{\partial p_0} \right)_{p_0 = iM_1^{[0]}} \right] e^{-M_1^{[0]}}.
\end{aligned} \qquad (6.34)
$$

Results for kinetic terms

We present results for the various kinetic quantities, using both the Wilson and improved gluon actions. The results for the Wilson action are already known, so they provide a valuable cross-check. Furthermore the logarithmic dependencies of these quantities on the infrared regulator (in this case a gluon mass) and the lattice spacing (or the dimensionless combination $m_0 a$) are universal. In all cases, our results for the improved action reproduce these known results.

In keeping with the Fermilab approach, we present all of our results for the full range of bare masses. The connection between the small and large mass limits is, in all cases, smooth. For the improved action we can report new results for various quantities. For $M_1(m_0)$ we have

$$M_1^{[1]} = \frac{4}{3} \tanh\left(M_1^{[0]}\right) \left\{ 0.12050(9) - \frac{3}{16\pi^2} \log\left(\left[M_1^{[0]}\right]^2\right) - 0.047(1)M_1^{[0]}, \right\} \quad (6.35)$$

when the bare mass is small, and

$$M_1^{[1]} = \frac{4}{3}\left(0.10937(9) - \frac{0.051(4)}{m_0}\right), \quad (6.36)$$

for large bare mass. The full mass dependence is shown in figure 6.1. For the kinetic mass renormalization factor, we find $Z_{M_2}^{[1]} \to 0$ as $m_0 \to 0$, and

$$Z_{M_2}^{[1]} = -\frac{4}{3}\left(0.07753(9) - \frac{0.097(2)}{m_0}\right), \quad (6.37)$$

in the infinite mass limit. Figure 6.2 shows the full mass dependence. Finally we present results for the wavefunction renormalization factor Z_2. These results are somewhat complicated by the fact that $Z_2^{[1]}$ has an infrared divergence. Fortunately, the coefficient of the divergence is known exactly. We have

$$Z_2^{[1]} = \tilde{Z}_2^{[1]} - \frac{1}{6\pi^2} \log\left(\lambda^2\right), \quad (6.38)$$

for a gluon mass (λ) IR regulator. Figure 6.3 shows results for $\tilde{Z}_2^{[1]}$ over the whole mass range. At small bare mass we have

$$\tilde{Z}_2^{[1]} = \frac{4}{3}\left\{ 0.0182(5) + \frac{3}{16\pi^2} \log\left(\left[M_1^{[0]}\right]^2\right) + 0.072(9)M_1^{[0]} \right\}, \quad (6.39)$$

and in the static limit

$$\tilde{Z}_2^{[1]} = \frac{4}{3}\left(0.1333(2) - \frac{0.182(5)}{m_0}\right). \quad (6.40)$$

Note that these results used $c_E = c_B = 1$. This is the value of c_E used in simulations by the Fermilab group. If we use the correct value of c_E from (5.15) we find very small differences. For example, with a correctly tuned c_E, $\tilde{Z}_2 = \frac{4}{3}0.1327(3)$, a 0.5(3)% difference.
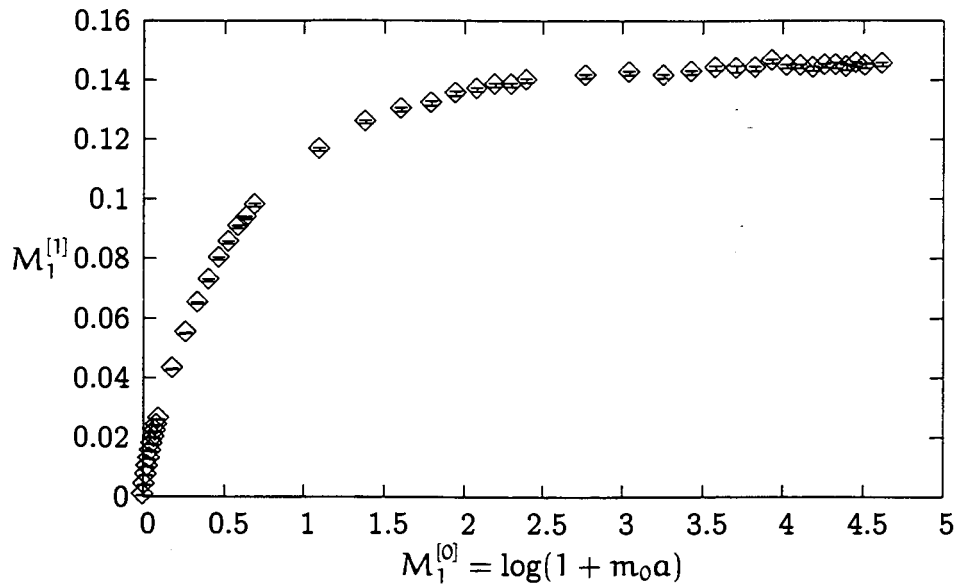
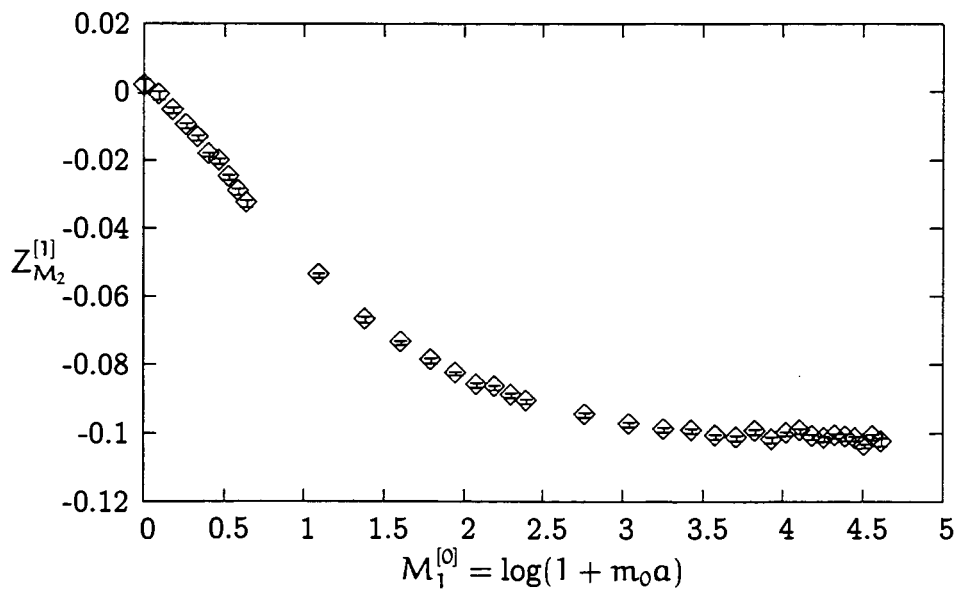Figure 6.1: One loop determination of the rest mass M_1.

Figure 6.2: One loop determination of the kinetic mass renormalization Z_{M_2}.
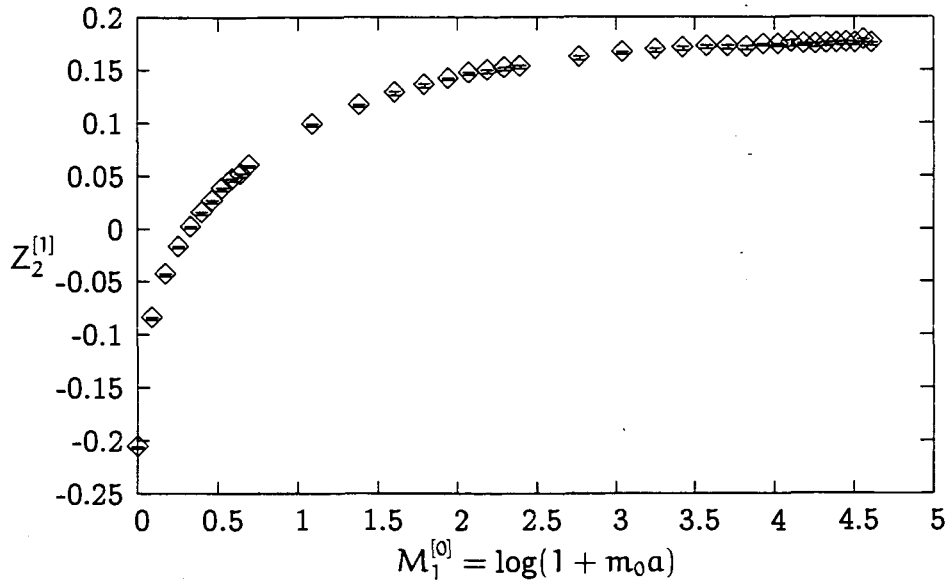
Figure 6.3: One loop determination of the wavefunction renormalization $\tilde{Z}_2$.

Numerical Integration Issues

There are a number of technical issues that arise in the integrations, both for the kinetic terms and for the numerical matching calculations presented below. There are two sources of difficulties; the pole structure of the heavy quark propagator, and the wide separation of scales in the integrals. We have implemented techniques to deal with both of these.

The first trouble stems from the behaviour of the quark propagator in the heavy quark limit. For large mass we have a pole in the gluon propagator at $p_0 \approx i \log(m_0)$. This pole is integrable, however it is numerically unstable. Fortunately, the solution to this problem is straightforward; we shift the integration contour away from the pole, by a complex constant [28]. Shifting the energy component of the loop momentum $k_4' = k_4 + i\frac{\lambda}{2}$, where λ is the gluon mass, works to stabilize the numerical integrations. Note that the gluon propagator has a pole at $k_4 = i\lambda$ so the shift uses half of the gluon mass to insure we do not hit the gluon mass pole.

The second difficulty with the numerical integrations is the separation of scales. The trouble is that we are integrating from 0 to $\pi/a >> 1$, which means the integral gets contributions from widely separated scales. This can cause trouble with VEGAS's adaptation routines. Furthermore, the integrands are dominated by the infrared divergences, which we expect to cancel in any matching calculations. These problems are somewhat lessened by transforming to spherical coordinates

$$\int_0^\pi dk_1 dk_3 dk_3 dk_4 = \int_0^{2\pi} dk \int_0^\pi d\chi \int_0^\pi d\theta \int_0^{2\pi} d\phi k^3 \sin^2(\chi) \sin(\theta). \tag{6.41}$$

The factor of k^3 significantly improves the infrared behavior of the integrals.

The convergence can be made better by a further transformation. To start, we cutoff the lower limit of the k integral at ϵ, where we choose ϵ to be much less than any other scale. Next we make the transformation

$$\kappa = \log(k/\lambda).$$

This transforms the k integral to

$$\int_\epsilon^{2\pi} k^3 dk = \int_{\log(\epsilon)}^{\log(\pi/\lambda)} k^4 d\left(e^{k/\lambda}\right). \tag{6.42}$$

The addition factor of k improves the infrared behaviour further, and taking the logarithm of the limits narrows the range that needs to be integrated over.

For the calculations of the kinetic terms these variable transformations are not necessary (though the complex energy shift is). Good results can be obtained without them. However, for the matching of action parameters, and currents, they are crucial.

6.3 Matching calculations for c_B and c_E

We adopt a very simple method to compute c_B. We consider the scattering of a quark off of a background chromo-magnetic field, with momentum transfer q. The

continuum tree level amplitude for this process is

$$M_{cont}^{[0]} = g_0 \frac{i\vec{\sigma} \cdot \vec{q}}{2m_Q}. \tag{6.43}$$

The tree level lattice amplitude will be similar, also linearly dependent on $\vec{q}$, we will call it $M_{latt}^{[0]}$. Likewise the one loop amplitudes will indicated by a superscript [1].

There are three pieces to the one loop lattice amplitude $M_{latt}^{[1]}$. First there are the one-loop diagrams, calculated with the tree level renormalized action, which we will denote $\bar{M}_{latt}^{[1]}$. This contains all of the one loop diagrams, including the contributions from the wavefunction renormalization counterterms (that is, computed using the first term in (6.21)). Then there is term, $\delta_B^{[1]}$, times the tree level scattering from $\Sigma \cdot \vec{B}$. δ_B is the one loop counterterm defined above in (6.24). Finally there is a contribution coming from the $-\zeta^{[1]}\bar{\psi}\vec{\gamma} \cdot \vec{D}\psi$ part of the counterterm Lagrangian. We write the full one loop lattice amplitude as

$$M_{latt}^{[1]} = \bar{M}_{latt}^{[1]} + \delta_B^{[1]} M_{\vec{\Sigma} \cdot \vec{B}}^{[0]} - \zeta^{[1]} M_{\vec{\gamma} \cdot \vec{D}}^{[0]}. \tag{6.44}$$

The continuum amplitude is just $M_{cont}^{[1]}$, and it includes the one loop wavefunction counterterms as well (but not the δ_B, or $\zeta^{[1]}$ parts)

To compute the matching factor $c_B^{[1]}$ we subtract the one loop continuum amplitude from (6.44) and solve for the unknown $\delta_B^{[1]}$. This gives

$$\delta_B^{[1]} = \frac{M_{cont}^{[1]} - \bar{M}_{latt}^{[1]} + \zeta^{[1]} M_{\vec{\gamma} \cdot \vec{D}}^{[0]}}{M_{\vec{\Sigma} \cdot \vec{B}}^{[0]}}. \tag{6.45}$$

We want this equation to hold up to $\mathcal{O}(q^2 a^2)$, which means we can consider the $q \to 0$ limit of (6.45). From $\delta_B^{[1]}$ we can use (6.24) to get $c_B^{[1]}$ by accounting for the renormalization of ζ, that is

$$\zeta_0 c_B^{[1]}(\zeta_0, m_0) = \delta_B^{[1]} + \zeta^{[1]} c_B^{[0]}(\zeta_0, m_0). \tag{6.46}$$

This gives our final expression

$$c_B^{[1]}(\zeta_0, m_0) = \frac{M_{cont}^{[1]} - \bar{M}_{latt}^{[1]}}{M_{\vec{\Sigma} \cdot \vec{B}}^{[0]}} + \zeta^{[1]}\omega + \zeta^{[1]} c_B^{[1]}(\zeta_0, m_0) \tag{6.47}$$

where

$$\omega = \frac{M^{[0]}_{\vec{\gamma}\cdot\vec{D}}}{M^{[0]}_{\vec{\Sigma}\cdot\vec{B}}}.$$

(6.48)

In an exactly similar manner we can consider scattering of a background chromo-electric field. By demanding the continuum and lattice amplitudes be equal to one loop we find

$$\delta^{[1]}_E = \frac{M^{[1]}_{\text{cont}} - M^{[1]}_{\text{latt}_0}}{M^{[0]}_{\vec{\alpha}\cdot\vec{E}}}.$$

(6.49)

From this calculation and equation (6.25) we can read off the result we want

$$\zeta_0 c^{[1]}_E(\zeta_0, m_0) = \delta^{[1]}_E + \zeta^{[1]} c^{[0]}_E(\zeta_0, m_0) + \zeta_0 \left[\zeta^{[1]} \frac{\partial}{\partial \zeta_0} + \frac{M^{[1]}_1}{1 + m_0} \frac{\partial}{\partial m_0} \right] c^{[0]}_E(\zeta_0, m_0).$$

(6.50)

Note that in this case there is no additional term for the tree level $\gamma_4 D^4$ part as it receives no additional renormalization in the Fermilab formalism.

Background Field Quantization

One potential issue with this calculation is the renormalization of the external gluon field and the bare coupling. These would be generated by loop diagrams correcting the gluon propagator and give a charge renormalization and a field renormalization. That is the combination Ag_0 gets renormalized to $A^r g_r$.

These renormalizations can be eliminated by working in background field gauge. This scheme was developed in the continuum (see [1]) and greatly aids in the calculation of certain processes. In background field gauge the combination Ag does not get renormalized. The price to be paid is that the gluon field is split into two parts, the background field (denoted in Feynman diagrams by a zigzag line) and the quantum gluon (denoted by a wavy line).

The background field method can also be implemented on the lattice, and the same property between the bare and renormalized gA holds [57]. To use it with

our automatic vertex generator we write the link field as

$$U_\mu(x) = U_\mu^{\text{background}}(x) U_\mu^{\text{quantum}}(x) \qquad (6.51)$$

considering two link fields at every point. Then we apply our vertex generator, taking care to distinguish quantum and background gluons. Finally we symmetrize over each gluon type separately. For these one loop calculations this method only saves us two diagrams, however as we increase the number of loops, the savings will increase rapidly.

6.3.1 Lattice to Lattice matching

Clearly in order to use (6.47) we need to be able to compute the continuum one loop amplitude. Of course, one-loop calculations in the continuum theory are feasible, however there is a problem with using them in lattice matching calculations

The trouble is that the lattice and continuum theories should be identical in the infrared. Given that our calculations will turn out to be infrared divergent this means that we need to use the same infrared regulator for both the lattice and the continuum parts of (6.47). The lattice matching computations that have been done to date have typically used a gluon mass to regulate the IR in both the lattice and continuum theories. This is the method we will use for our present calculation, however, it may pose significant problems with gauge invariance at higher order.

Another solution might be to use twisted boundary conditions, which provide a gauge invariant IR regulator. However this regulator is somewhat difficult to combine with dimensional regularization for continuum calculations. This can be avoided by rethinking the continuum UV regulator that we use. We are calculating matching coefficients, so there is no particular reason to use dimensional regularization. In fact, we can use any UV regulator we want.

Following a suggestion of Peter Lepage we have simply used a lattice cutoff to regulate the continuum theory. This allows us to do the "continuum" side of the computation using the same lattice techniques as we have developed for the heavy

quark actions. This procedure is straightforward, as we can pick a simple lattice theory (Wilson glue + naive quarks) and run the lattice spacing down. As long as the spacing is made small enough, this theory will be very close to the continuum theory. Then we can subtract off our heavy quark results, and get the matching coefficients.

We will see illustrations of how this works in the following sections. For the present work we have used a gluon mass to perform these matching calculations, however the procedure will work with twisted boundary conditions as well[2]. We suspect that for higher order calculations these will be needed.

Tree level matching

As an illustration of our lattice to lattice matching technique, we will outline in some detail the tree level matching for c_B and c_E. The tree level lattice amplitude for scattering off of a chromo-magnetic field is

$$M^{[0]}(pa, \bar{p}a) - M^{[0]}_{c_B = 0}(pa, \bar{p}a) + c_B^{[0]} M^{[0]}_{\Sigma \cdot B}(pa, pa). \qquad (6.52)$$

We have shown the dependence on the incoming and outgoing momenta (p and $\bar{p}$ respectively). The continuum amplitude is approximated using the Wilson quark action

$$M^{[0]}_{cont}(p, \bar{p}) = \lim_{a' \to 0} M^{[0]}_{c_B = 0}(pa', \bar{p}a'). \qquad (6.53)$$

Demanding that the difference between the two amplitudes vanish as $qa \to 0$ gives

$$c_B^{[0]} = \frac{\lim_{a' \to 0} M^{[0]}_{c_B = 0}(pa', \bar{p}a') - M^{[0]}_{c_B = 0}(pa, \bar{p}a)}{M^{[0]}_{\Sigma \cdot B}(pa, \bar{p}a)}. \qquad (6.54)$$

This is straightforward to implement in the computer. The only issue is that we must use dimensionless numbers in the computer. In practice what we do is to specify $m_0 a$, then compute $M_2 a$. Independently we specify $M_2 a' \ll 1$. This allows

---

[2]We can use a gluon mass because the tree-level amplitude involves only one coupling, so the effect of breaking gauge invariance will not show up until two-loop order.
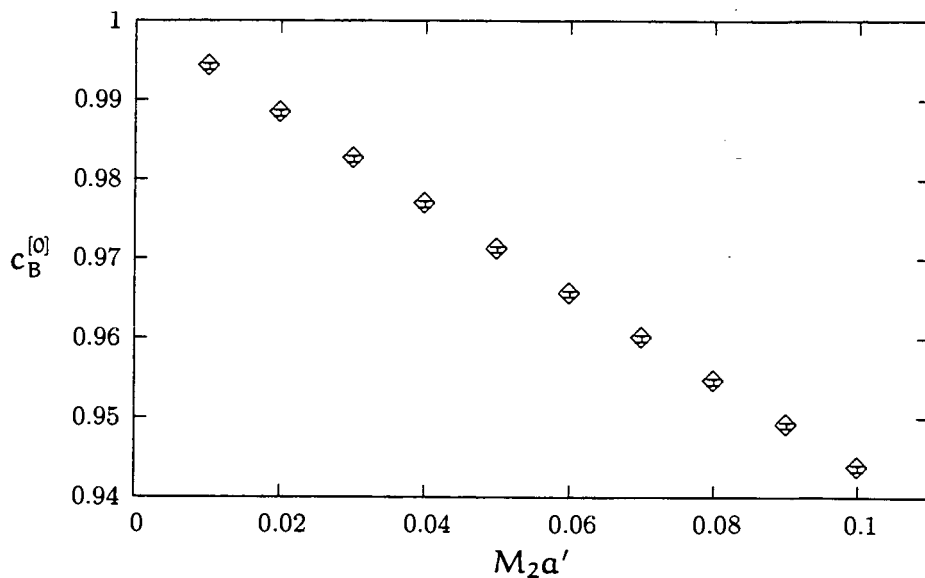
Figure 6.4: Tree level determination of c_B, for $m_0 a = 10.0$.

us to get the ratio of a'/a. This lets us convert from our specified values for pa and $\bar{p}a$ to those involving a' by multiplying by the known a'/a ratio. Note that analogous formulas hold for $c_E^{[0]}$.

Figure 6.4 illustrates the matching for $c_B^{[0]}$. This is the matching factor for $m_0 a = 10.0$. The linear $\mathcal{O}(a')$ errors of Wilson fermions are clear in this plot. The extrapolation is clearly to $c_B^{[0]} = r_s = 1$. This holds for all masses, and for general r_s. For the tree level $c_E^{[0]}$ figure 6.5 shows that we reproduce the known tree level result given in chapter 5.

These methods have also been used to cross check the complicated tree level matching for the dimension six Fermilab action [52]. The expressions for the tree coefficients of that action get quite involved, so these numerical cross checks are very useful.
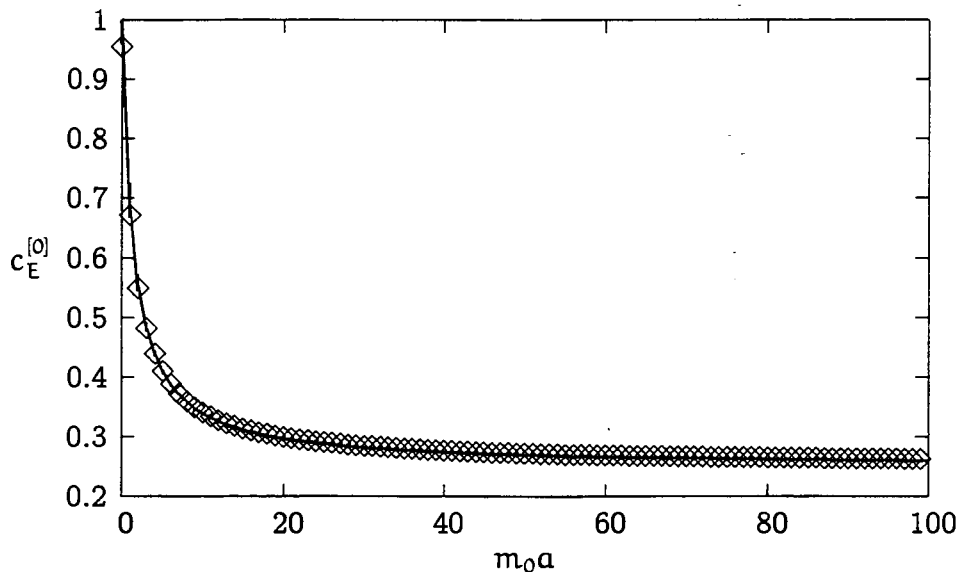
Figure 6.5: Tree level determination of c_E, fixed matching mass $M_2 a' = 0.0001$. The line is the exact result.

6.3.2 One loop results for c_B and c_E

The lattice to lattice matching procedure can be implemented at one loop to determine $c_{B,E}^{[1]}$. We can subtract lattice from continuum amplitudes, and divide by the appropriate tree level amplitude, to get the final result for δ_B. This is the same as the tree level procedure, with only difference being one of complexity. It requires considerably more effort to evaluate the one-loop diagrams.

We have performed the lattice to lattice matching for two different types of matching fermions, naive and clover. We expect that the naive fermions will have $\mathcal{O}(a^2)$ errors and the clover fermions will have $\mathcal{O}(a)$ errors. Figures 6.6 and 6.7 show that this is the case, for both gluon actions. The naive fermions clearly are much closer to the "continuum" result for a given $m_2 a'$, because of this, the one loop results for c_E and c_B presented below all use naive fermions to do the matching.

The diagrams (apart from the wavefunction renormalization) are shown in figure 6.8. We evaluate these diagrams in both the lattice and "continuum" theory. This
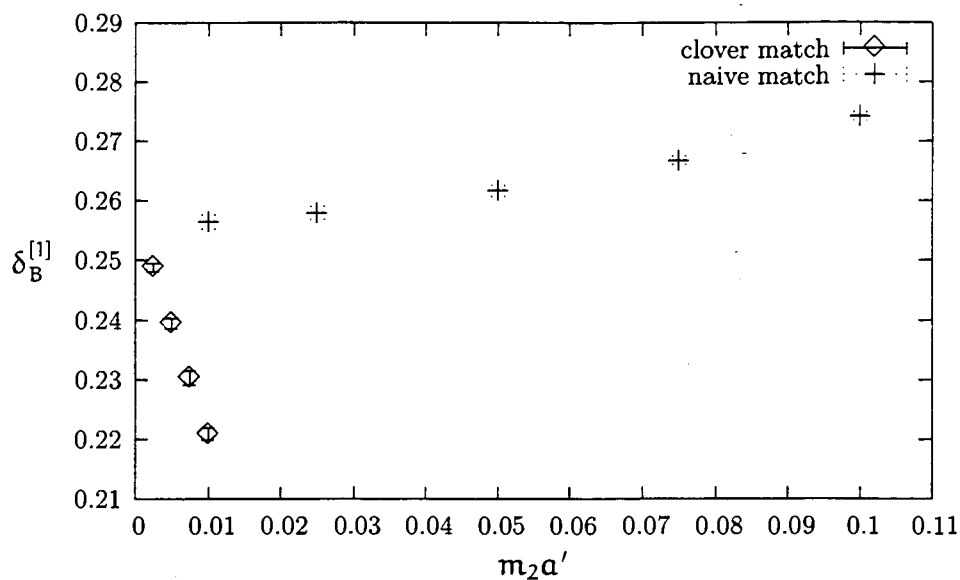
Figure 6.6: One loop lattice to lattice matching of c_B at $m_0 a = 0.1$, with Wilson glue.
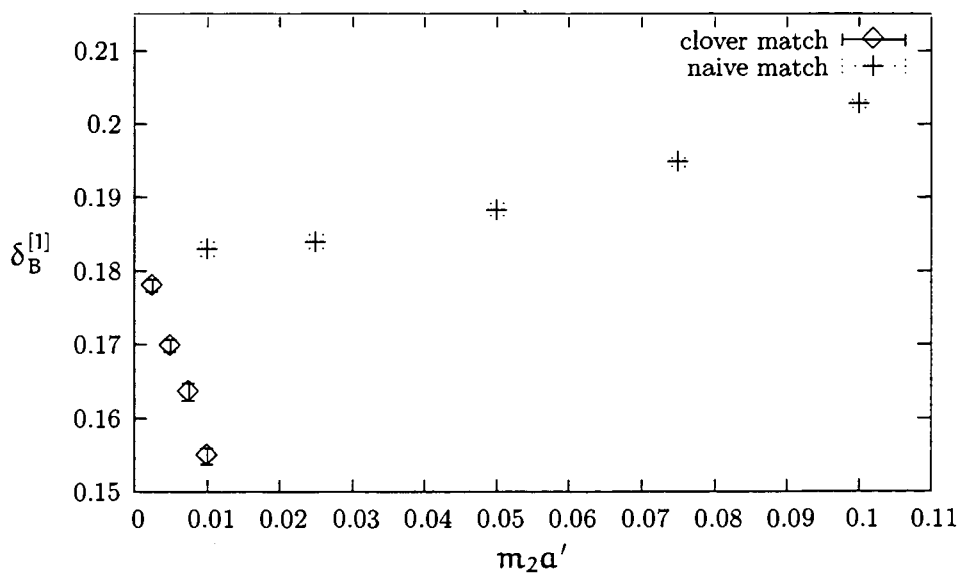

Figure 6.7: One loop lattice to lattice matching of c_B at $m_0 a = 0.1$, with improved glue.
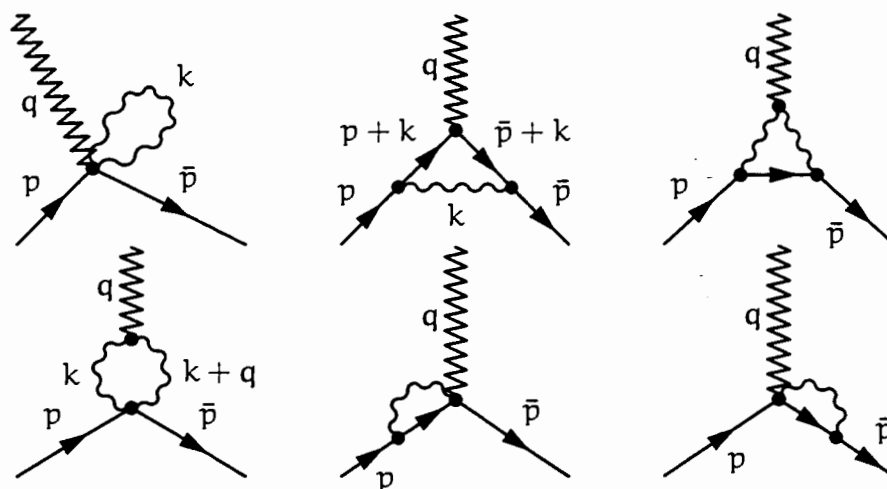
Figure 6.8: One Loop diagrams for quark scattering off of a background field.

gives us $\delta_{B,E}$. To extract $c_{B,E}$ we also need the wavefunction renormalization factors and, for the lattice theory, the factors of Z_{M_2} and M_1 as required by (6.24) and (6.25).

6.3.3 Results for $c_B^{[1]}$

Figure 6.9 shows $c_B^{[1]}$ over the whole mass range, with Wilson glue. Along with our data we show the known point at $m_0 a = 0$ ([58][40]), and the known result in the heavy quark limit[3] [59]

$$c_B^{[1]}(m \to \infty) = \frac{58.091 - 3\log\left(m_2^2 a^2\right)}{16\pi^2}. \tag{6.55}$$

Comparing with [59] requires some care. They performed their calculation in HQET which has no rest mass term. This means that there is no ζ parameter in their action, and the connection between c_B and δ_B (6.46) becomes

$$\delta_B^{[1]} = c_B^{[1]}.$$

---

[3]Note that this result is in terms of $M_2^{[0]}$ and the x-axis in figure 6.9 is $M_1^{[1]}$.
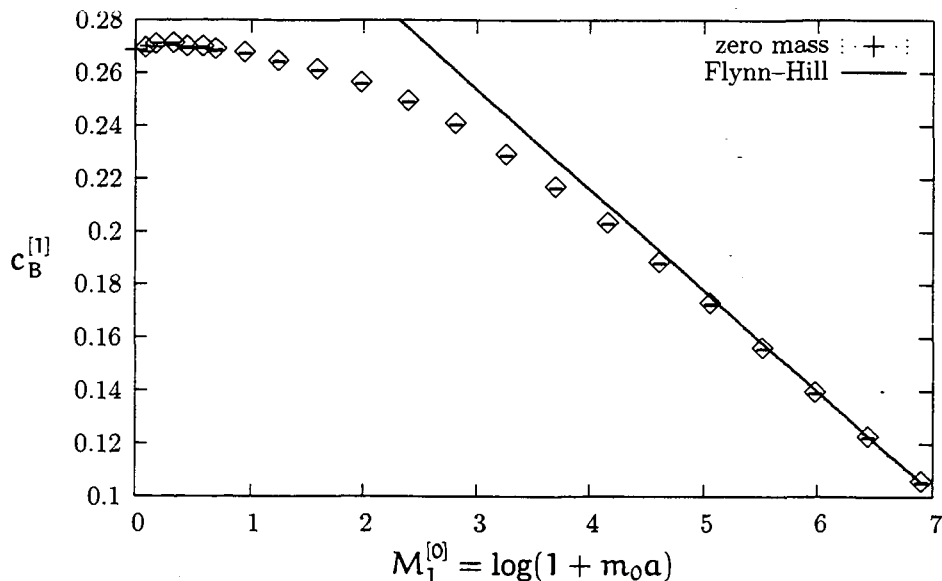
Figure 6.9: One loop determination of c_B, with Wilson glue.

In order to compare to our result we add the term δ_ζ to their result. In the heavy mass limit this merely shifts the constant they report 42.459 to that reported here 58.091. Figure 6.10 shows the same mass range, only with the improved gluon action. In this case the heavy quark result is not known, however we reproduce the corrected logarithmic dependence on m_0, and the known result at $m_0 a = 0$. We summarize all the perturbative pieces for $c_B^{[1]}$ in tables 6.1, 6.2, 6.3 and 6.3.

Tadpole Improvement

Tadpole improvement of the Fermilab action was outlined in chapter 5. To convert from our bare values for $c_B^{[1]}$ to the tadpole improved values $\tilde{c}_B^{[1]}$ we simply use (5.19). This gives

$$\tilde{c}_B^{[1]} = c_B^{[1]} + 3u_0^{[1]}, \tag{6.56}$$

where u_0 is the tadpole improvement term, either the mean link, or the fourth root of the average plaquette. In either case, $u_0^{[1]} < 0$ so the tadpole improvement tends
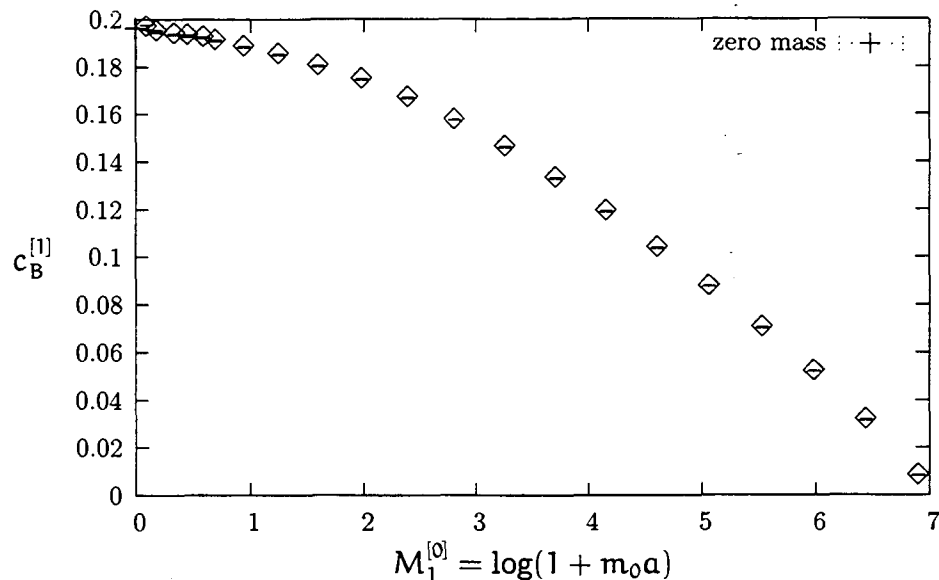
Figure 6.10: One loop determination of c_B, with improved glue.

to lower one loop correction, as expected.

6.3.4 Impact on the Hyperfine splittings

In order to fully assess the impact of our one-loop determination of c_B a non-perturbative simulation would have to be done. This is because, in the Fermilab formalism, the hyperfine splitting receives contributions from both $\vec{\gamma} \cdot \vec{D}$ and $\vec{\Sigma} \cdot \vec{B}$. To get a truly correct result, we would have to know the relative contributions of both these terms.

There is a way we can estimate the hyperfine splitting without the need for a new, non-perturbative, simulation. We start with the observation that the ratio of the tree level expectation values

$$\frac{\langle \vec{\gamma} \cdot \tilde{D} \rangle}{\langle \vec{\Sigma} \cdot \tilde{B} \rangle} = \omega \tag{6.57}$$

is, for $pa <\sim 1$, only weakly dependent on the momentum transfer. We are using the tadpole improved link fields here $\tilde{U} = U/u_0$ since they will have the most

"continuum-like" behaviour and $\langle \vec{\Sigma} \cdot \tilde{B} \rangle$ denotes the spin-flip computed from the clover part of the action, including the overall factor of 1/2. The fact that the ratio is nearly independent of $p\alpha$ suggests that it is insensitive to the bound state effects, and the tree level value will be a reasonable approximation to the exact result. We can use this fact to get an estimate for the correction to the hyperfine splitting.

The hyperfine splitting is a product of two spin flips, so we can write the *corrected* hyperfine splitting in terms of the tadpole improved c_B as

$$\mathcal{HF}_{\text{correct}} = \left[\langle \vec{\gamma} \cdot \tilde{D} \rangle + \tilde{c}_B \langle \vec{\Sigma} \cdot \tilde{B} \rangle \right]^2. \tag{6.58}$$

The Fermilab group used $\tilde{c}_B = 1$ in their calculation [50]. This means we can take

$$\mathcal{HF}_{\text{measured}} = \left[\langle \vec{\gamma} \cdot \tilde{D} \rangle + \langle \vec{\Sigma} \cdot \tilde{B} \rangle \right]^2. \tag{6.59}$$

Multiplying and dividing by the Fermilab result gives

$$\mathcal{HF}_{\text{correct}} = \frac{\left[\langle \vec{\gamma} \cdot \tilde{D} \rangle + \tilde{c}_B \langle \vec{\Sigma} \cdot \tilde{B} \rangle \right]^2}{\left[\langle \vec{\gamma} \cdot \tilde{D} \rangle + \langle \vec{\Sigma} \cdot \tilde{B} \rangle \right]^2} \mathcal{HF}_{\text{measured}}. \tag{6.60}$$

This allows us write $\mathcal{HF}_{\text{correct}} = \Delta \mathcal{HF}_{\text{measured}}$ where the correction factor is

$$\Delta = \frac{\left[\langle \vec{\gamma} \cdot \tilde{D} \rangle + \tilde{c}_B \langle \vec{\Sigma} \cdot \tilde{B} \rangle \right]^2}{\left[\langle \vec{\gamma} \cdot \tilde{D} \rangle + \langle \vec{\Sigma} \cdot \tilde{B} \rangle \right]^2}. \tag{6.61}$$

Using $\langle \vec{\gamma} \cdot \tilde{D} \rangle = \omega \langle \vec{\Sigma} \cdot \tilde{B} \rangle$ gives

$$\Delta = \frac{\left[1 + \frac{\tilde{c}_B}{\omega} \right]^2}{\left[1 + \frac{1}{\omega} \right]^2}. \tag{6.62}$$

Expanding to one loop order, we find

$$\Delta = 1 + g_0^2 \frac{2\tilde{c}_B^{[1]}}{1 + \omega} = 1 + \alpha_V \frac{8\pi \tilde{c}_b^{[1]}}{1 + \omega}. \tag{6.63}$$

We would like to use (6.63) to find the corrections to the Fermilab determination of the hyperfine splitting. To do this we need three things, the mass that was input

to the simulation, the type of tadpole improvement used, and the value of the average plaquette measured in the simulation. These three things give us $c_B^{[1]}$, $u_0^{[1]}$, and α_V. The latter can be extracted from the perturbative expansion of the plaquette, and the connection between α_V and α_0, using either the results of chapter 4 or the higher order results described in [45].

We have obtained, from the Fermilab group [60] the quantities, from their $\beta = 6.8$ simulations, needed to do this analysis. They give their masses in terms of two dimensionless parameters

$$\kappa = 0.119, \quad \kappa_c = 0.13788, \quad m_0 a = \frac{1}{2\kappa} - \frac{1}{2\kappa_c} = 0.575.$$

The Fermilab group uses mean link tadpole improvement ($u_0^{[1]} = -0.059591(8)$), and a measured plaquette of $P = 0.567060$. For this quark mass we calculate, using improved glue, $c_B^{[1]} = 0.1931 g_0^2$. Note that we are not propagating errors through this calculation, since the ratio ω is only an estimate anyway and could easily be wrong by 10%. Using our one loop expression for u_0 we find the tadpole improved result

$$\tilde{c}_B^{[1]} = 0.01433. \tag{6.64}$$

Note that in terms of α_V the tadpole improved c_B is

$$\tilde{c}_B = 1 + 0.1800\alpha_V, \tag{6.65}$$

so the improvement has produced a very small coefficient (it would have been 2.427 without the tadpole improvement).

To extract a value for α_V we have the average plaquette

$$-\log(P) = 3.068395\alpha_V(3.32/a)\left[1 - 1.0661(2)\alpha_V(3.32/a)\right], \tag{6.66}$$

where we have used the conversion from α_0 to α_V outlined in [45] since it is more accurate than the one computed in chapter 4 (for the one loop c_B we can freely interchange α_0 and α_V). Solving (6.66) for α_V gives

$$\alpha_V(3.32/a) = 0.2533.$$

Using this and the tree level ratio $\omega = 2.12749$, gives the final result for the correction factor $\Delta(3.32/a) = 1.029$ a 3% increase. The smallness of this result is due to the tadpole improvement. Over the whole range of interest, $m_0 a = 0 \ldots 1.1$ the tadpole improved c_B is very small. Given this, we expect that for the Fermilab action the uncorrected $\mathcal{O}(a^2)$ errors will have a major impact on the hyperfine splittings. It would be interesting to repeat this calculation for NRQCD, where a $\mathcal{O}(a^2)$ accurate action is already known. In this case, we expect that the one loop matching of $\Sigma \cdot \vec{B}$ would have a more pronounced effect.

6.3.5   Results for $c_E^{[1]}$

To have a fully one loop improved Fermilab action the one loop term for c_E must be included. The calculation of $c_E^{[1]}$ proceeds in the same manner as that for $c_B^{[1]}$, however there is a significant complication.

We consider a spin-flip amplitude off of an external chromo-electric field. The tree level amplitude for this process is proportional to $\vec{p} \times \vec{p}$. Choosing $\vec{p} = -p\hat{x}$ and $\vec{p} = p\hat{z}$ we find that the amplitude is proportional to p^2. This is in contrast to the magnetic field scattering, which was proportional to p. Since we are working in the small momentum limit, the extra power of p substantially reduces our signal.

The solution to this problem is to project out only the components of the amplitude that we want. The remaining components will integrate to zero anyway, however they form a noisy background which hurts our ability to extract the signal.

To do the projection, we note that our amplitude can be written as

$$\bar{u}_\uparrow(\vec{p})\mathcal{M}u_\downarrow(\vec{p}), \tag{6.67}$$

where $\mathcal{M}$ is a four by four matrix in spin space. A general four by four matrix can be written as

$$\mathcal{M} = \sum_{\text{bilinears}} \frac{\text{Tr}(\mathcal{M}\Gamma)\Gamma}{\text{Tr}(\Gamma^2)}, \tag{6.68}$$

where the sum runs over all sixteen Dirac bilinears Γ. For our problem we only have three possible directions to pick from $\hat{x}$ and $\hat{y}$, the incoming and outgoing
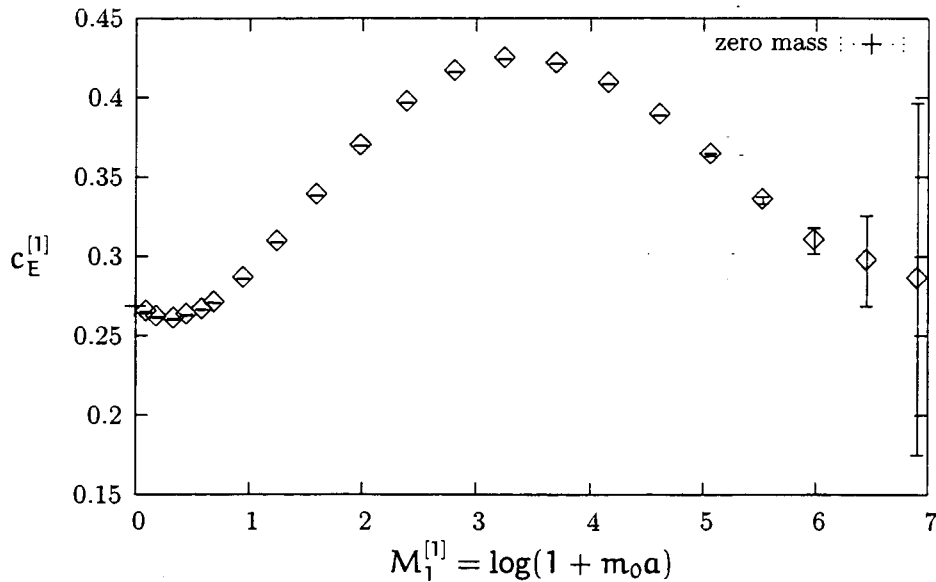
Figure 6.11: One loop determination of c_E with Wilson glue.

momenta directions, and $\hat{t}$ the polarization of the background field gluon. So of the sixteen choices we only have to include eight,

$$\gamma^1, \quad \gamma^3, \quad \gamma^4, \quad \gamma^1\gamma^3, \quad \gamma^1\gamma^4, \quad \gamma^3\gamma^4, \quad \gamma^2\gamma^5, \quad \text{and I.} \tag{6.69}$$

The identity is included here, along with $\gamma^2\gamma^5 = -\gamma^1\gamma^3\gamma^4$. All we have to do is keep the terms in the general projection equal to these, as the rest would have integrated to zero. Setting them to zero beforehand, the signal is greatly improved.

Figures 6.11 and 6.12 show the results for $c_E^{[1]}$ from small to large masses. In the small mass limit $c_E^{[1]} \to c_{SW}^{[1]}$, just as $c_B^{[1]}$ did. The tadpole improvement procedure for $c_E^{[1]}$ is the same as for $c_B^{[1]}$. We summarize our results for $c_E^{[1]}$ in tables 6.1, 6.2, 6.3 and 6.3.

$m_0 a$	ω	$Z_{M_2}^{[1]}$	$M_1^{[1]}$
1000.000	0.001998	-0.098897(38)	0.167869(39)
631.000	0.003165	-0.098840(38)	0.167716(46)
398.000	0.005013	-0.098650(40)	0.167566(38)
251.000	0.007937	-0.098528(35)	0.167447(34)
158.000	0.012579	-0.098158(39)	0.167086(41)
100.000	0.019804	-0.097539(34)	0.166708(44)
63.100	0.031209	-0.096796(35)	0.166030(43)
39.800	0.049050	-0.095490(36)	0.164920(41)
25.100	0.076742	-0.093372(34)	0.163253(38)
15.800	0.119472	-0.090296(33)	0.160715(38)
10.000	0.183335	-0.085795(31)	0.157222(36)
6.310	0.278819	-0.079292(32)	0.152332(36)
3.980	0.418485	-0.070540(27)	0.145609(35)
2.510	0.620142	-0.059458(31)	0.136454(27)
1.580	0.912250	-0.046768(33)	0.124287(26)
1.000	1.333340	-0.034118(35)	0.109282(26)
0.800	1.607150	-0.028380(35)	0.101007(22)
0.575	2.127490	-0.020793(31)	0.087963(16)
0.400	2.916670	-0.014132(36)	0.073378(13)
0.202	5.404630	-0.006077(40)	0.048342(8)
0.100	10.476200	-0.002284(40)	0.029076(5)

Table 6.1: Wilson glue perturbative results needed to convert $\delta_{B,E}$ to $c_{B,E}$.

m_0a	$\delta_B^{[1]}$	$\delta_E^{[1]}$	$c_B^{[1]}$	$c_E^{[1]}$
1000.000	0.00637(31)	0.26(11)	0.10527(31))	0.29(11)
631.000	0.02339(26)	0.272(29)	0.12223(26))	0.300(29)
398.000	0.04035(25)	0.285(82)	0.13900(25))	0.3097(81)
251.000	0.05718(22)	0.3105(24)	0.15572(22))	0.3350(24)
158.000	0.07425(26)	0.33927(91)	0.17242(26))	0.36369(91)
100.000	0.09031(23)	0.36471(49)	0.18788(23))	0.38890(49)
63.100	0.10587(22)	0.38452(36)	0.20275(22))	0.40841(36)
39.800	0.12083(22)	0.39789(33)	0.21653(22))	0.42127(33)
25.100	0.13496(21)	0.40165(32)	0.22881(22))	0.42421(32)
15.800	0.14899(24)	0.39480(27)	0.24033(24))	0.41614(27)
10.000	0.16102(21)	0.37719(26)	0.24892(22))	0.39671(26)
6.310	0.17250(23)	0.35213(24)	0.25574(23))	0.36898(24)
3.980	0.18369(29)	0.32477(23)	0.26096(29))	0.33799(23)
2.510	0.19457(26)	0.30014(24)	0.26424(26))	0.30878(24)
1.580	0.20665(30)	0.28226(24)	0.26720(30))	0.28589(24)
1.000	0.21778(30)	0.27139(24)	0.26844(31))	0.27066(24)
0.800	0.22370(35)	0.26846(26)	0.26947(35))	0.26615(26)
0.575	0.23069(38)	0.26659(38)	0.26939(38))	0.26274(38)
0.400	0.23893(44)	0.26468(34)	0.27066(44))	0.26043(34)
0.202	0.24933(69)	0.26463(41)	0.27044(70))	0.26170(42)
0.100	0.2553(11)	0.26551(55)	0.2690(11)	0.26468(59)

Table 6.2: Wilson glue perturbative results for $\delta_{B,E}$ and $c_{B,E}$.

$m_0 a$	ω	$Z_{M_2}^{[1]}$	$M_1^{[1]}$
1000.000000	0.001998	-0.102890(28)	0.145339(34)
631.000000	0.003165	-0.102796(30)	0.145261(28)
398.000000	0.005013	-0.102625(30)	0.145100(34)
251.000000	0.007937	-0.102443(30)	0.144969(35)
158.000000	0.012579	-0.102033(29)	0.144636(33)
100.000000	0.019804	-0.101476(29)	0.144216(28)
63.100000	0.031209	-0.100556(31)	0.143519(33)
39.800000	0.049050	-0.099128(30)	0.142455(33)
25.100000	0.076742	-0.096906(26)	0.140825(31)
15.800000	0.119472	-0.093513(30)	0.138387(29)
10.000000	0.183335	-0.088675(24)	0.135039(29)
6.310000	0.278819	-0.081688(26)	0.130481(23)
3.980000	0.418485	-0.072348(24)	0.124425(27)
2.510000	0.620142	-0.060749(28)	0.116489(22)
1.580000	0.912250	-0.047524(25)	0.106224(23)
1.000000	1.333340	-0.034547(28)	0.093690(16)
0.800000	1.607150	-0.028679(30)	0.086854(16)
0.575000	2.127490	-0.020971(28)	0.075996(12)
0.400000	2.916670	-0.014189(30)	0.063740(11)
0.202000	5.404630	-0.006000(30)	0.042511(07)
0.100000	10.476200	-0.002244(36)	0.025864(04)

Table 6.3: Improved glue perturbative results needed to convert $\delta_{B,E}$ to $c_{B,E}$.

$m_0 a$	$\delta_B^{[1]}$	$\delta_E^{[1]}$	$c_B^{[1]}$	$c_E^{[1]}$
1000.000	-0.09465(20)	-0.12(65)	0.00824(20)	-0.10(65)
631.000	-0.07138(19)	-0.10(18)	0.03142(19)	-0.08(18)
398.000	-0.05068(20)	0.132(50)	0.05195(20)	0.158(50)
251.000	-0.03214(18)	0.135(13)	0.07031(18)	0.161(13)
158.000	-0.01454(21)	0.1664(38)	0.08751(21)	0.1920(38)
100.000	0.00205(17)	0.1972(13)	0.10357(17)	0.2226(13)
63.1000	0.01826(16)	0.22156(55)	0.11891(17)	0.24683(55)
39.800	0.03373(17)	0.23953(32)	0.13308(18)	0.26450(32)
25.100	0.04874(19)	0.25076(24)	0.14614(19)	0.27524(24)
15.800	0.06290(16)	0.25456(21)	0.15749(16)	0.27828(21)
10.000	0.07614(21)	0.24936(19)	0.16700(21)	0.27192(19)
6.310	0.08877(19)	0.23734(18)	0.17454(19)	0.25807(18)
3.980	0.10094(19)	0.22186(17)	0.18019(19)	0.23992(17)
2.510	0.11382(18)	0.20696(16)	0.18499(18)	0.22139(16)
1.580	0.12674(20)	0.19572(18)	0.18827(20)	0.20568(18)
1.000	0.13971(26)	0.18931(19)	0.19101(26)	0.19494(19)
0.800	0.14609(29)	0.18829(20)	0.19235(29)	0.19207(20)
0.575	0.15405(29)	0.18722(22)	0.19309(29)	0.18886(23)
0.400	0.16191(35)	0.18766(26)	0.19377(35)	0.18795(26)
0.202	0.17411(52)	0.18970(34)	0.19495(53)	0.18934(35)
0.100	0.1832(10)	0.19238(42)	0.1966(10)	0.19291(47)

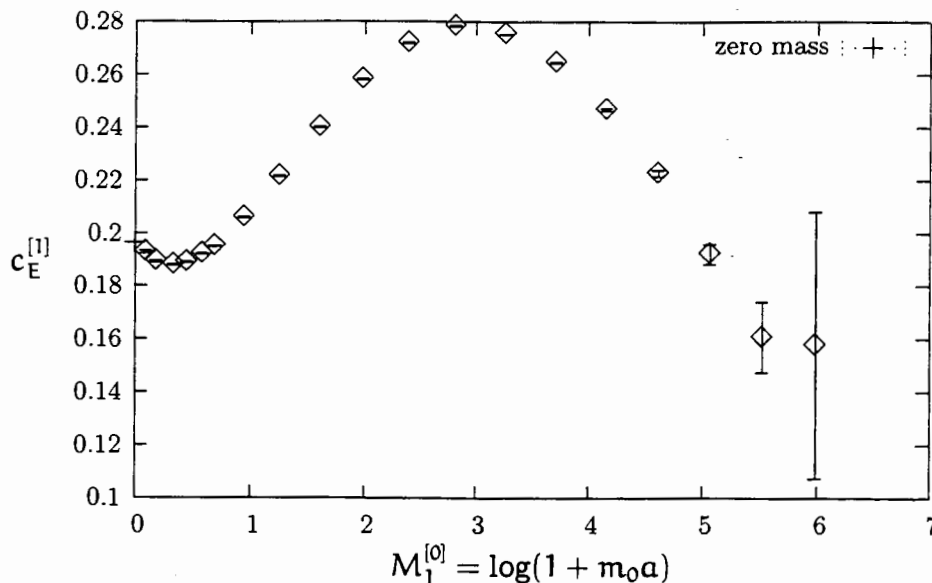Table 6.4: Improved glue perturbative results for $\delta_{B,E}$ and $c_{B,E}$.

Figure 6.12: One loop determination of c_E with improved glue.

6.4 Matching Currents

The second calculation that we report is the one-loop matching of bilinear quark currents[4]. Recall from chapter 2 that the connection between a continuum operator and the lattice operators is

$$\hat{O}_c = Z(g,\ldots)\left\{\hat{O}_0 + \sum_n C_n(g,\ldots)\hat{O}_n\right\}. \qquad (6.70)$$

Here O_0 is the lattice operator with the same dimension as the continuum operator. The remaining operators are higher-dimensional, and in our case they will contain $O(a)$ errors.

The operators we want to consider are the bilinear currents that connect a "light" quark and a "heavy" quark. The quotations emphasize that our calculations will be completely general: "light" and "heavy" here serve only to distinguish the two quarks (henceforth we'll drop the quotes). We consider the heavy quark in it's

---

[4]The calculations in this section were done in collaboration with Aida El-Khadra.

rest frame. It's four-velocity is $v_4 = i$, $\vec{v} = \vec{0}$. The continuum currents we consider are

$$
\begin{aligned}
V_\parallel^c(x) &= \bar{q}^c(x) i\gamma_4 Q^c(0) \\
\vec{A}_\perp^c(x) &= \bar{q}^c(x) i\gamma_5 \vec{\gamma} Q^c(0),
\end{aligned}
$$

where $Q^c(q^c)$ is the heavy(light) continuum quark field. The analogous lattice operators with the same quantum numbers ($\mathcal{O}_0$ in 6.70) are defined identically

$$
\begin{aligned}
V_\parallel^l(x) &= \bar{q}^l(x) i\gamma_4 Q^l(0) \\
\vec{A}_\perp^l(x) &= \bar{q}^l(x) i\gamma_5 \vec{\gamma} Q^l(0),
\end{aligned}
$$

where now the quark fields are defined from the desired lattice actions. These matching calculations have been done for Wilson gluons with Wilson and SW quarks in [61] and [62], we are continuing this work for the more complicated actions we have considered. In particular most modern simulations use the Symanzik improved gluon action.

We can, at this point, consider the matching of the two operators, ignoring the correction terms in (6.70), and just focusing on the Z factor. The procedure for doing this should now be familiar, we demand that

$$
\langle q | \mathcal{O}_c | Q \rangle - Z \langle q | \mathcal{O}_0 | Q \rangle = 0. \tag{6.71}
$$

We can write the Z factor in (6.70) as $Z = Z^{[0]} + g^2 Z^{[1]}$ and the lattice current as

$$
\langle q | \mathcal{O}_0 | Q \rangle = \langle q | \mathcal{O}_0 | Q \rangle^{[0]} + g^2 \langle q | \mathcal{O}_0 | Q \rangle^{[1]}. \tag{6.72}
$$

This gives, at tree and one-loop levels, our matching conditions

$$
Z^{[0]} = \frac{\langle q | \mathcal{O}_c | Q \rangle^{[0]}}{\langle q | \mathcal{O}_0 | Q \rangle^{[0]}}, \quad Z^{[1]} = \frac{\langle q | \mathcal{O}_c | Q \rangle^{[1]} - Z^{[0]} \langle q | \mathcal{O}_0 | Q \rangle^{[1]}}{\langle q | \mathcal{O}_0 | Q \rangle^{[0]}}. \tag{6.73}
$$

As we saw with the matching for the action parameters, Wilson-like fermions have a tree level contribution to their self energy. This means that

$$
\langle q | \mathcal{O}_0 | Q \rangle^{[0]} = T_F \langle q | \mathcal{O}_c | Q \rangle^{[0]}, \tag{6.74}
$$

where

$$T_F = \frac{1}{\sqrt{(1 + m_q)(1 + m_Q)}}, \tag{6.75}$$

when both q and Q are Wilson-like fermions, and

$$T_F = \frac{1}{\sqrt{1 + m_Q}}, \tag{6.76}$$

when only Q is. This suggests that we should define a renormalization factor with this contribution removed, $\mathcal{Z} = T_F Z = 1 + g^2 \mathcal{Z}^{[1]} + \cdots$. With this definition we have

$$\mathcal{Z}^{[1]} = \frac{T_F \langle q | \mathcal{O}_c | Q \rangle^{[1]} - \langle q | \mathcal{O}_0 | Q \rangle^{[1]}}{\langle q | \mathcal{O}_0 | Q \rangle^{[0]}}. \tag{6.77}$$

A final technical point; the tree level self energy is actually momentum dependent, however we will only be considering terms linear in the external momenta, and since the tree level Z_2's momentum dependence starts at $\mathcal{O}(\vec{p}^2)$ we do not need to consider it.

To do the matching we compute each of the matrix elements and evaluate the $\mathcal{Z}$ factors. Unlike the matching of c_B and c_E these currents are not part of the QCD action. Therefore lattice to lattice matching has to be used with much more care. A finite renormalization could be generated by the lattice theory that does not go away in the $a \to 0$ limit. Rather than deal with this complication, we simply compute the continuum quantities numerically with a Pauli-Villars ultraviolet cutoff. This amounts to replacing the continuum gluon propagator (with a small gluon mass λ)

$$D_{\mu\nu} = \frac{\delta_{\mu\nu}}{k^2 + \lambda^2}, \tag{6.78}$$

with

$$D_{\mu\nu}^R = \delta_{\mu\nu} \left[\frac{1}{k^2 + \lambda^2} - \frac{1}{k^2 + \Lambda^2} \right], \tag{6.79}$$

where Λ is the UV cutoff, set to be much greater than any other scale in the calculation (in this case, the heavy quark mass). For the quantities we are calculating the dependence on the continuum regulator cancels.

In both cases, lattice and continuum, we need to include the wavefunction renormalization factor $\sqrt{Z_2^h Z_2^l}$, as well as the renormalization of the operator diagram. The full one loop expression can be written schematically in diagram form as

$$\langle q|\mathcal{O}_0|Q\rangle^{[1]} = \frac{1}{2}\frac{\partial}{\partial p_0}\left(\text{diagram} + \text{diagram} \right) \times \text{diagram}$$

$$+ \frac{1}{2}\frac{\partial}{\partial p_0}\left(\text{diagram} + \text{diagram} \right) \times \text{diagram}$$

$$+ \text{diagram} \qquad\qquad (6.80)$$

where the double lines represent the heavy quark, and the hatched dot is the operator. The continuum calculation has the same diagrams, without the tadpoles. Also note that the terms in brackets have to be differentiated to get the self energy.

With these definitions we can compute the matching factors. However, we neglected the higher dimensional operators in (6.70). These are the $\mathcal{O}(a)$ errors, which must be corrected. For the current operators we are considering the necessary corrections are relatively simple. The reason is the the current operators we are considering are constants (for example γ_4), so the only mismatch between lattice and continuum theories is in the definitions of the external states.

In the continuum theory we have

$$\hat{\psi}_c|q(\xi,\vec{p})\rangle = \left[1 - \frac{i\vec{\gamma}\cdot\vec{p}}{2m_q}\right] u(\xi,\vec{0}) + \mathcal{O}(p^2) \qquad (6.81)$$

where $\xi = 1, 2$ is the spin of the quark with

$$u_1(1,\vec{0}) = 1, \quad u_2(2,\vec{0}) = 1, \qquad (6.82)$$

and all other components zero. In the lattice theory,

$$\hat{\psi}_l|q(\xi,\vec{p})\rangle = e^{-M_1/2}\left[1 - \frac{i\zeta\vec{\gamma}\cdot\vec{p}}{2\sinh M_1}\right] u(\xi,\vec{0}) + \mathcal{O}(p^2) \qquad (6.83)$$

where $M_1 = \log(1 + m_0)$ is the tree level rest mass. The $\mathcal{O}(pa)$ terms are clearly not the same in this expression. As well there is a mismatch stemming from the exponential factor $\exp(-M_1/2)$. This mismatch is taken into account by using the $\mathcal{Z}$ matching factor. Recall we defined

$$\mathcal{Z} = \frac{Z}{\sqrt{(1 + m_q)(1 + m_Q)}} = e^{-M_1^q/2}e^{-M_1^Q/2} = T_F. \qquad (6.84)$$

The lattice spinors $|Q\rangle$ and $|q\rangle$ generate a factor T_F, so the overall mismatch due to this factor cancels in the division by $\langle q|\mathcal{O}|Q\rangle$ in (6.77). To correct the other mismatch we need to make the two terms in the square brackets equal.

We can accomplish this by using a different lattice spinor than the one we get from solving the discretized Wilson–Dirac equation. This is permissible so long as the new spinor has the correct continuum limit. With this in mind we define the "rotated" spinor:

$$\Psi_1(x) = [1 + ad_1\vec{\gamma} \cdot D]\,\psi(x). \qquad (6.85)$$

In momentum space, at tree level, this is

$$\Psi_1(p) = [1 + ad_1\vec{\gamma} \cdot \vec{p}]\,\psi(p) \qquad (6.86)$$

which gives

$$\hat{\psi}_1|q(\xi, \vec{p})\rangle = e^{-M_1/2}\left[1 - \frac{i\vec{\gamma} \cdot \vec{p}}{2\sinh M_1} + id_1\vec{\gamma} \cdot \vec{p}\right]u(\xi, \vec{0}) + \mathcal{O}(p^2) \qquad (6.87)$$

for the external state. Setting the square bracket equal to that in (6.81), gives

$$d_1 = \frac{\zeta}{2\sinh M_1} - \frac{1}{2m_q}. \qquad (6.88)$$

Setting the quark mass equal to the tree level kinetic mass M_2 (see 5.10) we find

$$d_1 = \frac{\zeta(1 + m_0 - \zeta)}{m_0(2 + m_0)} - \frac{r_s\zeta}{2(1 + m_0)}. \qquad (6.89)$$

With $r_s = \zeta = 1$ this simplifies to

$$\frac{m_0}{2(1 + m_0)(2 + m_0)}.$$

If we use (6.85) to compute the external states for our current calculations we will correct tree level $\mathcal{O}(a)$ errors. With a one loop calculation of the matching factor using the rotated spinors the errors will be reduced to $\mathcal{O}(a^2, \alpha_s a, \alpha_s^2)$.

The outline of the calculation we presented above is the same with the rotated spinors, the only difference is that there are more diagrams, stemming from the D in the rotation term.

Results for Current Matching

We have computed the current matching factors $\mathcal{Z}$ for a number of different combinations of masses. We present a few results here. First, for degenerate masses we recover the correct $m_0 \to 0$ limits for the Wilson quark action $\mathcal{Z}_V^{[1]} = -0.1294$. For the improved action, we report $\mathcal{Z}_V^{[1]} = -0.1003(6)$. Of most phenomenological interest is the case where one quark is "heavy" and the other is massless. In this case, we set the outgoing quark mass to be zero, leaving only one quark mass (m_0) to vary. We consider this case in the results we present.

In the heavy quark limit we expect [61] that the current matching factors should all have the form

$$z_J^{[1]} = \frac{z_J + \log(1 + m_0)}{12\pi^2}. \qquad (6.90)$$

We have verified this for both the Wilson and improved gluon actions. For the improved action we can report

$$z_{V_\parallel} = -8.67(5), \quad z_{A_\perp} = -11.12(3). \qquad (6.91)$$

Figures 6.13 and 6.14 show $\mathcal{Z}_{V_\parallel}$ and $\mathcal{Z}_{A_\perp}$ over a wide range of masses. We can easily rerun this code for any masses of interest in simulations.

We have also computed the q^* scale for these processes, as outlined in chapter 3. Figure 6.15 shows the results for the range of masses of interest to simulations. The diverging behaviour near $M_1 = 2$ is do to the vanishing of the one loop Z near this point. This means the denominator of (3.68) is going to zero, and, as discussed
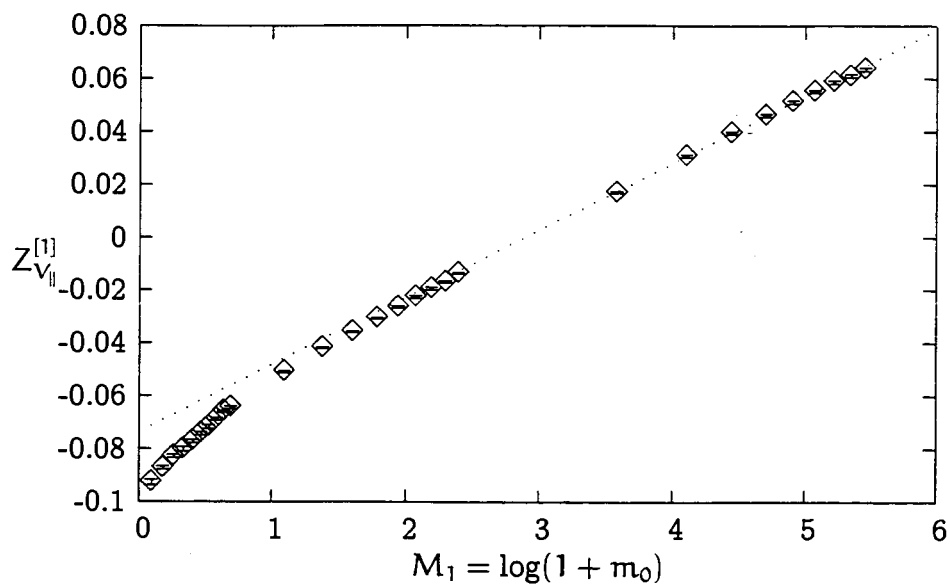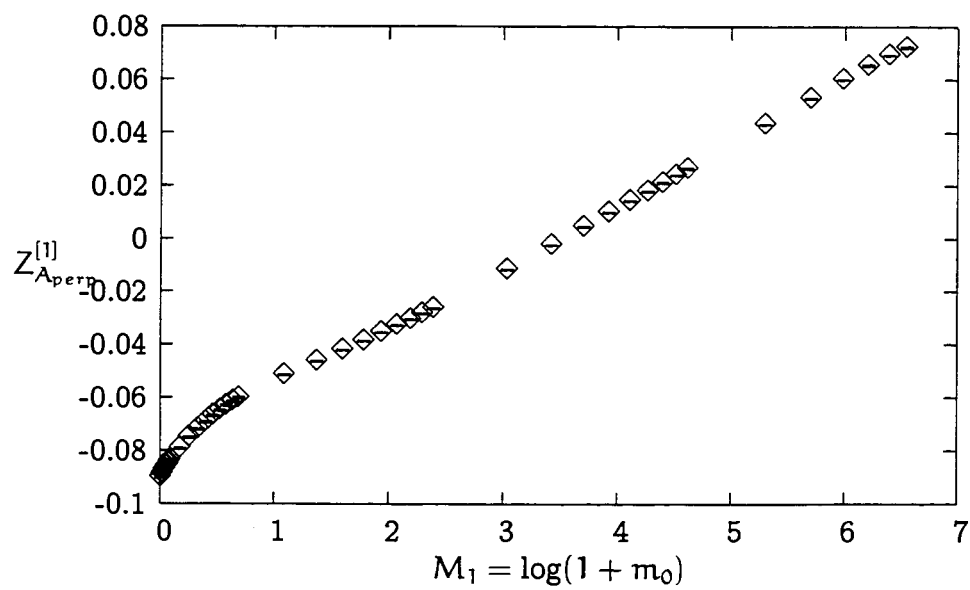
Figure 6.13: $\mathcal{Z}_{V_{\|}}$ for improved glue.

Figure 6.14: $\mathcal{Z}_{A_{\perp}}$ for improved glue.

$m_0 a$	$Z_{V_\parallel} \times 10^2$	$m_0 a$	$Z_{V_\parallel} \times 10^2$
0.9000	-6.590(43)	4.0000	-3.586(39)
0.8000	-6.876(49)	5.0000	-3.061(30)
0.7000	-7.163(66)	6.0000	-2.637(28)
0.6000	-7.421(60)	7.0000	-2.264(42)
0.5000	-7.709(62)	8.0000	-1.940(42)
0.3999	-8.011(91)	9.0000	-1.686(36)
0.2999	-8.283(55)	10.000	-1.358(32)
0.2000	-8.722(50)	35.00	1.685(41)
0.1000	-9.266(93)	60.00	3.069(46)
1.0000	-6.442(48)	85.00	3.943(50)
2.0000	-5.095(37)	110.0	4.607(51)
3.0000	-4.196(35)	135.0	5.109(54)
		160.0	5.506(54)

Table 6.5: Table of values for $Z_{V_\parallel}$ for improved glue.

$m_0 a$	$Z_{A_\perp} \times 10^{-2}$	$m_0 a$	$Z_{A_\perp} \times 10^{-2}$
0.10	-8.371(43)	5.00	-3.870(26)
0.20	-7.933(40)	6.00	-3.560(27)
0.30	-7.515(33)	7.00	-3.284(24)
0.40	-7.199(40)	8.00	-3.062(31)
0.50	-6.932(35)	9.00	-2.842(32)
0.60	-6.687(33)	10.00	-2.640(26)
0.70	-6.487(34)	20.00	-1.182(26)
0.80	-6.304(33)	30.00	-0.244(24)
0.90	-6.146(35)	40.00	0.421(23)
1.00	-6.010(34)	50.00	0.959(22)
2.00	-5.130(32)	60.00	1.405(21)
3.00	-4.616(28)	70.00	1.768(32)
4.00	-4.209(26)	80.00	2.097(30)

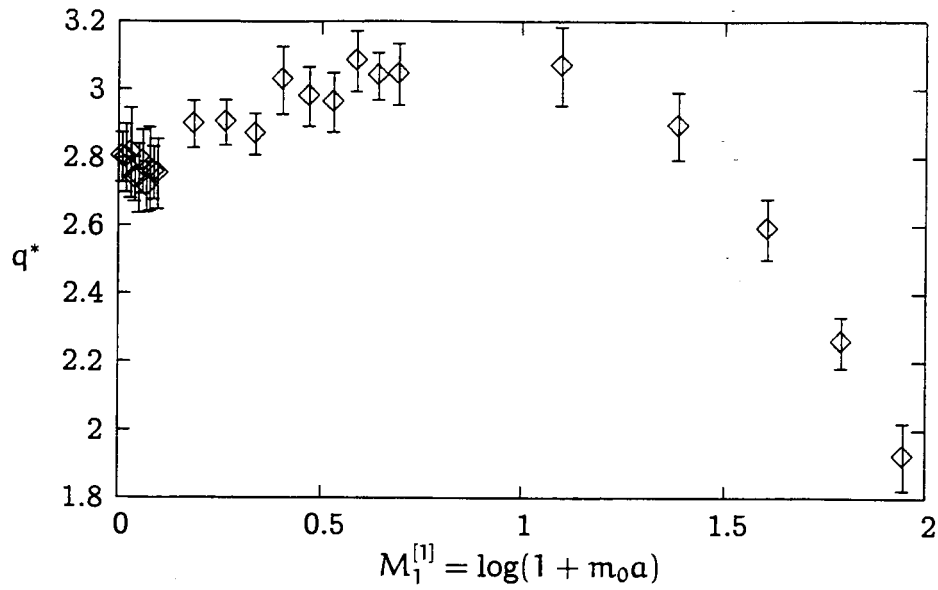Table 6.6: Table of values for $Z_{A_\perp}$ for improved glue.

Figure 6.15: The scale q^* for $V_{\parallel}$ with improved glue.

in chapter 3 more involved procedures must be used [36]. Fortunately, for the $m_0 a$ values relevant to numerical simulations, these methods are not necessary.

Chapter 7

Conclusion

7.1 Summary

In order to provide high-precision results to the wider particle physics community, it is imperative that lattice field theorists make use of improved actions. Such actions, built based on effective field theory approaches, allow for control over systematic errors present in all lattice simulations. One approach to improvement, the one we have adopted here, is to use perturbation theory to match the lattice theory to the continuum at high energy. Such a program requires one- and two-loop perturbative calculations. Several of these calculations have been reported here.

Owing to the lattice cutoff, lattice perturbation theory is much more complicated than in the continuum. A lattice perturbation theory calculation will have more diagrams, and the Feynman rules will be much more complicated. In order to overcome these problems we have developed a number of tools to simplify and automate the calculations.

The first is an implementation of the Lüscher–Weisz vertex generation algorithm for arbitrary quark and gluon actions. This automatically generates n-gluon Feynman rules, in a quick and error-free manner. By setting up the resulting loop integrals in a modular way, it is easy to change which action is used. This is a very important feature, since the number of improved actions in use by the lattice

community is very large.

Twisted periodic boundary conditions are another tool which greatly simplifies calculations. With a gauge invariant infrared regulator many issues which come up in continuum perturbative calculations are avoided.

In order to make use of twisted boundary conditions in matching calculations, we need to use them for both the lattice and continuum parts. We have introduced lattice-to-lattice matching, which allows us to do this in a convenient way.

7.1.1 New Results

This thesis presents several new results, calculated using the tools we have developed. First, there are the results for the link operators. We computed small Wilson loops, the static quark potential, static quark self energy, and the mean link, to next to leading order for three different gauge actions. Several of the results for the improved actions (self energy and potential) were new. These results, along with the calculations of small Wilson loops, are crucial in determining the strong coupling constant α_s.

We also present new results for the Fermilab action. The one-loop matching of c_B and c_E across the whole mass range was not known for either the Wilson or improved action. Furthermore we computed the kinetic terms $(M_1^{[1]}, Z_{M_2}^{[1]}, Z_2^{[1]})$ for the improved action; another new result. With these calculations as input, results from the Fermilab action are now accurate to $\mathcal{O}(a^2)$, the $\mathcal{O}(\alpha a)$ errors have been removed.

The same holds true for the Fermilab currents. We matched the vector and axial vector currents at one loop order using the improved gluon action, and the improved ("rotated") spinors. These results will improve the accuracy of results for heavy quark decay constants and form factors.

7.2   Future Work

There is no shortage of work that could be done to continue the program outlined in this thesis. One obvious direction is the one loop matching of the action parameters and currents for the NRQCD action. There is also the dimension 6 Fermilab action [52], which has over ten new parameters which need one-loop matching.

For true high-precision work many two-loop calculations will also be needed. The strong coupling is, on the $a \approx 0.09$ fm lattices used by MILC, (optimistically) 0.15, so two loop calculations will be needed to get perturbative errors down below few percent. A good candidate calculation would be to continue the current matching to two loops. This would have a major impact on the determination of the CKM matrix elements.

The techniques outlined in this thesis have all been developed with their extension to higher orders in mind. The combination of twisted boundary conditions and lattice to lattice matching should allow for two loop determinations of action parameters, and (partially) conserved currents. While new issues will arise, the techniques presented here will provide the basics for doing higher order lattice perturbation theory.

Bibliography

[1] M. E. Peskin and D. V. Schroeder. *An Introduction to Quantum Field Theory*. Frontiers in Physics. Addison-Wesley, 1995.

[2] D. Griffiths. *Introduction to Elementary Particles*. John Wiley and Sons, Inc., 1987.

[3] K. Hagiwara et al. Review of particle physics. *Phys. Rev.*, D66:010001, 2002. Updates are available online at http://pdg.lbl.gov.

[4] E. Fermi. An attempt of a theory of beta radiation. 1. *Z. Phys.*, 88:161–177, 1934.

[5] N. Cabibbo. Unitary symmetry and leptonic decays. *Phys. Rev. Lett.*, 10:531–532, 1963.

[6] M. Kobayashi and T. Maskawa. CP violation in the renormalizable theory of weak interaction. *Prog. Theor. Phys.*, 49:652–657, 1973.

[7] Lincoln Wolfenstein. Parametrization of the Kobayashi-Maskawa matrix. *Phys. Rev. Lett.*, 51:1945, 1983.

[8] Matthew A. Nobes and R. M. Woloshyn. Decays of the B_c meson in a relativistic quark-meson model. *J. Phys.*, G26:1079–1094, 2000.

[9] Kenneth G. Wilson. Confinement of quarks. *Phys. Rev.*, D10:2445–2459, 1974.

[10] K.G. Wilson. Quarks and strings on a lattice. In A. Zichichi, editor, *New Phenomena in Subnuclear Physics*, page 69. Plenum Press, New York, 1975.

[11] G. Peter Lepage. Flavor-symmetry restoration and Symanzik improvement for staggered quarks. *Phys. Rev.*, D59:074502, 1999.

[12] C. T. H. Davies et al. (26 authors, including M. Nobes) High-precision lattice QCD confronts experiment. *Phys. Rev. Lett.*, 92:022001, 2004.

[13] Matthew A. Nobes, Howard D. Trottier, G. Peter Lepage, and Quentin Mason. Second order perturbation theory for improved gluon and staggered quark actions. *Nucl. Phys. Proc. Suppl.*, 106:838–840, 2002.

[14] Howard D. Trottier, G. Peter Lepage, Paul B. Mackenzie, Quentin Mason, and Matthew A. Nobes. Highly improved naive and staggered fermions. *Nucl. Phys. Proc. Suppl.*, 106:856–858, 2002.

[15] C. Davies, A. Gray, M. Alford, E. Follana, J. Hein, P. Lepage, Q. Mason, M. Nobes, J. Shigemitsu, H. Trottier, and M. Wingate. The determination of $alpha_s$ from lattice QCD with 2+1 flavors of dynamical quarks. *Nucl. Phys. Proc. Suppl.*, 119:595–597, 2003.

[16] Ruedi Burkhalter. Recent results from the CP-PACS collaboration. *Nucl. Phys. Proc. Suppl.*, 73:3–15, 1999.

[17] S. Gottlieb. Results on improved KS dynamical configurations: spectrum, decay constants, etc. Plenary talk presented at Lattice 2003, Tsukuba, Japan, July 15-19. Available online at http://www.arxiv.org/abs/hep-lat/0310041.

[18] J. Gasser and H. Leutwyler. Chiral perturbation theory: Expansions in the mass of the strange quark. *Nucl. Phys.*, B250:465, 1985.

[19] Sinead M. Ryan and Andreas S. Kronfeld. Remark on the theoretical uncertainty in B_0 anti-B_0 mixing. *Nucl. Phys. Proc. Suppl.*, 119:622–624, 2003.

[20] C. Bernard et al. Panel discussion on chiral extrapolation of physical observables. *Nucl. Phys. Proc. Suppl.*, 119:170–184, 2003.

[21] Noam Shoresh. *Applications of Chiral Perturbation Theory*. PhD thesis, Washington University, Seattle, 2001.

[22] C. Aubin and C. Bernard. Staggerd chiral perturbation theory. In *Lattice 2003 Proceedings*, 2003. Talk presented at Lattice 2003, Tsukuba, Japan. Writeup availble as hep-lat/0308036.

[23] K. Symanzik. Continuum limit and improved action in lattice theories. 1. principles and ϕ^4 theory. *Nucl. Phys.*, B226:187, 1983.

[24] Mark G. Alford, W. Dimm, G. P. Lepage, G. Hockney, and P. B. Mackenzie. Lattice QCD on small computers. *Phys. Lett.*, B361:87–94, 1995.

[25] B. Sheikholeslami and R. Wohlert. Improved continuum limit lattice action for QCD with Wilson fermions. *Nucl. Phys.*, B259:572, 1985.

[26] M. Lüscher and P. Weisz. Efficient numerical techniques for perturbative lattice gauge theory computations. *Nucl. Phys.*, B266:309, 1986.

[27] H. J. Rothe. Lattice gauge theories: An introduction. *World Sci. Lect. Notes Phys.*, 59:1–512, 1997.

[28] Colin J. Morningstar. The heavy quark selfenergy in nonrelativistic lattice QCD. *Phys. Rev.*, D48:2265–2278, 1993.

[29] B. Alles, M. Campostrini, A. Feo, and H. Panagopoulos. Lattice perturbation theory by computer algebra: A three loop result for the topological susceptibility. *Nucl. Phys.*, B413:553–566, 1994.

[30] Stefano Capitani and Gaincarlo Rossi. The use of schoonschip and form in perturbative lattice calculations. 1995. hep-lat/9504014.

[31] Mark Lutz and David Ascher. *Learning Python.* O'Reilly and Associates, 1999.

[32] Istvan Montvay and Gernot Munster. *Quantum Fields on a Lattice.* Cambridge Monographs on Mathematical Physics. Cambridge University Press, 1994.

[33] G. Peter Lepage. A new algorithm for adaptive multidimensional integration. *J. Comput. Phys.*, 27:192, 1978.

[34] Rainer Sommer. Non-perturbative renormalization of HQET and QCD. *Nucl. Phys. Proc. Suppl.*, 119:185–197, 2003.

[35] G. Peter Lepage and Paul B. Mackenzie. On the viability of lattice perturbation theory. *Phys. Rev.*, D48:2250–2264, 1993.

[36] K. Hornbostel, G. P. Lepage, and C. Morningstar. Scale setting for α_s beyond leading order. *Phys. Rev.*, D67:034023, 2003.

[37] Claude Bernard, Tom Blum, Thomas A. DeGrand, Carleton DeTar, Steven Gottlieb, Urs M. Heller, James Hetrick, Craig McNeile, K. Rummukainen, Bob Sugar, and Doug Toussaint. Quenched hadron spectroscopy with improved staggered quark action. *Phys. Rev.*, D58:014503, 1998.

[38] Gerard 't Hooft. A property of electric and magnetic flux in nonabelian gauge theories. *Nucl. Phys.*, B153:141, 1979.

[39] Quentin Mason. Treatise on colour factors. Unpublished notes.

[40] R. Wohlert. Improved continuum limit lattice action for quarks. DESY-87-069, 1987.

[41] G. Parisi. Prolegomena to and future computer evaluation of the QCD mass spectrum. In G. 't Hooft et al., editors, *Progress in Gauge field theory.* Plenum Press, New York, 1984.

[42] H. D. Trottier, N. H. Shakespeare, G. P. Lepage, and P. B. Mackenzie. Perturbative expansions from monte carlo simulations at weak coupling: Wilson loops and the static-quark self- energy. *Phys. Rev.*, D65:094502, 2002.

[43] G. P. Lepage, B. Clark, C. T. H. Davies, K. Hornbostel, P. B. Mackenzie, C. Morningstar, and H. Trottier Constrained curve fitting. *Nucl. Phys. Proc. Suppl.*, 106:12–20, 2002.

[44] Urs M. Heller and F. Karsch. One loop perturbative calculation of Wilson loops on finite lattices. *Nucl. Phys.*, B251:254, 1985.

[45] Howard D. Trottier. Higher-order perturbation theory for highly-improved actions. Plenary talk presented at Lattice 2003, Tsukuba, Japan, July 15-19. Available online at http://www.arxiv.org/abs/hep-lat/0310044.

[46] Aneesh V. Manohar and Mark B. Wise. Heavy quark physics. *Cambridge Monogr. Part. Phys. Nucl. Phys. Cosmol.*, 10:1–191, 2000.

[47] G. P. Lepage, L. Magnea, C. Nakhleh, U. Magnea, and K. Hornbostel Improved nonrelativistic QCD for heavy-quark physics. *Phys. Rev. D*, 46(9):4052, 1992.

[48] Howard D. Trottier. Quarkonium spin structure in lattice NRQCD. *Phys. Rev.*, D55:6844–6851, 1997.

[49] Aida X. El-Khadra, Andreas S. Kronfeld, and Paul B. Mackenzie. Massive fermions in lattice gauge theory. *Phys. Rev.*, D55:3933–3957, 1997.

[50] Massimo di Pierro, Aida X. El-Khadra, Steven Gottlieb, Andreas S. Kronfeld, Paul B. Mackenzie, Damian P. Menscher, Mehmet B. Oktay, Masataka Okamoto, and James N. Simone. Properties of charmonium in lattice QCD with 2+1 flavors of improved staggered sea quarks. Talk presented at Lattice 2003, Tsukuba, Japan. Writeup available at hep-lat/0310042. 2003.

[51] Massimo di Pierro, Aida X. El-Khadra, Steven Gottlieb, Andreas S. Kronfeld, Paul B. Mackenzie, Damian P. Menscher, Masataka Okamoto, and James N. Simone. D_s spectrum and leptonic decays with fermilab heavy quarks and improved staggered light quarks. Talk presented at Lattice 2003, Tsukuba, Japan. Writeup available at hep-lat/0310045.

[52] M. B. Oktay, A. X. El-Khadra, A. S. Kronfeld, and P. B. Mackenzie. A more improved lattice action for heavy quarks. Talk presented at Lattice 2003, Tsukuba, Japan. Writeup available at hep-lat/0310016. 2003.

[53] A. Kronfeld B.P.G. Mertens and A.X. El-Khadra. Self energy of massive lattice fermions. *Phys. Rev.*, D58:04505, 1998.

[54] C. T. H. Davies, K. Hornbostel, G. P. Lepage, A. J. Lidsey, J. Shigemitsu, and J. Sloan. Precision charmonium spectroscopy from lattice QCD. *Phys. Rev.*, D52:6519–6529, 1995.

[55] A.X. El-Khadra. The charmonium spectrum on the lattice: A status report. *Nucl. Phys B (Proc. Suppl.)*, 30:449, 1993.

[56] Chris Stewart and Roman Koniuk. Unquenched charmonium with nrQCD. *Phys. Rev.*, D63:054503, 2001.

[57] Martin Lüscher and Peter Weisz. Background field technique and renormalization in lattice gauge theory. *Nucl. Phys.*, B452:213–233, 1995.

[58] Sinya Aoki and Yoshinobu Kuramashi. Determination of the improvement coefficient c_{SW} up to one-loop order with the conventional perturbation theory. *Phys. Rev.*, D68:094019, 2003.

[59] Jonathan M. Flynn and Brian R. Hill. B-B* splitting: A test of heavy quark methods. *Phys. Lett.*, B264:173–177, 1991.

[60] J. Simone and A. El-Khadra. List of fermilab parameters. Private Communications. 2003.

[61] Junpei Harada, Shoji Hashimoto, Ken-Ichi Ishikawa, Andreas S. Kronfeld, Tetsuya Onogi, and Norikazu Yamada. Application of heavy-quark effective theory to lattice QCD. II: Radiative corrections to heavy-light currents. *Phys. Rev.*, D65:094513, 2002.

[62] Junpei Harada, Shoji Hashimoto, Andreas S. Kronfeld, and Tetsuya Onogi. Application of heavy-quark effective theory to lattice QCD. III: Radiative corrections to heavy-heavy currents. *Phys. Rev.*, D65:094514, 2002.